universität wien

DISSERTATION / DOCTORAL THESIS

Titel der Dissertation /Title of the Doctoral Thesis

„The Ebreichsdorf 2013 earthquake series: location, interaction and wave propagation“

verfasst von / submitted by

Dipl.-Ing. Maria-Theresia Apoloner, BSc

angestrebter akademischer Grad / in partial fulfilment of the requirements for the degree of

Doktorin der Naturwissenschaften (Dr. rer.nat.)

Wien, 2015 / Vienna 2015

Studienkennzahl lt. Studienblatt / degree programme code as it appears on the student record sheet:	A 796 605 416
Dissertationsgebiet lt. Studienblatt / field of study as it appears on the student record sheet:	Geophysik
Betreut von / Supervisor:	Univ.-Prof. Dr. Götz Bokelmann

Acknowledgements

Firstly, I would like to thank my advisor Prof. Bokelmann for the continuous support of my research and my PhD study. Besides my advisor I would like to thank the other employees of the Department of Geophysics and Meteorology of the University of Vienna, especially from the geophysics working group: for stimulating discussions, insightful comments and their encouragement.

My sincere thanks also goes to all people, institutions and organisations who supplied data for this research: Technical University of Vienna, Zentralanstalt für Meteorologie und Geodynamik, GeoRisk Earthquake Engineering, and Observatories and Research Facilities for European Seismology. Without this input, this research would not have been possible.

Last but not least, I give my thanks to my family: my parents and my sister, who have always showed great interest in my work, and supported and encouraged me in conducting this thesis.

Abstract

Due to Vienna's location in a seismogenic region, it is important to characterize seismicity in the vicinity well. The Austrian seismological network is built of very high quality stations, but those are spread too widely to determine earthquake depths accurately for small earthquakes. Therefore I attempt to optimize use of the network and available data for locating earthquakes, with a comprehensive dataset from the Ebreichsdorf 2013 earthquake series, complemented by data from earlier events in the area.

Two location methods are applied: one by Lomax et al. (2000) to get precise absolute location of the series. Afterwards, HypoDD by Waldhauser and Ellsworth (2000) is used to get a better picture of the spatio-temporal pattern of the series. Following this analysis the interaction between the events is examined. Due to the network geometry hypocentral depths are not as well-constrained as lateral location. Regional depth phases can improve depth estimation if they can be identified. To detect those phases data from the GERES seismic array were processed additionally. To understand RDP propagation in this area, synthetic seismograms are calculated with regional focal mechanisms and a locally adapted velocity model.

Location with NonLinLoc puts the epicentres to the south-east of Ebreichsdorf and reveals a south-west to north-east pattern. After relocation with hypoDD, the earthquake series clusters on a smaller area and depth range. Also the main shocks collocate, which was confirmed by coherence measurements. The application of Coulomb failure stress modelling for analysing interaction between the 2013 main shocks shows that Coulomb stress transfer from the main shocks does not explain aftershock triggering. Complementary comparison with the 2000 series indicates that the previous main shocks are located 4 km apart to the north-east. Subsequent analysis of the 2013 earthquakes at GERES, identifies clear arrivals of PmP

and PbP, but not of their corresponding depth phases, which is consistent with the synthetic data. Examination of the modelled seismograms also shows, that RDP propagation is dependent not only on depth but is also strongly influenced by the focal mechanism. Also a low-velocity top-layer, like a sedimentary basin, renders RDP invisible, as it complicates the resulting seismograms considerably.

Kurzfassung

Aufgrund der Lage Wiens in einer seismisch aktiven Region ist es wichtig, diese Seismizität gut zu bestimmen. Das seismologische Netz Österreichs besteht aus hochwertigen Stationen, jedoch sind die Stationen zu weit voneinander entfernt, um Lage und Tiefe von kleineren Erdbeben genau zu charakterisieren. Deshalb versuche ich in dieser Doktorarbeit die Menge der der verwendeten Daten zur Lokalisierung zu erhöhen. Dafür wurde ein umfassender Datensatz der Erdbebenserie in Ebreichsdorf von 2013 zusammengestellt, ergänzt durch die Erdbebenserie von 2000.

Zwei Lokalisierungsmethoden werden verwendet: die absolute Lage wird mit NonLinLoc von Lomax et al. (2000) bestimmt. Danach wird HypoDD von Waldhauser und Ellsworth (2000) verwendet, um das raumzeitliche Muster der Erdbebenserie zu berechnen. Nach dieser Analyse wird die Wechselwirkung zwischen den Ereignissen untersucht. Da aufgrund der Netzgeometrie die Lagegenauigkeit beschränkt ist, wird versucht diese durch regionale Tiefenphasen zu verbessern, sofern diese identifiziert werden können. Dafür wurden Daten des seismischen Arrays GERES verwendet. Um die Wellenausbreitung um das Wiener Becken besser zu verstehen, werden weiters synthetische Seismogramme mit regionalen Herdmechanismen und einem lokal angepassten Geschwindigkeitsmodell berechnet.

NonLinLoc setzt die Epizentren in den Südosten von Ebreichsdorf und zeigt eine längliche Verteilung von Südwesten nach Nordosten. Mit der Relokalisierung mit HypoDD verkleinert sich die Fläche und der Tiefenbereich, auf dem die Beben auftreten. Auch die Hauptbeben sind nun kollokalisiert, wie auch die Kohärenzmessungen bestätigen. Die Modellierung von Coulomb-Bruchspannungen zeigt, dass Coulomb-Spannungsübertragung nicht stark genug ist, um die Nachbeben auszulösen. Ein ergänzende Vergleich mit der 2000-Serie ergibt, dass sich die Hauptbeben

4 km entfernt im Nordosten befinden. Die anschließende Analyse der 2013 Erdbeben in GERES, identifiziert die Phasen PmP und PbP, aber nicht ihre entsprechenden Tiefenphasen. Dies steht im Einklang mit den synthetischen Daten. Prüfung der modellierten Seismogramme zeigt des weiteren, dass die Wellenausbreitung stark vom Herdmechanismus beeinflußt wird. Auch eine langsame oberflächennahe Schicht, wie ein Sedimentbecken, beeinflusst die Sichtbarkeit von Tiefenphasen stark negativ.

Contents

Abstract v

Kurzfassung vii

1. Introduction 1
- 1.1. Regional tectonic setting and seismicity . . . 1
- 1.2. Earthquake localisation . . . 3
- 1.3. Earthquake interaction . . . 4
- 1.4. Complementary earthquake depth estimation . . . 5
  - 1.4.1. Regional depth phases (RDP) . . . 5
  - 1.4.2. Regional Rayleigh phases (Rg) . . . 8
- 1.5. Thesis outline . . . 9

2. Ebreichsdorf dataset 11
- 2.1. Historical and recent seismicity . . . 11
- 2.2. Surrounding seismic networks and available stations . . . 13
- 2.3. Location methods and stations used . . . 15
  - 2.3.1. Earthquake catalogue and ZAMG-bulletin . . . 15
  - 2.3.2. Additional locations and methods used . . . 16
- 2.4. Additional data products . . . 16
  - 2.4.1. Isoseismal maps . . . 16
  - 2.4.2. Focal mechanisms . . . 17

3. The 2013 Earthquake Series in the Southern Vienna Basin: location 21
- 3.1. Abstract . . . 21
- 3.2. Introduction . . . 22
- 3.3. Dataset . . . 23
  - 3.3.1. Seismicity . . . 23
  - 3.3.2. Velocity models . . . 23

3.3.3. Seismic stations 23
3.4. Hypocenter location 25
3.4.1. Routine processing with 3 local stations 25
3.4.2. Advanced processing routine with comprehensive consistent dataset 26
3.5. Conclusions 27

4. The Ebreichsdorf 2013 earthquake series: Relative location 29
4.1. Abstract 29
4.2. German abstract 30
4.3. Introduction 31
4.4. Ebreichsdorf 2013 series 33
4.4.1. Additional data 35
4.5. Event location and relocation 35
4.5.1. HypoDD 36
4.5.2. Parameters and settings 38
4.6. Results 39
4.7. Discussion 45
4.8. Conclusion 46
4.9. Acknowledgements 47

5. Earthquake interactions during the 2013 Ebreichsdorf aftershock sequence 49
5.1. Abstract 49
5.2. German abstract 50
5.3. Introduction 52
5.4. Ebreichsdorf sequence in 2013 53
5.5. Coulomb stress interactions 57
5.6. Parameters and results 59
5.7. Discussion 60
5.8. Conclusion 62
5.9. Acknowledgements 63
5.10. Appendix: Hydrological observations in Ebreichsdorf area 63

6. Modeling and detection of regional depth phases at the GERES array 69
6.1. Abstract 69
6.2. Introduction 70

6.3. Tectonic setting . . . 71
6.4. Seismic data . . . 72
6.5. Regional depth phase (RDP) propagation . . . 73
6.5.1. Waveform modeling . . . 74
6.6. Array analysis with vespagrams . . . 77
6.7. Polarization analysis of 3-component stations . . . 78
6.8. Results . . . 79
6.8.1. Regional depth phase spreading . . . 79
6.8.2. Array analysis . . . 79
6.8.3. Polarization analysis . . . 80
6.9. Conclusions . . . 80
6.10. Acknowledgements . . . 81

7. Influences on regional depth phase identification 83
7.1. Travel times . . . 85
7.1.1. Phase overlaps . . . 85
7.1.2. Minimum time difference between RDP pairs . . . 85
7.2. Amplitudes and waveforms . . . 87
7.2.1. Influence of low-velocity surface layer . . . 88
7.2.2. Influence of focal mechanism . . . 89
7.3. Summary . . . 96

8. Summary and conclusions 99

A. Improving identification of regional depth phases in sparse networks 105
A.1. Overview . . . 105
A.2. Region and seismic data . . . 106
A.3. Polarization filtering . . . 107
A.4. Depth phase stacking . . . 107
A.5. Current research - Northern California . . . 109
A.6. Summary and further research . . . 110

B. Modeling local and regional wave propagation 113
B.1. Overview . . . 113
B.2. Local and regional phases . . . 114
B.3. Synthetic Seismograms . . . 115
B.3.1. Model and methods . . . 115

B.3.2. Explosion source 116
B.3.3. Strike slip source at at 0° and 45° azimuth 116
B.4. Results and outlook 116

C. Academic curriculum vitae **125**

List of Figures **129**

List of Tables **139**

Bibliography **141**

1. Introduction

Everybody remembers the reports of earthquakes, which have caused huge damages. They are thoroughly covered by the media, and also lots of research focuses on them like the Tohoku 2011 earthquake with many thousands of research contributions in multiple fields of research.

It is important to study those big events, due to their impact on humans and their environment. However, in many areas of the world only small non-damaging magnitude earthquake have occured in the instrumental period. Conclusions on earthquake hazard assessment have therefore often be drawn based on those small earthquakes, and it is imperative to well-characterise their locations and frequencies of occurence.

Usually small earthquakes cannot be analysed thoroughly because the number of recordings that are available is much smaller (i. a. no strong-motion records because of triggering, not enough movement for GPS). This leads to less background knowledge on seismicity in the area investigated, which is fundamental for thorough analysis such as fault location or underground velocity. To fill this knowledge gap multiple efforts can be undertaken: deployment of temporary seismic networks, analysis of seismic profiles to characterise the underground velocity - in summary: additional data to be recorded and analysed.

1.1. Regional tectonic setting and seismicity

One of the areas where this was done in the last decades is the Vienna Basin, wedged between the Eastern Alps and the Western Carpathians (see Figure 1.1). Ongoing convergence between the Adriatic Plate from the south and the European Plate from the north, lead to lateral extrusion of blocks to the east into the Pannonian Basin (e.g. Gutdeutsch et al.,

1987). Both the Salzach-Enns-Mariazell-Puchberg fault (SEMP) and the seismically active Mur-Mürz-Line (MML) show this process by forming sinistral strike-slip fault systems.

The Vienna Basin lies in the northeastern extension of the MML, and it and its faults, the Vienna Basin Fault Sysem (VBFS), are particularly interesting, due to their vicinity to Vienna. As this region is one of the most densely populated and developed areas of Austria. The pull-apart basin originates from the Middle Miocene (e.g. Royden, 1985) and is filled with several kilometres of slow-velocity sediments. The Bohemian Massif forms the underlying basement beneath. The overview of the tectonic setting and seismic activity in the area is given in Figure 1.1.

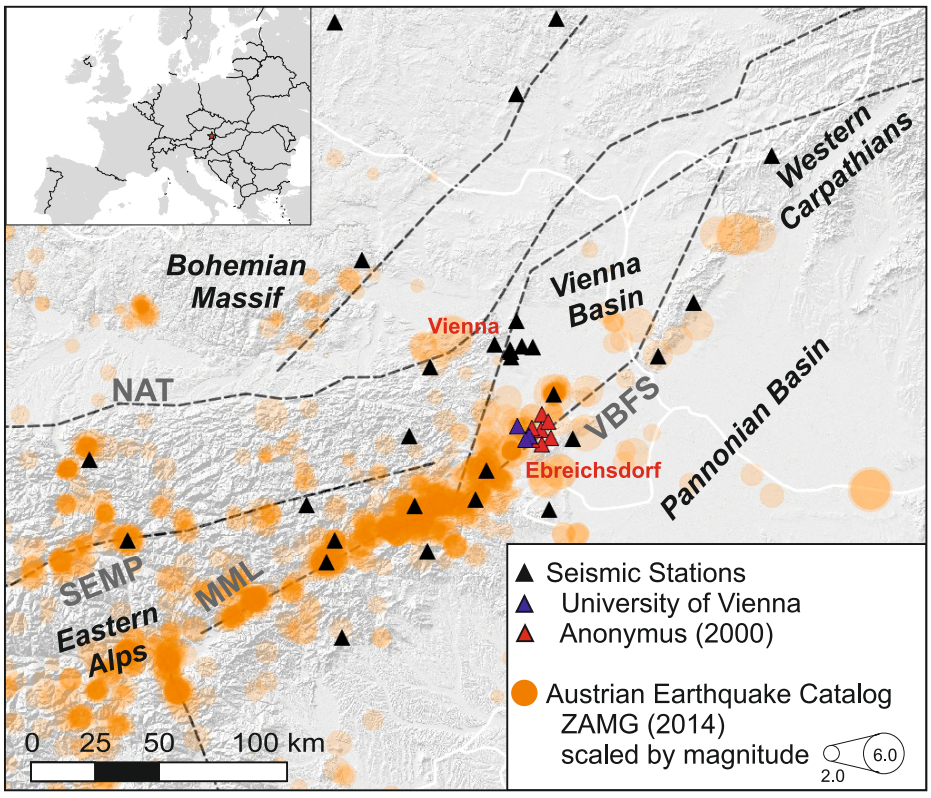

Figure 1.1.: Seismotectonic overview of the Vienna Basin: main tectonic units and generalized faults from GBA (2010) combined with earthquakes from the Austrian Earthquake Catalogue scaled by magnitude (ZAMG, 2014). Triangles indicate the positions of seismic stations available for this thesis.

At present, the Austrian seismological network is used to detect and locate earthquakes and other seismic events in this area. The network

is built of high quality stations, but their station coverage is relatively sparse. The sparse network combined with the standard procedure used for earthquake localization by the ZAMG (Zentralanstalt für Meteorologie und Geodynamik) is not able to detect all earthquakes nor to give precise focal depths for most earthquakes.

So, instrumentally recorded seismicity in the area is moderate, but recorded magnitudes reach values larger than 5. There are historical records of earthquakes with intensities equivalent to magnitudes around 6, and even larger events have been suggested based on paleoseismicity, e.g. by Hintersberger et al. (2010).

Research, mostly since 2000, produced much additional measurements and analysis, which was used in further studies to create P- and S-velocity models (Behm et al., 2007a,b), to calculate Moho-depths (Bianchi et al., 2015) and to analyse seismic anisotropy (Qorbani et al., 2015a,b). Also data from temporary seismological deployments entered into the standard location procedure, and has so increased the number and quality of events localized (see Chapter 2).

1.2. Earthquake localisation

Earthquake localisation is a fundamental challenge of seismology and often the basis for further studies. The earthquake location consists of three spatial coordinates (longitude, latitude and depth) and the origin time. Due to the geometry (all stations are on the surface or close to it) longitude and latitude can be estimated well using P- and S-picks, if station coverage is sufficiently dense. On the other hand the depth and origin time are dependent on each other. Yet, not all earthquakes can be localized and for even more hypocentral depth can only be estimated based on former knowledge, e.g. depths from catalogue (ZAMG, 2014) or macroseismic studies (Lenhardt et al., 2007).

To improve the accuracy of an earthquake location data can be added: e.g. more and/or higher-quality stations. Also, the method can be improved to be able use more information like additional phases or 3D-velocity models. However, those methods need to be adjusted carefully to the data and the

regional settings. For this study I selected two different methods, due to their different advantages:

- NonLinLoc by Lomax et al. (2000) is a probabilistic, non-linear, global-search earthquake location software package for 3D media. Absolute locations are calculated individually for each event. Aside from P- and S-picks also pick and model accuracies are used as input. If, as in the case of the 3D model for the area, the model is very crude, station corrections can be calculated and applied to reduce model errors and improve location. More about this method and the results can be found in Chapter 3.
- HypoDD implements the double-difference earthquake mechanism published by Waldhauser and Ellsworth (2000). In contrast to NonLinLoc it needs inital earthquake locations, which are jointly and iterativly relocated. HypoDD can also use cross-correlations between the earthquakes. With these data accurate relative locations within a dataset of earthquakes can be determined. More about this method and the results can be found in Chapter 4.

To test these two methods in the Vienna Basin and to create a dataset of accurate locations for further research they were applied to Ebreichsdorf and its vicinity. This city in the Southern Vienna Basin was selected because it has experienced two series of earthquakes recently: one in 2000 and another in 2013. The focus lies on those, because the main shocks (local magnitude 4.2 - 4.8) were big enough to calculate i.a. focal mechanisms, which in turn were crucial for modelling waveforms. Also, records of the aftershocks from temporary local stations are available. The aftershocks can be used for example to reduce location errors, by calculating station corrections and applying them.

1.3. Earthquake interaction

From the Austrian Earthquake Catalogue it is known that in both series of earthquakes the events are located close to each other. Location and relocation undertaken in this thesis, confirms this and locates the main shocks of the Ebreichsdorf 2013 series even closer together (less than 100

m). However, collocation of similar magnitude main shocks with short inter-event times are unexpected, because tectonic stresses should have been released in the first main shock. So this raises questions of the nature of the interaction between the earthquakes in this sequence. Therefore, this phenomena is studied in detail in Chapter 5.

1.4. Complementary earthquake depth estimation

Although, NonLinLoc gives absolute locations and HypoDD is used for precise relative location, both have something in similar: they both search jointly for the location and depth of the event using P- and S-Picks /pick-differences. As depth is proportional to origin time, neither of these parameters can be determined without affecting the other. Therefore, hypocentral depth usually has less accuracy than lateral location. To improve depth estimation additional data are needed.

1.4.1. Regional depth phases (RDP)

One possible solution is mentioned in Bormann et al. (2012):

"In summary, observational seismologists should be aware that depth phases are vital for improving source locations and making progress in understanding earthquakes in relation to the rheological properties and stress conditions in the lithosphere and upper mantle. Therefore, they should do their utmost to recognize depth phases in seismograms despite the fact that they are not always present and that it may be difficult to identify them reliably." New Manual of Seismological Observatory Practice-2, Ch. 11

This excerpt emphasizes the utility of using depth phases to improve source locations and thereby constraining epicentral depths. Regional depth phases such as sPg, sPmP and sPn have been studied by numerous scientists: Helmberger and Engen (1980); Saikia (2000); Langston (1987);

Uski et al. (2003); Stroujkova (2009); Bock (1993). However, they are seldom used, because identification is complicated.

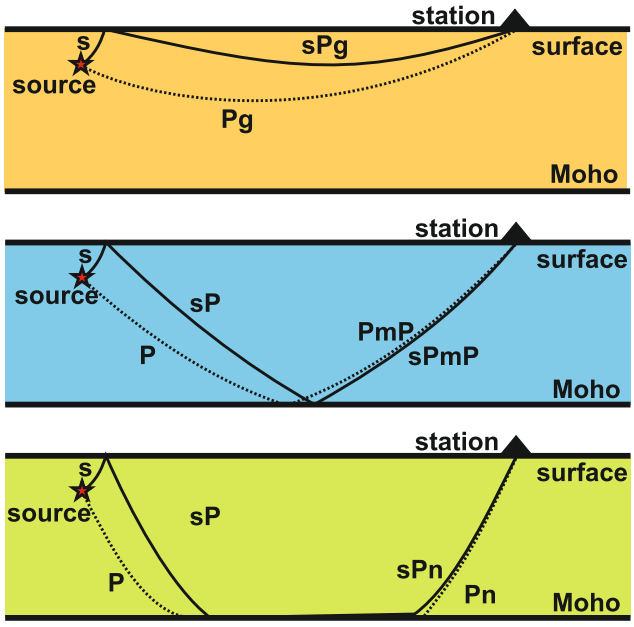

Figure 1.2.: Schematic RDP wavepaths adapted from Ma and Eaton (2011).

In theory, regional depth phases such as sPg, sPmP and sPn in combination with their reference phases Pg, PmP and Pn can be used to estimate focal depths of regional earthquakes. Wavepaths of those are sketched in Figure 1.2. In principle, a single station with one phase pair may be sufficient for accurately determining earthquake depth from the difference in their arrival times. Different studies, (e.g. Ma and Atkinson, 2006; Ma and Eaton, 2007; Ma, 2010) show that regional depth phases develop differently well, depending on epicentral distance and magnitude. Values by Ma (2010) are compiled in Table 1.4.1.

Phases	Distance	Magnitude
Pg & sPg	< 100 km	> 1.5
PmP & sPmP	200-300 km	> 2.0
Pn & sPn	> 300 km	> 4.0

Table 1.1.: RDP detectability adapted from Ma (2010).

Figure 1.3 shows the region around Ebreichsdorf combined with the distance ranges for RDP given in Table 1.4.1. This figure indicates that

some RDP (Pg and sPg, PmP and sPmP) should be easily detectable in this area. However, previous research (Apoloner and Bokelmann, 2012, Appendix A) showed that they cannot be seen directly with regional data from this area. Neither single station polarization filtering by Schimmel and Gallart (2004) nor stacking improved phase detection on more than a few cases, which could not be confirmed by depth values given in the catalogue.

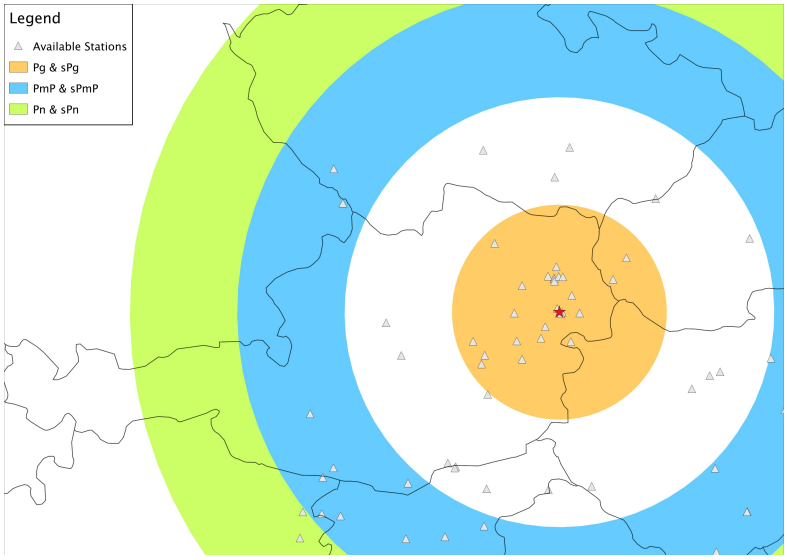

Figure 1.3.: Regions with zones of detectable regional depth phases after Ma (2010) around Ebreichsdorf.

A different approach to improve the signal to noise ratio to detect RDP is array processing. In the area of interest shown in Figure 1.3 the GERES array (Figure 1.4) is available at 220 km distance to Ebreichsdorf, a distance where PmP and sPmP should be well developed according to Ma (2010). In Chapter 6 the visibility of RDP at this array is investigated with real and synthetic data and two different types of analysis: 1D array processing and 3D polarization.

Even with these techniques and concurrent modelling only few RDP could be detected and no full RDP pair like PmP and sPmP identified. So, in the last part of this thesis (Chapter 7) I investigate two cases which could cause the invisibility of RDP with synthetic seismograms:

- Most studies using RDP are based on normal/thrusting earthquakes (e.g. Bock, 1993; Ebel and Bonjer, 1990; Gamage et al., 2009; Ma, 2012;

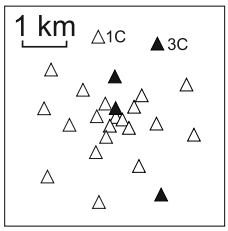

Figure 1.4.: Stations of the seismic array GERES. White triangles mark seismic station positions with one component, black with three components.

Ma and Atkinson, 2006). The impossibility to detect both at the same station could result from the focal mechanism, which is typically strike-slip in the area (see Chapter 2).

- From the previous study by Apoloner and Bokelmann (2012) (see Appendix A), it is also known that RDP are generally not directly visible, but need further preprocessing. One author, Ma (2010) also mentions that surface sediment layers reduce RDP development. As the Vienna Basin is above the epicentres investigated, this information is also integrated in the final modelling.

1.4.2. Regional Rayleigh phases (Rg)

Another type of phase was considered in this thesis as well: If the earthquake is very shallow, a Rg wave develops. One important characteristic of this wave is the approximately exponential attenuation with focal depth. At the same time a Sg wave is produced, which is less dependent on focal depth. The MPSR by Ma and Motazedian (2012) uses the different attenuation behaviour of these two waves to estimate focal depth.

The seismogram gets split into different parts containing either one of these phases or noise. Afterwards a spectrum for each part is calculated. The ratio of the Sg and the Rg spectrum then gives an indication of the focal depth. In Figure 1.5 an example for the MPSR method is shown.

However, as mentioned before this method only works with very shallow events (less than 5 km). From location, relocation and array processing (Chapters 3, 4 and 6) it is clear that the earthquakes in the area around

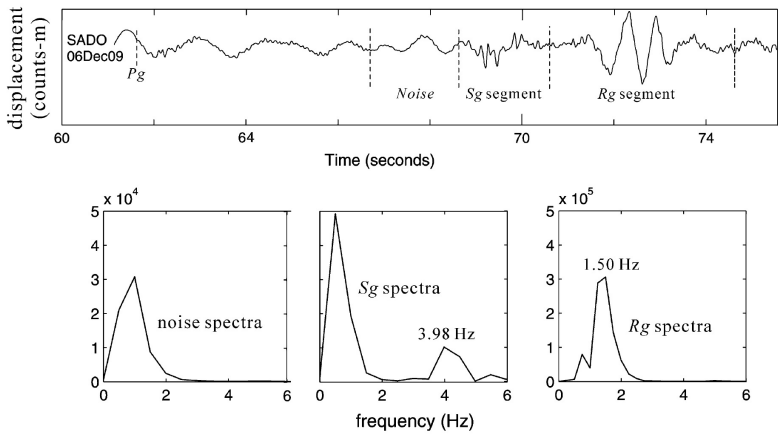

Figure 1.5.: Maximum power Rg/ Sg spectral ratio by Ma and Motazedian (2012).

Ebreichsdorf are much deeper (8-11 km), so this method is not applicable. This is also shown in Appendix B, which was presented by Apoloner and Bokelmann (2012).

1.5. Thesis outline

This thesis explores the possibilities of using different methods, additional data and multiple processing methods in the Vienna Basin, based on recent earthquakes in the vicinity of Ebreichsdorf.

The research is divided into the following parts:

- Chapter 2: Compilation of a comprehensive data set for the Ebreichsdorf 2000 and 2013 earthquake series
- Chapter 3: Determine absolute location of 2013 earthquake series
- Chapter 4: Determine relative location of 2013 earthquake series, and comparison to main shocks from 2000
- Chapter 5: Investigation of interaction between earthquakes in the 2013 earthquake series
- Chapter 6: 1-component array analysis and 3-component polarization analysis of the selected events from the 2013 earthquake series and synthetic data

- Chapter 7: Investigation of the effect of a sediment layer and of different focal mechanisms for the Vienna Basin with synthetic seismograms

A final summary for all parts together is given in Chapter 8. Additional material concerning RDP identification in the Vienna Basin can be found in Appendix A. Appendix B shows an example for waveform modelling of Rg phases.

2. Ebreichsdorf dataset

The focus of this thesis is on the area around Ebreichsdorf, a town 30 km south of Vienna. The area was selected because its recent seismic activity led to unprecedented high data availability for it. This chapter gives an overview of data and data products available for the area:

- historical and recent seismicity from different sources
- available seismic networks and stations
- macroseismic data
- velocity models for the subsurface

Although some of the figures in this chapter have a larger extent, only earthquakes in a 10 km radius around the seismic station VB01 (at the castle of Ebreichsdorf) are considered. VB01 was selected, because of its close vicinity to the church of Ebreichsdorf, which has been used as earthquake location in historical analysis.

2.1. Historical and recent seismicity

Research on historical earthquake activity in Lower Austria (Niederösterreich), clearly shows that the area around Ebreichsdorf is seismically active (Hammerl and Lenhardt, 2013): The first earthquake listed occurred in 1874 with an estimated intensity of 5 and magnitude of 3.3. The next record dates from 1899, with a magnitude of 3.2 and intensity above 5. In the 20^{th} century, with the start of instrumental seismic records 5 earthquakes were observed with intensities of at least 5. The highest intensity until now (10/2015) with 7 was reported on the 8^{th} November 1938 by Mifka and

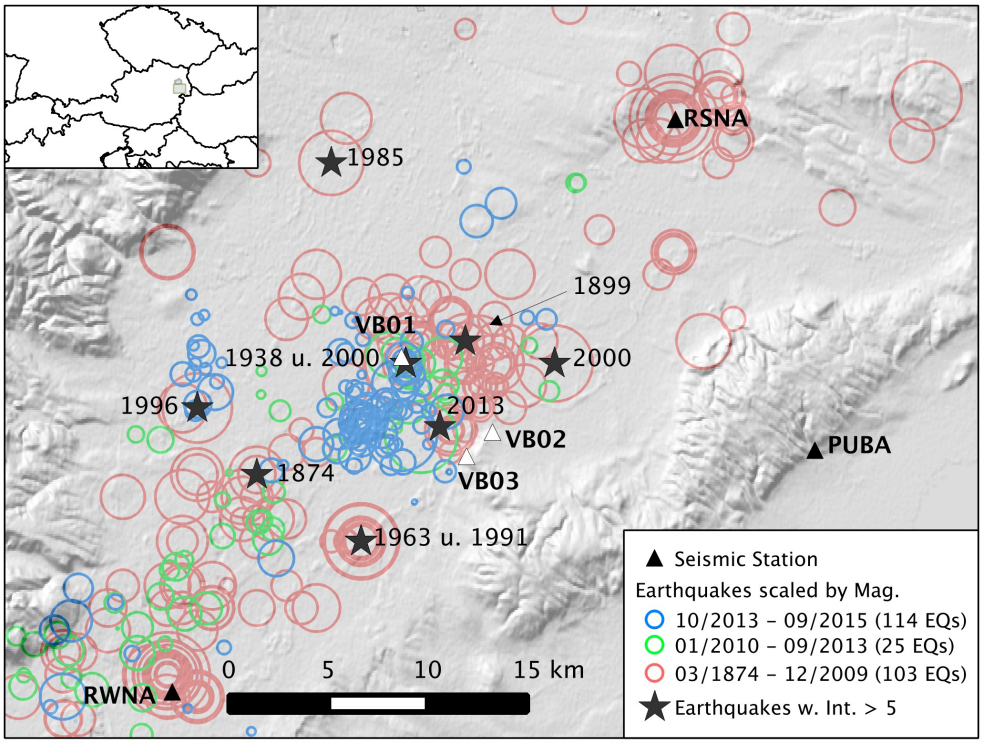

Figure 2.1.: Historical and recent seismicity in a 10 km radius around station VB01 at Ebreichsdorf Castle: Data until 12/2009 from Hammerl and Lenhardt (2013), 01/2010 - 09/2013 from ZAMG (2014), 10/2013 - 09/2015 from AutoDRM Bulletin using station VB01.

Trapp (1941). A complete list is given in Table 2.1 and Figure 2.1 shows the locations.

In 2000, for the first time in this area, not only the main shocks, but a whole series of earthquakes were recorded instrumentally. The main shocks with local magnitudes of 4.8 and 4.5 (intensities 5-6) were followed by more than 30 aftershocks. They were recorded by a temporary seismometer deployment by the Comprehensive Test Ban Treaty Organisation (CTBTO) (Anonymous, 2002).

With additional data from semi-permanent stations deployed by the Technical University of Vienna such as the ALPAACT project (Brückl et al., 2014), more than 20 earthquakes were recorded between 2001 and 2012 in the vicinity of Ebreichsdorf. All earthquakes with intensities $\geq$5 are listed in Table 2.1.

Table 2.1.: Earthquakes from the revised Earthquake Catalog for Lower Austria by Hammerl and Lenhardt (2013) with intensity $\geq$ 5.0 in a 10 km radius around Ebreichsdorf, supplemented by the main shocks from 2013.

Origin Time UTC	Latitude [°]	Longitude [°]	Depth [km]	Magnitude	Intensity
1874-03-10 —:—	47.91	16.30	7	3.3	5
1899-06-11 00:30	47.97	16.44	5	3.2	5-6
1938-11-08 03:12	47.96	16.40	10	5.0	7
1963-12-02 06:49	47.88	16.37	8	4.5	6-7
1985-06-05 23:45	48.05	16.35	11	3.8	5
1991-05-02 10:15	47.88	16.37	11	4.3	5-6
1996-01-09 01:07	47.94	16.26	8	4.1	6
2000-07-11 02:49	47.96	16.40	13	4.8	6
2000-07-11 10:56	47.96	16.50	22	4.5	5
2013-09-20 02:06	47.93	16.41	11	4.3	5-6
2013-10-02 17:17	47.93	16.41	12	4.2	5-6

In autumn 2013, another earthquake series was recorded in this area. In less than a month the Zentralanstalt für Meteorologie and Geodynamik (ZAMG) located almost 30 earthquakes with two main shocks with a local magnitude of 4.2. Localization was aided by a temporary deployment of three local stations (VB01, VB02 and VB03).

To monitor ongoing seismic activity one of the seismic stations (VB01) was left in Ebreichsdorf castle. With the assistance of this local additional station, and stations deployed for different projects by the University of Vienna more than 100 earthquakes were detected and located by the ZAMG in the two following years. Locations of all earthquakes since the deployment of VB01 are jointly plotted as blue circles in Figure 2.1.

2.2. Surrounding seismic networks and available stations

Although the first seismometers were already installed in Austria around 1900, the current broadband network was only deployed starting from 1990. The earthquakes listed in Table 2.1 were selected from the earthquake catalogue for Lower Austria released by Hammerl and Lenhardt (2013). In

this catalogue, earthquakes were reconstructed using historical records, macroseismic data and seismic recordings, depending on data availability. After 2000, multiple projects investigated the area around the Vienna Basin by deploying seismic stations.

Most important for this study was the ALPAACT project (Brückl et al., 2014) by the Technical University of Vienna. Since the beginning of 2015 the AlpArrayAustria network (Fuchs et al., 2015) has been set up by the University of Vienna in the context of the international AlpArray project (Kissling et al., 2014). Also a double-profile of stations was deployed along longitude 13.5°E from summer 2014 to summer 2015 in the context of the EASI project (Plomerova et al., 2015). Yet, those stations were not used in this thesis, as they were deployed after the two earthquake series investigated. An overview of stations is given in Figure 2.2 in the left panel.

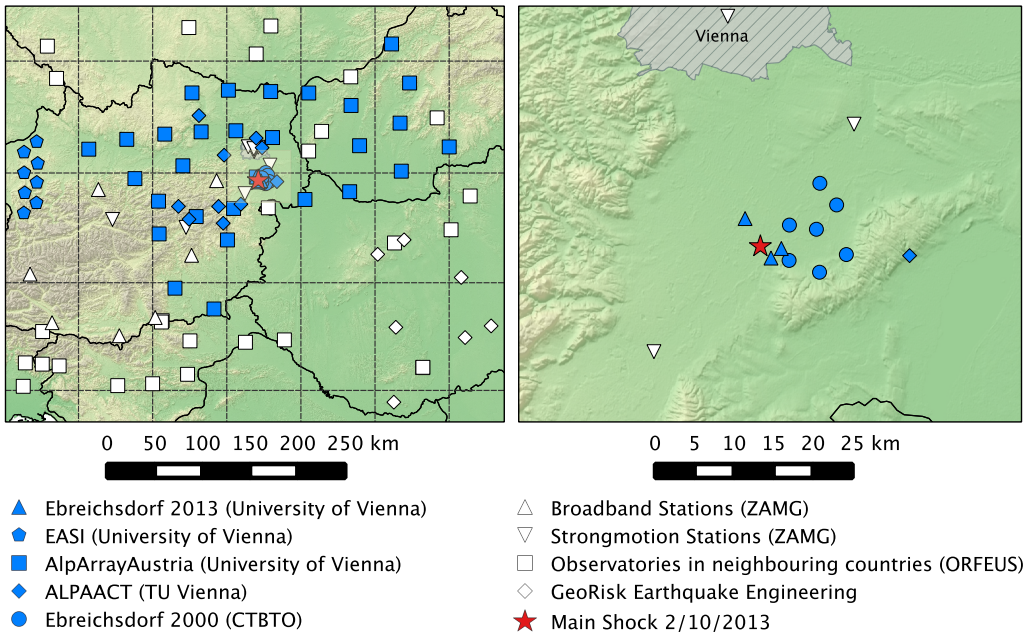

Figure 2.2.: Seismic stations in and around Eastern Austria used in this thesis (ALPAACT, Ebreichsdorf 2000 and 2013) and from deployments starting afterwards (EASI in 2014 and AlpArrray in 2015). Permanent stations are marked in white, temporary ones in blue colour.

However, most important for this thesis was the deployment of two temporary networks: 7 stations for 3 days after the main shocks of 2000 by the

CTBTO and another 3 stations by the DMG (department of meteorology and geophysics of university of Vienna) for almost 2 months after the main shocks of 2013 surrounding the preliminary epicentre. The recorded data from the deployment of 2013 was used in Chapter 3 and Chapter 4. Additionally, the records from 2000 entered into Chapter 4. Locations of these stations together with the main shocks of 2013 are shown in the right panel of Figure 2.2..

Furthermore, additional stations can be used in this area, e.g. the stations from GeoRisk Earthquake Engineering, which are used to monitor seismicity around a nuclear power plant in Hungary. A few other projects collected passive seismic data in this area after 2000: the ALPASS (Wilde-Piórko et al., 2008) or the CBP (Dando et al., 2011). As no data was used from these stations, they are not shown in any of the figures.

2.3. Location methods and stations used

2.3.1. Earthquake catalogue and ZAMG-bulletin

As mentioned previously in section2.1, locations in the earthquake catalogue of Lower Austria were estimated using macroseismic data points, if no seismic records were available. Later locations, using the ZAMG seismic network and surrounding international observatories are calculated using the LOCSAT (Nagy, 1996) algorithm with a 1D velocity model. Since 2009 seismic stations from the ALPAACT project were used. Also, the station VB01 that was deployed after the 2013 series, enters into the standard location procedure, when available. From summer 2014 to 2015 it was also possible to use data from the Austrian part of the EASI project - a profile from North to South through the Alps (see Plomerova et al., 2015). In spring of 2015 the deployment of the Austrian part of the AlpArray project (Fuchs et al., 2015) started, which also forwards the seismic records to the ZAMG.

Due to the higher number of stations at regional distances a much higher number of earthquakes were detected and located in the last years:

- 1000 - 12/2009: 103 earthquakes in 2000 years,

- 01/2010 - 09/2013: 25 earthquakes in 2.75 years,
- 10/2013 - 09/2015: 114 earthquakes in 2 years,

which shows the importance of local stations for earthquake detection.

2.3.2. Additional locations and methods used

The aftershocks of 2000 were relocated jointly with a local velocity model inversion, for details, see Anonymous (2002). To improve location accuracy in the Vienna Basin, another study was done by Hausmann et al. (2010) using Hypo71 (Lee and Lahr, 1975) and NonLinLoc (Lomax et al., 2000). An overview of all relocations using the ALPAACT seismic stations until 2012 is given in Brückl et al. (2012).

Location of the 2013 earthquake series is discussed in detail in Chapter 3 and 4.

2.4. Additional data products

Because of their larger intensities and more extensive records, additional data products were created for the earthquakes in 1938, 2000, 2010 and 2013. The following subsections show a collection of this data.

2.4.1. Isoseismal maps

For three earthquakes, assigned to Ebreichsdorf, isoseists were published. All isoseists are collected in Figure 2.3. The bottom right panel shows all three together at an intensity of 5.

The strongest earthquake was analysed by Mifka and Trapp (1941) - using the original Mercalli-Siebergscale. Meurers et al. (2004) investigated the earthquakes in 2000. Isoseists were computed for the EMS-98 (Grünthal, 1998), a scale based on the Mercalli-Sieberg-Scale. For 2013 the ZAMG published isoseists for the first main shock also for the EMS-98.

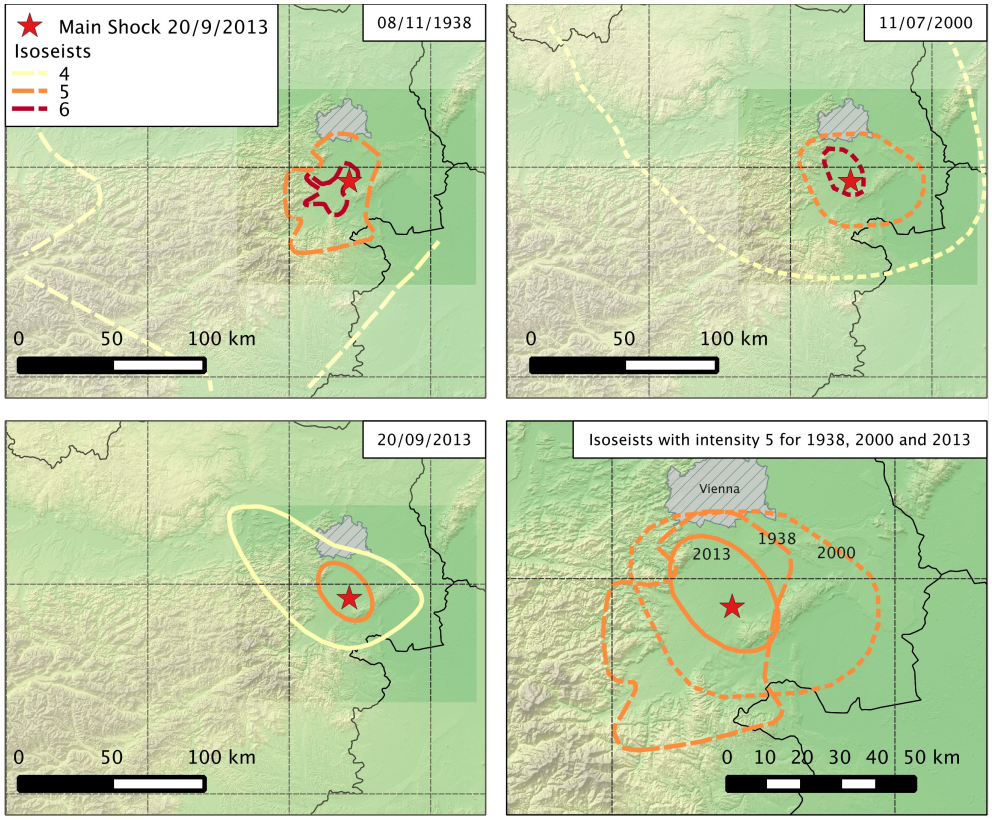

Figure 2.3.: Isoseists available for earthquakes close to Ebreichsdorf: 1938 by Mifka and Trapp (1941) (top left), 2000 by Meurers et al. (2004) (top right), 2013 by ZAMG (bottom left), all intensity 5 isoseists (bottom right).

Although, there is a difference in intensity by one, the areas for an intensity of 5 have a similar size for the earthquakes in 1938 and 2000. The earthquake in 2013 had a much smaller intensity 5 area.

A feature visible in all isoseists, is the much stronger propagation to the Northwest, which is also confirmed (e.g. by Hammerl and Lenhardt, 2013) using macroseismic data points from all earthquakes in the catalogue for Lower Austria. More similarly shaped isoseismal maps for the area are available, e.g. for 1963 from GBA (1980).

2.4.2. Focal mechanisms

Another common data product for earthquakes with sufficiently high magnitude and/or dense seismic networks are focal mechanisms. For the

Table 2.2.: Nodal planes and sources of focal mechanisms in the vicinity of Ebreichsdorf.

Origin Time	Reference	Nodal Plane 1 strike/dip/rake	Nodal Plane 2 strike/dip/rake
11/07/2000 02:00	SED (2006)	232/88 /3	142/87/178
	Meurers et al. (2004)	74/72/-8	166/83/-162
11/07/2000 10:00	SED (2006)	47/82/-12	139/78/-171
18/12/2010 06:19	Weginger and Brückl (2014)	55/71/37	311/55/157
20/09/2013 02:00	Hausmann et al. (2014)	62/73/31	323/60/161
	Weginger and Brückl (2014)	245/88/32	154/58/177
02/10/2013 17:00	Hausmann et al. (2014)	63/79/5	332/85/166
	GEVN (2013)	55/80/0	325/90/170

area around Ebreichsdorf eight focal mechanisms for five earthquakes from five different sources were published. All of them are plotted as beach balls in Figure 2.4 and the nodal planes are listed in Table 2.2.

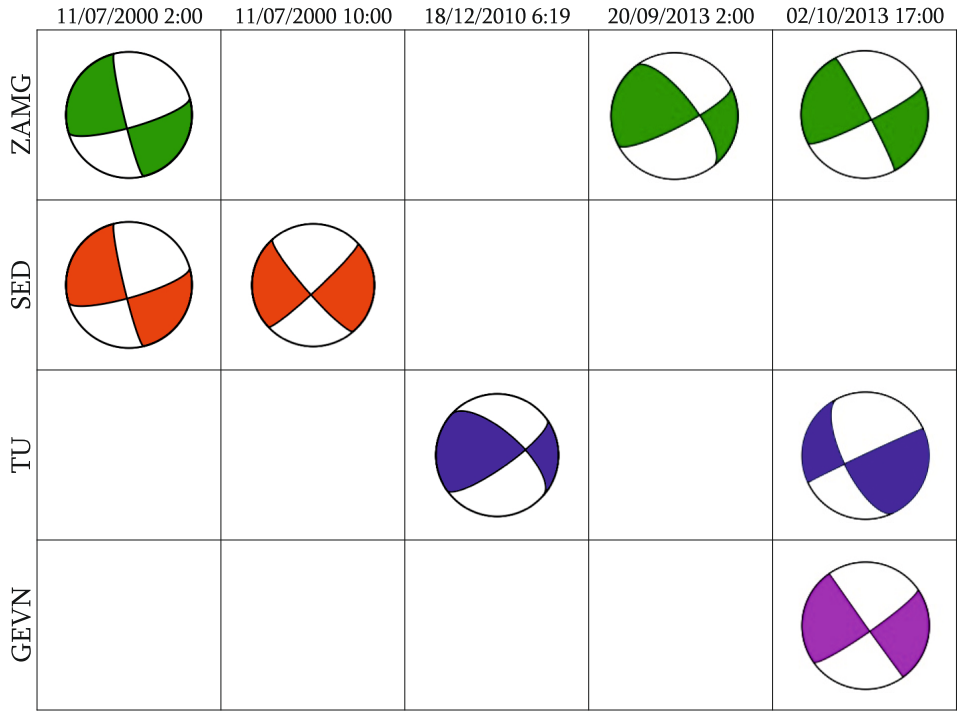

Figure 2.4.: Beachballs of available focal mechanisms in the vicinity of Ebreichsdorf (for a complete list of references see Table 2.2.

All of the available focal solutions in Table 2.2 strike in North-East direction and dip steeply around 80°, which matches well with the tectonic setting

with a sinistral strike-slip assumed for this area (e.g. Royden, 1985). The focal mechanism for December 18, 2010 is mentioned for completeness of the available focal mechanisms, and not used in this thesis. The magnitude of 3.6 was low for focal mechanism estimation and creation was only possible because data provided by the ALPAACT station and a new waveform stacking method (see Weginger and Brückl, 2014, for details).

3. The 2013 Earthquake Series in the Southern Vienna Basin: location

This chapter has been published as:

M.-T. Apoloner, G. Bokelmann, I. Bianchi, E. Brueckl, H. Hausmann, S. Mertl, and R. Meurers, 2014, The 2013 Earthquake Series in the Southern Vienna Basin: location, Advances in Geosciences, 36, 77-80.

3.1. Abstract

Eastern Austria is a region of low to moderate seismicity, and hence the seismological network coverage is relatively sparse. Nevertheless accurate earthquake location is very important, as the area is one of the most densely populated and most developed areas in Austria.

In 2013 a series of earthquakes with magnitudes up to 4.2 was recorded in the Southern Vienna Basin. With portable broadband, semi-permanent, and permanent installed seismic sensors from different institutions it was possible to record the main- and aftershocks with an unusual multitude of close-by seismic stations.

In this study we combine records from all available stations up to 240 km distance in one dataset. First, we stabilize the location with three stations deployed in the epicentral area. The higher network density moves the location of smaller magnitude events closer to the main shocks, with respect to preliminary locations achieved by permanent and semi-permanent networks. Then we locate with NonLinLoc using consistent

picks, a 3D velocity model and apply station corrections. This second approach results in stable epicentres, for limited and even changing station availability.

This dataset can then be inspected more closely for the presence of regional phases, which then can be used for more accurate localizations and especially depth estimation. Further research will address directivity effects and the asymmetry in earthquake intensity observed throughout the area, using double differences and cross-correlations.

3.2. Introduction

The study area is situated at the transition of the Eastern Alps to the Pannonian Basin and the Western Carpathians. The Vienna Basin is, due to the vicinity to Vienna, one of the most densely populated and developed areas in the region.

Instrumentally recorded seismicity in the area is moderate, with a maximum registered magnitude of around 5. The Vienna Basin Fault System occasionally shows earthquakes with magnitudes larger than 4 for example in 1938 close to Ebreichsdorf one event with a magnitude of 5.0. Historical records (e.g. Gutdeutsch et al., 1987) and paleoseismicity (e.g. Hintersberger et al., 2010) indicate that even stronger earthquakes occur, more infrequently.

The Austrian seismological network is built of very high quality stations. However, due to large inter-station distances the allocation of an events to a fault is not always definite. Earthquake location and depth estimation accuracy can be increased with different approaches: Additional seismic stations, particularly close to the epicentre, are the easiest way of improvement. As most location techniques are strongly dependent on the velocity model, the use of a regionally adapted model has a significant impact. The location technique itself has a big influence as well, in particular as seismic data and the velocity model enter in different ways.

In this article, we show an earthquake series south of Vienna in fall 2013 and which steps can be taken to improve and stabilize location. We deployed additional stations and collected all available data up to 240 km

distance to form a comprehensive dataset. We use two different location techniques with two distinct velocity models.

This article illustrates the change in location and tries to allocate the earthquakes to known faults.

3.3. Dataset

3.3.1. Seismicity

In fall 2013 an earthquake series was recorded in the Southern Vienna Basin close to Ebreichsdorf. Two main shocks with a local magnitude of 4.2 as well as about 30 aftershocks with magnitudes below 3.0 were observed. Although in 2000 a similar earthquake swarm was registered, with an epicentral distance to the closest permanent station of 20 km, hypocentral parameter estimation can be only constrained within limits. This time the events were recorded by a multitude of networks as shown in Figure 3.1 and listed in Table 3.1

3.3.2. Velocity models

We used two velocity models for this investigation. The global IASP91 (Kennett, 1991) 1D velocity model, which is used for event location in the ZAMG bulletin. The 3D P- and S-velocity models by Behm et al. (2007b) and Behm et al. (2007a), which are available for eastern Austria, where also used.

3.3.3. Seismic stations

The Zentralanstalt für Meteorologie und Geodynamik (ZAMG) operates a seismic network of permanent broadband and strong motion stations in Austria. As part of the ALPAACT Project (Mertl and Brückl, 2010), by the Technical University of Vienna (TU) 10 temporary seismic stations record seismic data in and around the Vienna Basin. Also, seismic records of the

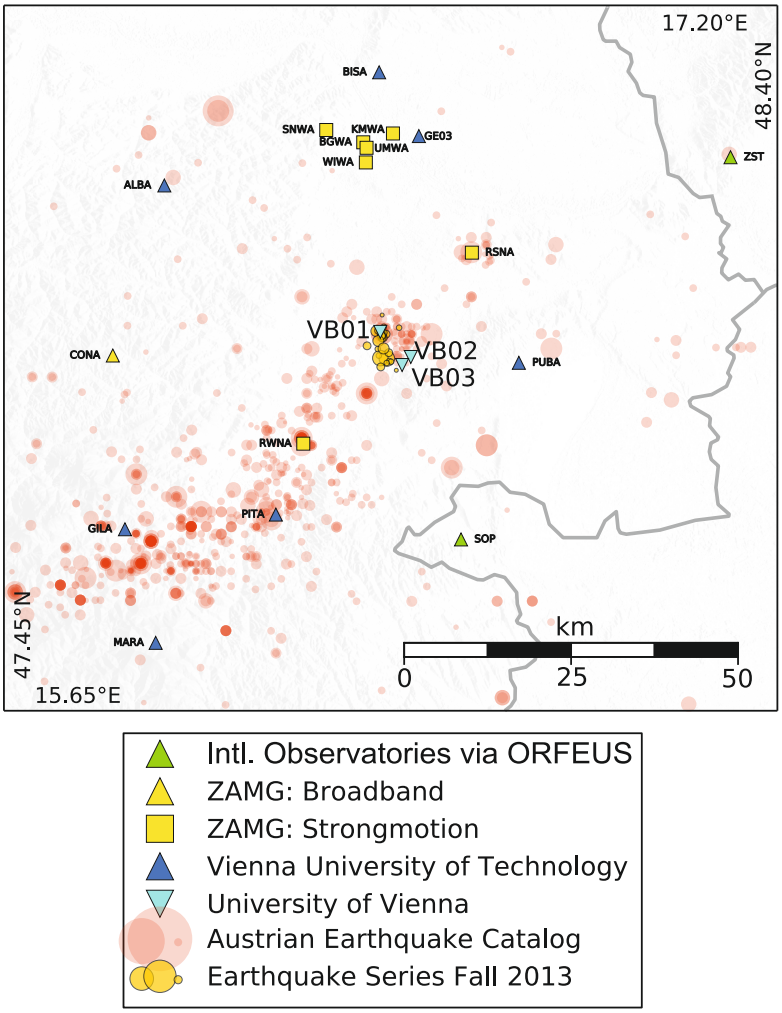

Figure 3.1.: Local station networks and earthquake distribution.

national networks surrounding Austria have been obtained via ORFEUS web service. Supplementary data from the nuclear power plant monitoring stations in Hungary was made available by GeoRisk Earthquake Engineering. After the second main shock, the University of Vienna deployed three seismic broadband stations (VB01, VB02 and VB03) as close as possible to the epicentres of the magnitude 4.2 events, as given in the ZAMG bulletin. We assembled all available data from the stations in above-mentioned networks to a comprehensive dataset for this study. We used stations up to 240 km distance, as the 3D model has limited coverage.

3.4. Hypocenter location

3.4.1. Routine processing with 3 local stations

The locations given in the bulletin are calculated using the LOCSAT (Nagy, 1996) algorithm with the 1D velocity model. P- and S-arrivals of the Austrian station network and international stations close to the border are automatically picked and manually reviewed. Besides, the stations PUBA, MARA, SITA and GUWA of the ALPAACT network are included in routine analysis. Six aftershocks were also recorded with the close-by deployed stations VB01, VB02 and VB03. P- and S-Picks from those stations were added to the routine processing.The locations with the local stations are marked with * in Table 3.1.

The mean inter-event distance of the newly located earthquakes decreases from 2.0 km to 0.9 km with inclusion of the VB-stations. The use of these stations also moves the smaller aftershocks closer to the main events.

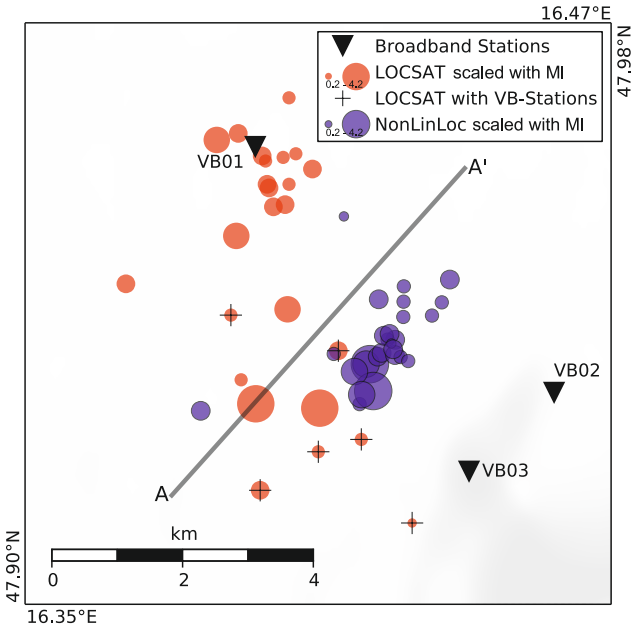

Figure 3.2.: Comparison of epicentral locations calculated with different approaches. Profile A parallel to fault direction by Peresson and Decker (1997).

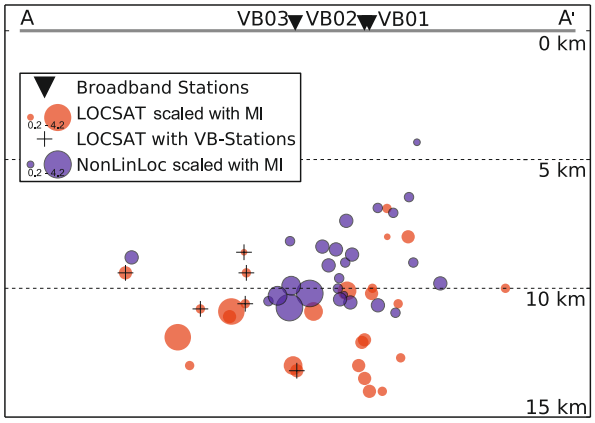

Figure 3.3.: Earthquake depth distribution along profile A (see Figure 3.2 for details).

3.4.2. Advanced processing routine with comprehensive consistent dataset

We picked all to us available station data to compile a consistent arrival dataset. With the program NonLinLoc (Lomax et al., 2000) it was possible to use the 3D velocity model. However, it does not map small-scale inhomogeneities like the underground beneath a station. This leads to shifts in event location, depending on station availability.

This influence was reduced by calculating station corrections in the first location run and applying them in the final run. The improvement in location can be deduced from the mean inter-event distance, which is reduced from 1.8 km to 1.1 km after applying station corrections. Especially smaller events with less picks move closer to the rest of the swarm. Events with magnitudes bigger than 2.0 do change their location only negligibly. Hence, it was possible to get stable epicentres even for sparse station configurations. According to Geller (1976) the source radius of the two 4.2 earthquakes was estimated at less than 200 m, based on their Mb of 3.6, which was taken from the ZAMG Bulletin.

The final epicentre locations are mostly on an area of 1 x 2 km as shown in Figure 3.2. The mean hypocentral depth is around 9 km, which is typical in this region as described, e.g. in Lenhardt et al. (2007). This means that the hypocenters are beneath the principal displacement zone of the flower structure which is assumed for this area (Beidinger and Decker, 2011).

Furthermore, the epicentres show a south-west to north-east pattern which maps them to the Vienna Basin Fault System. Final locations are listed in Table 3.1.

3.5. Conclusions

In this study we used a multitude of data available for post-processing. As expected, a higher network density around the epicentre improves the stability of earthquake locations, even if a global 1D velocity model is used. With NonLinLoc, 3D velocity model and station corrections it is possible to get stable epicentres even for changing and sparse station configurations.

Although the events can be associated with a nearby fault, no space-time pattern of the main shocks and their aftershocks can be seen with the methods applied and the data used. Therefore, we will investigate this earthquake swarm further using cross-correlation between events.

With this dataset it might be possible to identify additional regional phases like sP, PmP or sPmP. Those could then be used in further research to improve estimation of hypocentral parameters for other events, where less data is available.

Table 3.1.: Hypocentral parameters with LOCSAT and NonLinLoc, events located with LOCSAT using VB01, VB02 and VB03 are marked with * at the beginning of the line.

		LOCSAT			NonLinLoc		
Origin Time	ML	Lon	Lat	Depth	Lon	Lat	Depth
4.9.13 11:00	1.9	16.4088	47.9599	8.0	16.4369	47.9447	9.8
20.9.13 2:06	4.2	16.4103	47.9270	10.9	16.4206	47.9331	10.2
20.9.13 2:42	1.7	16.4032	47.9550	14.0	16.4257	47.9364	10.6
20.9.13 2:44	1.0	16.4028	47.9615	6.9	16.4274	47.9395	6.9
20.9.13 3:17	1.3	16.4040	47.9578	14.0	16.4242	47.9364	9.0
20.9.13 23:24	1.2	16.4054	47.9620	10.6	16.4353	47.9416	9.0
24.9.13 13:53	2.7	16.3892	47.9639	10.1	16.4198	47.9331	9.3
25.9.13 10:08	1.7	16.3936	47.9648	12.1	16.4222	47.9341	8.4
28.9.13 17:19	0.6	16.3942	47.9309	13.0	16.4185	47.9276	10.5
1.10.13 23:54	1.4	16.3992	47.9610	10.0	16.4275	47.9438	6.5
2.10.13 4:09	2.0	16.3985	47.9617	10.2	16.4230	47.9346	9.1
2.10.13 5:12	1.3	16.4040	47.9697	12.7	16.4275	47.9417	7.1
2.10.13 5:26	2.1	16.4008	47.9547	13.0	16.4257	47.9343	8.5
2.10.13 5:33	1.8	16.3999	47.9573	12.0	16.4234	47.9370	7.4
2.10.13 17:17	4.2	16.3972	47.9276	11.9	16.4212	47.9294	10.8
2.10.13 19:38	1.6	16.3995	47.9578	13.5	16.4246	47.9372	8.7
2.10.13 19:42	2.8	16.3932	47.9507	10.9	16.4174	47.9320	9.9
3.10.13 0:11	0.2	16.4008	47.9856	8.0	16.4152	47.9534	4.3
3.10.13 0:18	1.9	16.3706	47.9441	11.1	16.3859	47.9266	8.8
3.10.13 0:21	-.-	16.3590	47.9386	10.0	16.3964	47.9815	9.0
5.10.13 1:27	1.0	16.3921	47.9398	9.4	16.4333	47.9397	10.9
7.10.13 18:22	1.5	16.3981	47.9157	9.4	16.4224	47.9420	10.7
7.10.13 19:47	0.3	16.4292	47.9112	8.6	16.4249	47.9359	10.2
13.10.13 23:26	0.5	16.4188	47.9227	10.6	16.4269	47.9340	10.0
14.10.13 2:34	1.9	16.4141	47.9349	13.2	16.4253	47.9351	10.4
16.10.13 2:19	1.4	16.4100	47.9210	10.8	16.4284	47.9335	9.6
23.10.13 19:34	2.6	16.4037	47.9406	13.0	16.4189	47.9289	10.3
15.11.13 16:31	0.9	16.4348	47.9685	10.0	16.4132	47.9345	8.2

4. The Ebreichsdorf 2013 earthquake series: Relative location

This chapter is currently in press at the Austrian Journal of Earth Science as:

M.-T. Apoloner , J.-B. Tary and G. Bokelmann, Ebreichsdorf 2013 Earthquake Series: Relative Location

4.1. Abstract

We study recent moderate-size earthquakes in the southern Vienna Basin, focusing on the 2013 series of two earthquakes with local magnitudes of 4.2 and their aftershocks. Furthermore, we compare them to a similar series of earthquakes from 2000. Due to the superior dataset, we can jointly relocate all earthquakes from 2013 datasets. To reduce the influence of unmodeled velocity inhomogeneities, we use the "double-difference-times" implemented in the HypoDD software. Additionally, we use velocity models with different degrees of complexity (1-D to 3-D). We also test the stability of the results with different sets of initial locations.

After relocation the main shocks are located only 40 m apart; the collocation is confirmed by the high inter-event coherence. Moreover, the aftershocks show a clear pattern with larger earthquakes having deeper hypocentres and location in the South West and shallower, smaller earthquakes in the North East. We also locate the two main shocks from 2000

relative to the main shocks from 2013 using S-P-times. The main shocks from 2000 are located 4 km to the North East of the 2013 main shocks.

This suggests that the earlier notion of "event clustering" in the Southern Vienna basin needs to be reconsidered, since at least some of the earthquakes, here the aftershocks, seem to occur between the clusters that have been proposed previously. Still the question why earthquake collocation within short time intervals occurs, remains open.

4.2. German abstract

In dieser Studie untersuchen wir die Erdbebenserie von 2013 bei Ebreichsdorf im südlichen Wiener Becken. Hier wurden zwei Beben mit einer lokalen Magnitude von 4.2, sowie ca. 30 Nachbeben aufgezeichnet. Im ersten Schritt relokalisieren wir die Serie relativ zueinander, denn im Unterschied zu früheren Erdbebenserien ist der 2013er Datensatz wesentlich umfangreicher. Im Anschluss vergleichen wir die relokalisierten Erdbeben mit einem (ähnlichen) Bebenpaar des Jahres 2000. Um den Einfluss von unmodellierten Geschwindigkeitsänderungen zu reduzieren, verwenden wir den den HypoDD Algorithmus, welcher auf der Verwendung von Doppel-Differenz-Zeiten basiert. Zusätzlich verwenden wir unterschiedlich komplexe Geschwindigkeitsmodelle (1-D, 2-D und 3-D). Weiters testen wir die Stabilität der Ergebnisse mit unterschiedlichen Startlokalisierungen der Erdbeben.

Nach der Relokalisierung befinden sich die beiden Hauptbeben von 2013 nur 40 m voneinander entfernt. Diese Kollokation wird von der hohen Kohärenz zwischen den Wellenformen der beiden Hauptbeben bestätigt. Die Nachbeben zeigen ein klares Muster, wobei die stärkeren Ereignisse in größeren Tiefen auftreten, und weiter im Südwesten, als die kleineren Erdbeben. Zusätzlich lokalisieren wir die beiden Hauptbeben von 2000 - relativ zu den Hauptbeben von 2013 unter der Verwendung von S-P-Zeiten. Hier zeigt sich, das die beiden Bebenserien ca. 4 km voneinander stattfanden. Sie zeigen jedoch auch eine hohe Ähnlichkeit untereinander, wenn auch geringer als die Beben von 2013.

Dies lässt darauf schließen, dass die frühere Vorstellung des "event clustering" im südlichen Wiener Becken überdacht werden sollte. Offenbar treten auch Beben zwischen den Clustern auf. Weiterhin bleibt es eine offene Frage, warum Erdbeben innerhalb kurzer Zeiträume kollokiert auftreten können.

4.3. Introduction

Due to ongoing convergence between the European Plate from the north and the Adriatic plate from the south, crustal blocks extrude laterally to the east into the Pannonian Basin (e.g. Gutdeutsch and Aric, 1987). At larger scale, two sinistral strike-slip fault systems show this process: the Salzach-Enns-Mariazell-Puchberg fault (SEMP) and the seismically active Mur-Mürz-Fault (MMF). The Vienna Basin lies in the north-eastern extension of the MMF, in the transition of the Eastern Alps to the Western Carpathians. This pull-apart basin started forming in the Middle Miocene (e.g. Decker et al., 2005; Royden, 1985) is now filled with several kilometres of sediments. The MMF links up with the Vienna-Basin-Fault-System (VBFS), which consists of seismically active sinistral strike-slip faults and non-active normal faults. Beneath up to 5 km of slow velocity Miocene fill and medium-velocity sedimentary rocks of Northern Calcareous Alps and Greywacke Units (Wessely, 1983) the Bohemian Massif forms the basement of the Vienna Basin. An overview of the main tectonic units, faults and seismicity is given in Figure 4.1.

The Vienna Basin is not only one of the most densely populated areas in Austria; it is also one of its seismically active regions. Particularly the southern part of the basin is susceptible to earthquakes with a maximum instrumentally recorded local magnitude (Ml) of 5.2 (see Fig. 4.1; ZAMG, 2014). We will subsequently abbreviate it as AEC. Earthquakes in the Vienna Basin appear to cluster approximately every 15 to 20 km along the main fault of the VBFS. Most of the destructive earthquakes occur on that fault. Moment tensor and fault plane solutions usually show strike-slip earthquakes (Decker et al., 2005), with southwest-northeast oriented nodal planes that are subparallel to the direction of the faulting.

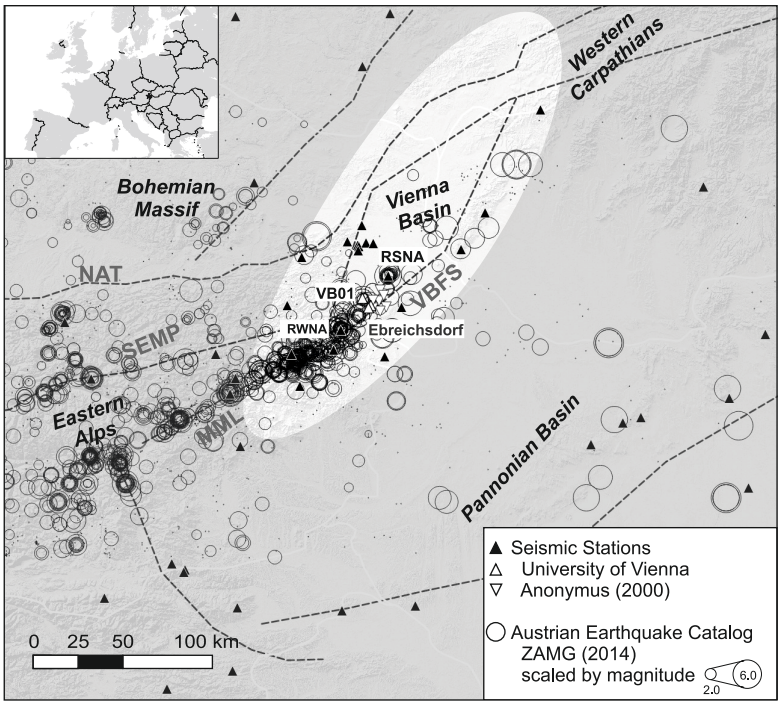

Figure 4.1.: Seismotectonic overview of the Vienna Basin: main tectonic units and generalized faults from GBA (2010). Earthquakes from the Austrian Earthquake Catalog scaled by Magnitude (ZAMG, 2014). Triangles indicate the positions of seismic stations used in this study.

Our study focuses on the area around Ebreichsdorf, 30 km south of Vienna shown in Figure 4.2: The first earthquake listed in the AEC for the vicinity of Ebreichsdorf occurred in 1899, with a magnitude above 3 and intensity above 5. In the 20^{th} century, with the start of instrumental seismic records only 12 earthquakes were observed within a radius of 7.5 km. Therefore, the earthquake from 1938 is the most notable with an estimated magnitude of 5.0 and intensity of 7.0.

In 2000 two earthquakes with a Ml of 4.8 and 4.5 (intensity 6.0 and 5.0) took place in the region of Ebreichsdorf within less than 10 hours. Most of the aftershocks could be recorded with temporary seismometer deployments by the Comprehensive Test Ban Treaty Organisation (CTBTO) (Anonymous, 2002). Locations of these aftershocks are shown in Figure 4.5 for comparison. With additional data from semi-permanent stations deployed by the Technical University of Vienna due to e.g. the ALPAACT project (Brückl et al., 2014), more than 20 earthquakes were recorded

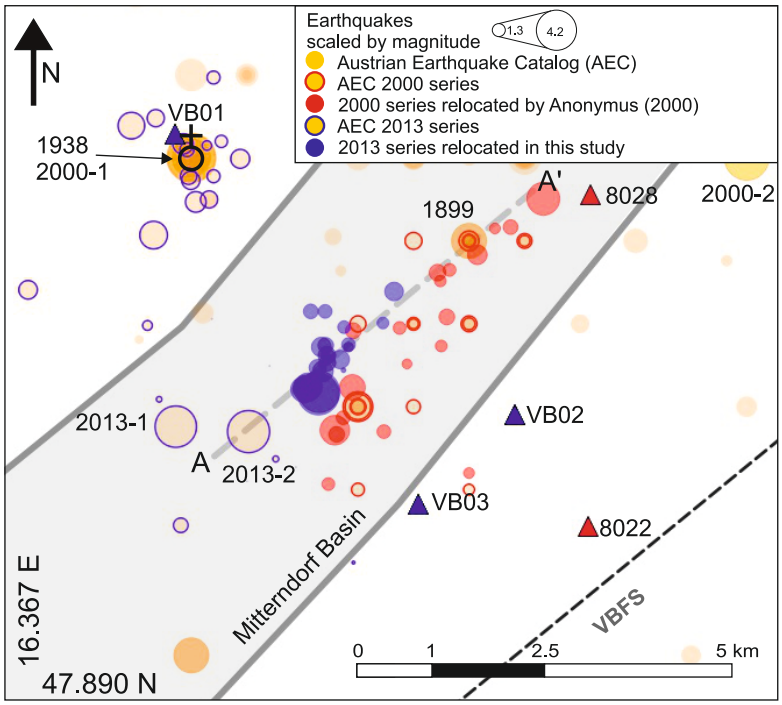

Figure 4.2.: Seismotectonic overview of the area around the VBFS close the Ebreichsdorf. Micone faults (Hinsch and Decker, 2010) as solid grey lines. Earthquakes from the Austrian Earthquake Catalogue scaled by Magnitude (ZAMG, 2014), events mentioned in the text are labelled with year of occurrence. Triangles indicate the positions of seismic stations used in this study. Profile A – A' parallel to VBFS is used in Figure 4.4.

between 2001 and 2012 in the vicinity of Ebreichsdorf.

In autumn 2013 an earthquake series was recorded in the South west of Ebreichsdorf. In a period of less than a month the Zentralanstalt für Meteorologie and Geodynamik (ZAMG) recorded two earthquakes with a Ml of 4.2 and almost 30 aftershocks. In this paper we discuss the recordings from 2013, and the constraints on (precise) earthquake locations that they provide.

4.4. Ebreichsdorf 2013 series

The earthquake that occurred on September 20^{th} 2013 at 02:06 UTC had a Ml of 4.25, and it was located close to Ebreichsdorf by the ZAMG. Over the

Table 4.1.: Location of temporary seismic stations deployed on 03/10/2013 around Ebreichsdorf for recording of aftershocks.

Station	Longitude	Latitude	Altitude	Location
VB01	16.3971° E	47.9629° N	200 m	Ebreichsdorf Schloss
VB02	16.4583° E	47.9291° N	241 m	Leithaprodersdorf Friedhof
VB03	16.4409° E	47.9183° N	236 m	Wimpassing Stall Szdenk

following days 8 smaller aftershocks were detected. After a few events in the night of October 2^{nd}, the second main shock with a Ml of 4.18 occurred at 17:17 UTC. 17 aftershocks followed in October. Until April, eight more earthquakes took place, all with a local magnitude smaller than 1.5. All of those events are listed in Table 4.4.

Numerous stations in various seismic networks recorded data from the events in autumn 2013: The ZAMG operates seismic broadband stations spread all over Austria, where continuous data is available online. Furthermore, strong-motion sensors are triggered for large magnitude events. Also, national institutes in the neighbouring countries operate seismic stations. Most of their data are collected by ORFEUS (Observatories and Research Facilities for European Seismology) and are available online. GeoRisk Engineering supplied this study with additional data from seismic stations in the Pannonian Basin.

Seismic data from the project ALPAACT with its focus on eastern Austria is of particular importance for this study, as they recorded all earthquakes in the 2013 series.

Following the second main shock, seismologists from the University of Vienna deployed 3 temporary seismic stations (VB01-03) close to Ebreichsdorf on October 3^{rd}. All three stations were equipped with 60-second 3-component broadband sensors and set to 100 Hz continuous recording. Table 4.1 lists the station locations. Station VB02 and VB03 were dismantled on December 5^{th}, and station VB01 was equipped with GSM for real-time data transmission to the datacentre of the Department of Meteorology and Geophysics (DMG) at the University of Vienna and to the ZAMG.

4.4.1. Additional data

Meurers et al. (2004) published isoseismals for the first main shock of 2000. The ZAMG offers an earthquake testimony map for the event from September 20^{th} 2013 online. Those maps show the same asymmetric intensity anomaly (e.g. Hammerl and Lenhardt, 2013) often observed in the area: the earthquakes were felt twice as far to the north-west than the south-east.

Due to the more numerous instrumental recordings for higher magnitude earthquakes it was possible to calculate focal mechanisms for events with a Ml above 4. Focal mechanisms for the two main shocks in 2000 by the Schweizer Erdbebendienst (SED) as well as for 2013 by the ZAMG are shown in Figure 4.3.

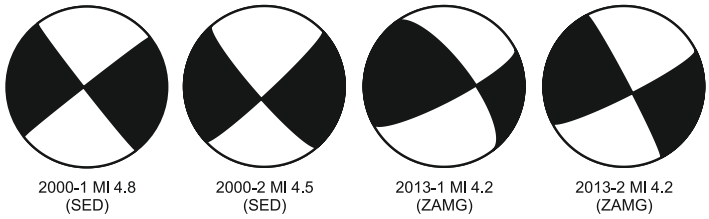

Figure 4.3.: Focal mechanisms from left to right: main shocks in 2000 around Ebreichsdorf from SED (2006) and for the two main shocks in 2013 from Hausmann et al. (2014).

Supplementary we estimate the fault area for the main shocks of 2013 using their local magnitude (4.2), corner frequencies (1-6 Hz), and scaling relationships (Geller, 1976; Madariaga, 1976; Stein and Wysession, 2009). The main shocks have a fault length of 500 m and a width of 250 m.

4.5. Event location and relocation

Primary locations for the earthquakes were taken from the AEC provided by ZAMG (2014) Standard processing uses only absolute arrival times and a 1-D velocity model, which is a considerable disadvantage in a subsurface with complex 3-D structure, such as the Eastern Alps. Advanced methods like NonLinLoc by Lomax et al. (2000) can handle 3-D velocity models,

but are strongly dependent on model accuracy. Apoloner et al. (2014) used NonLinLoc together with a 3-D P and S velocity model for obtaining accurate locations using all available seismic stations in a 240 km radius of Ebreichsdorf, which corresponds to the extent of the used 3-D models. Small scale homogeneities not modelled where included in the processing by using station corrections obtained in the location process.

4.5.1. HypoDD

For this study we use the software HypoDD, which is described in detail in Waldhauser and Ellsworth (2000). Double-difference relocation with HypoDD is based on the assumption that arrival times from events located close to each other will be perturbed similarly by the unknown subsurface structure. Events close to each other, with similar source mechanism and stress drop, produce similar signals at a seismic station. The distance to which this similarity persists is given by the $\lambda/4$-criterion (Geller and Müller, 1980), thus depending on the dominant frequency of the signal.

HypoDD uses "differential travel-times", which are calculated with Equation 4.1, to relocate pairs of events relative to each other. Calculation of double-difference dr for station k and events i and j:

$$dr_k^{ij} = (t_k^i - t_k^j)^{obs} - (t_k^i - t_k^j)^{cal} \tag{4.1}$$

To do so arrival time differences can be determined either by the difference of "picked" arrival times or by waveform correlation.

If the velocity model diverges from the real underground structure, residuals between calculated and observed travel-times increase. Calculating the difference between two wave arrivals of the same phase at one station removes this effect mostly, as is shown in Figure 4.4 (a). By minimizing the residuals between observed and calculated travel times (double-difference) for pairs of events, HypoDD adjusts the difference vector (Δx, Δy, Δz, Δt) between those events. The algorithm iteratively does this for all event pairs at each station. For datasets containing less than 100 events singular value decomposition solves the equation system and calculates error

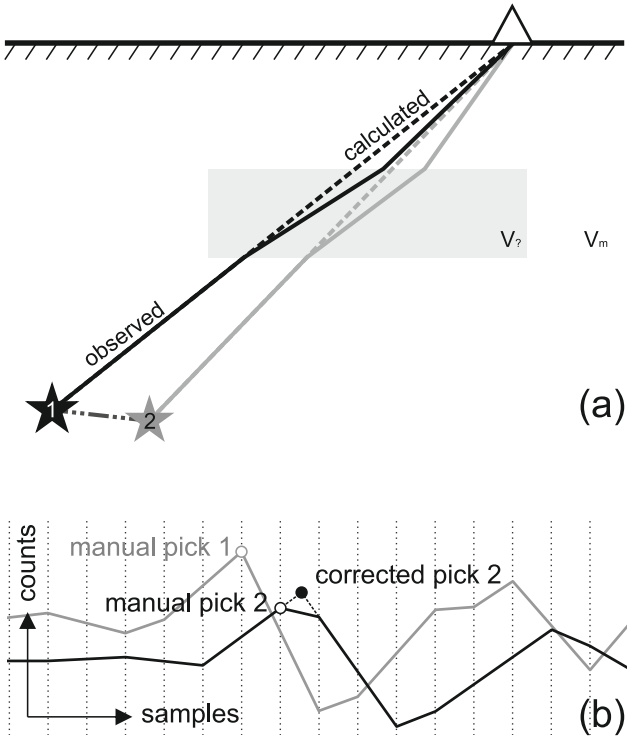

Figure 4.4.: (a) The principle of double-difference calculation: Two earthquakes (star 1 and 2) with close-by location produce similar arrivals at a station (triangle), as they are affected nearly equally by small-scale velocity inhomogeneities. Using double-differences between the observed and calculated arrival times for the events reduces the effect of unmodeled velocity changes. (b) Seismograms (P-phases) of two events at station VRAC, showing a sub-sample shift that can be resolved using cross-correlation.

estimates. The system only solves, if events are well linked through observations of multiple events at the same station. For this reason data has to preselected.

The differential travel-times mentioned above can be calculated from catalogue data. Time differences are calculated for one station and multiple events. In this case seismograms can be very similar. However, arrival time picks in catalogues are made for each event separately, irrespective of their similarity. If seismic waveforms are available it is possible to dramatically improve time difference accuracies (e.g. Schaff et al., 2004)with cross-correlation. Here, the relative arrival times between multiple events can be determined with sub-sample precision as shown in Figure 4.4 (b) and discussed in detail in Deichmann and Garcia-Fernandez (1992) and

Schaff et al. (2004). Furthermore,Waldhauser and Ellsworth (2000) mention that location accuracy can be improved 5 times using cross-correlation compared to using only catalogue data.

4.5.2. Parameters and settings

Depending on observation type (cross-correlation or catalogue), accuracy and distance, the effect of different types of observations on the results needs to be adjusted. For this reason an elaborate weighting scheme is part of HypoDD algorithm. We adapted the values as follows, to fit our dataset: The first set of 5 iterations removes double-differences from the catalogue data with high residual times, e. g. if Pn is picked instead of the Pg arrival. Travel time differences based on S waves enter the relocation with a smaller weight than P-waves. The second set of 5 iterations weights the cross-correlation and remaining catalogue double-differences similarly and simultaneously. Only double-differences from inter-event distances of less than 2 km are used and are re-weighted depending on distance. We derive the weights directly from picking accuracy for each pick individually.

To use HypoDD, we first calculate double-differences from the available picks. Furthermore, the data needs to be pre-selected to assure solvability with HypoDD. We calculate double-difference times for earthquakes with a maximum separation distance of 2 km and a minimum of 4 links in between them. From 738 picks we approximately compute 3400 phase-pairs. We cross-correlate the phase picks in a 2.0 – 7.0 Hz range, which corresponds to the dominant frequency in the observed earthquakes. P-phases were picked on the vertical components, for S-phase picking we use all 3 components. We obtain more than 500 difference times with a cross-correlation higher than 0.7.

In this study we use 3 different velocity models to evaluate their influence on location. The first is a 1-D model, taking only the top layer of IASP91, a widely-used velocity model for the earth. The second model is a layered 2-D model by Hausmann et al. (2010) composed of four layers above the crust-mantle boundary "Moho", the top layer being a 5 km thick slow velocity layer. With the last version of HypoDD 2.1b it is possible to use a

Table 4.2.: Location with different velocity models (initial locations are from Apoloner et al. (2014); see text.

Velocity model	1-D	2-D	3-D
Events located	17	21	20
Mean depth	5.9 km	9.3 km	9.3 km
Horizontal error	180 m	170 m	150 m
Vertical error	960 m	360 m	250 m
RMS cross-correlation	0.15 sec	0.17 sec	0.18 sec
RMS catalogue	0.14 sec	0.14 sec	0.15 sec
Mean number of difference-times per event used	191	250	305

3-D velocity model. We based our 3-D model on the P-velocity model of Behm et al. (2007a) and the S-velocity model of Behm et al. (2007b).

To check the dependence on initial location/s, we test HypoDD with different sets. In the first run we use the locations calculated with NonLinLoc and station corrections. HypoDD also offers the possibility to use the centre of the earthquake cluster as starting position. As it can be strongly influenced by outliers, we use the location of the Ml 4.2 main shock on the September 20^{th} 2013 as initial location for all events. In addition, we also compare the locations with those in the ZAMG-Bulletin.

4.6. Results

Using the 1-D velocity model destabilizes the result, as the algorithm removes one third of the observations due to large misfit and moves the entire earthquake series 10 km to the south-west. The 2-D and 3-D velocity models influence neither the location nor the mean depth of the earthquakes significantly. Apart from this the main influence is in the change in location errors, which is shown in Table 4.2. E. g. mean location errors for depth reduce from 960 m (1-D) to 360 m (2-D) to 250 m (3-D). Although, the RMS residual is almost the same for all models, the mean number of phase-pairs used is much higher for the 3-D model, indicating a better fit of observations to the model.

Initial locations are another important aspect, as they control the difference-times used as input for the relocation process. Also, the difference-vectors

Table 4.3.: Initial locations used for relative location calculation with HypoDD.

Initial locations	Initial depth mean	Result depth mean	Standard deviation	Distance between main shocks
Apoloner et al. (2014)	9.1 km	9.3 km	0.7	40 m
Apoloner et al. (2014), all 20/09/2013 4.2	10.6 km	10.7 km	0.7	75 m
ZAMG bulletin	11.7 km	11.7 km	1.9	70 m

between events are not recalculated at each iteration step, but only adjusted. Table 4.3 shows that the final locations are strongly constrained by the initial location used. For example, the initial mean depth controls the final location depth.

Final locations are given in Table 4.4 and plotted in Figure 4.5 (left) in top view and Figure 4.5 (right) in a cross section along the fault strike. Independently from initial locations, both Ml 4.2 earthquakes locate less than 100 m apart. Moreover, the depths of the earthquakes are between 7.5 and 10.5 km, which means that they are situated on the fault beneath the negative flower structure (Hinsch et al., 2005). In addition, the depth of events changes with magnitude, with smaller events being rather shallower than bigger events. However, even with relative locations, no distinct event pattern in time is apparent in Table 4.4.

In the next step we compare the 2013 series to the 2000 series. Each of the two earthquake series is composed of two main shocks with Ml >4 and an aftershock sequence of around 30 events. Figure 4.5 shows that the aftershocks of 2000 are close to the 2013 sequence, but shallower. However, the main shocks from 2000 given in the AEC are more than 7 km away from the events in 2013 and located 7 km apart from each other. The focal mechanisms computed by SED and ZAMG are very similar though (Fig. 3). To distinguish wether the location difference for the main shocks is due to the network geometry or different location, we compare the waveforms from stations, which recorded both pairs of main shocks.

The two closest strong motion stations RSNA (Schwadorf) and RWNA (Wr. Neustadt) of the ZAMG network are triggered and therefore recorded only the main shocks. Figure 4.6 shows the waveforms aligned at the P phase for all four events in chronological order. As a reference we use the pick of the S phase of the first main shock in 2013, due to its higher location

Table 4.4.: Relocated earthquakes from 2013 around Ebreichsdorf. Ml taken from ZAMG Bulletin. CC and Cat DT give the number of cross-correlation and catalogue double-difference times used for location.

Date D.M.Y	Time (UTC)	Ml	Lat. [°]	Lon. [°]	Depth [km]	CC DT	Cat DT	Ex [m]	Ey [m]	Ez [m]
04.09.13	11:00	1.9	47.9439	16.4365	9.4	15	176	158	178	456
20.09.13	02:06	4.2	47.9318	16.4230	10.5	55	293	97	100	202
20.09.13	02:42	1.7	47.9353	16.4245	9.6	41	283	82	87	223
20.09.13	03:17	1.3	47.9362	16.4246	9.7	42	255	78	101	218
20.09.13	23:24	1.2	47.9401	16.4345	9.0	23	228	98	120	313
24.09.13	13:53	2.7	47.9322	16.4207	9.8	68	339	72	77	166
25.09.13	10:08	1.7	47.9347	16.4227	9.1	39	209	82	99	210
01.10.13	23:54	1.4	47.9415	16.4241	7.5	5	33	237	290	868
02.10.13	04:09	2.0	47.9372	16.4234	9.2	47	376	70	82	177
02.10.13	05:12	1.3	47.9396	16.4275	8.0	10	89	164	235	565
02.10.13	05:26	2.1	47.9343	16.4237	8.9	51	299	74	85	193
02.10.13	05:33	1.8	47.9362	16.4244	8.4	23	156	102	121	278
02.10.13	17:17	4.2	47.9315	16.4229	10.5	46	275	99	105	211
02.10.13	19:38	1.6	47.9374	16.4242	8.9	50	273	75	85	196
02.10.13	19:42	2.8	47.9324	16.421	10.0	47	344	76	81	179
05.10.13	01:27	1.0	47.9372	16.4283	9.8	23	181	113	113	167
07.10.13	18:22	1.5	47.9415	16.4215	9.8	25	238	111	111	163
13.10.13	23:26	0.5	47.9344	16.4274	9.2	15	243	80	90	155
14.10.13	02:34	1.9	47.9357	16.4268	9.9	64	367	80	76	134
16.10.13	02:19	1.4	47.9375	16.4283	9.3	35	319	79	89	139
23.10.13	19:34	2.6	47.9321	16.4202	9.6	58	344	81	75	130

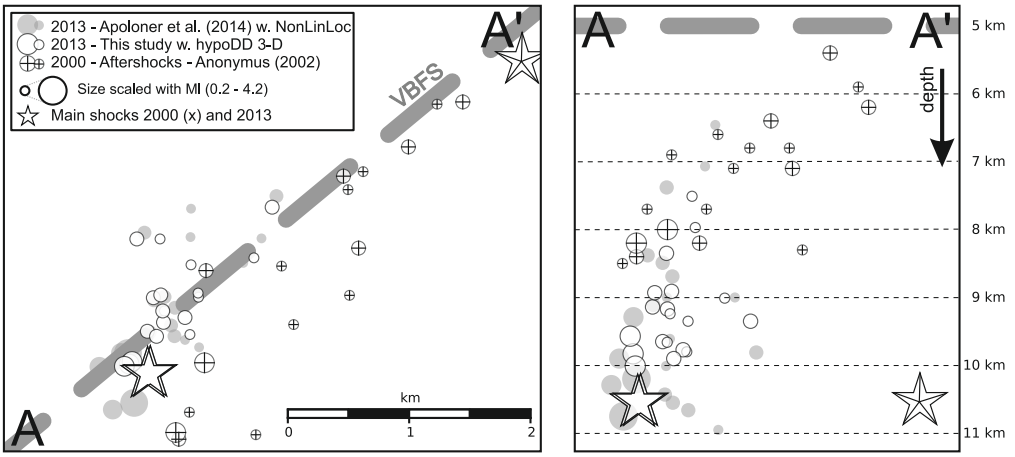

Figure 4.5.: (left) Map of earthquakes near Ebreichsdorf area from 2000 and 2013. Initial locations for 2013 (grey) by Apoloner et al. (2014) with NonLinLoc, relocations with HypoDD (blue). Red dots show aftershocks of the earthquakes in 2000 (Anonymous, 2002). The red star indicates the location of main shocks in 2000 relative to the two 2013 main shocks, determined with S-P-differences (right) .Vertical profile along the VBFS with events projected on a vertical fault plane.

accuracy. Since variations in S-P-time differences from event to event are associated with variations in distance with respect to the station, this allows investigating whether events are in the same place or not. The S-P-time difference between the 2000 and the 2013 events differs by about 0.6 seconds, which corresponds to a difference in distance of approximately 4 km. The events from 2013 have almost the same distance to the stations. However, to fit the data, the events from 2000 need to be around 4 km further away from station RWNA and 4 km closer to station RSNA. This suggests that the events from 2000 are located 4 km to the North East from the 2013 sequence. The type of constraint provided by the S-P times (distance), and the relative locations of the events are illustrated in Figure 4.7.

Collocation can be also determined by inspecting the inter-event coherence. The criterion of Geller and Müller (1980) states that waveforms can be similar up to an inter-event distance of $\lambda/4$, with wavelength λ. Figure 4.8 shows the inter-events coherence around the S wave arrival for the two main shocks in 2013 and 2000. We note for the 2013 events that coherence is very high at low frequencies, and it drops gradually with increasing

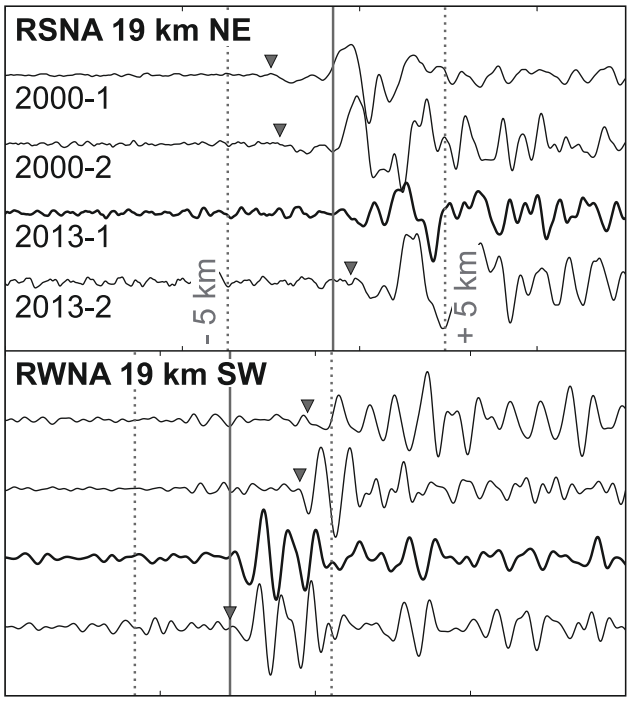

Figure 4.6.: S-arrivals of main shocks of 2000 (1^{st}: 2000-1, 2^{nd}: 2000-2) and 2013 (1^{st}: 2013-1, 2^{nd}: 2013-2) earthquake series aligned at the P-arrival. S-arrival on 2013-1 is marked by a continuous grey line (picked using all three components). Dashed lines show 5 km distance difference to the station, based on S-P-time difference with respect to 2013-1 suggested S pick. Main shocks from the 2000 series are 4 km closer to station RSNA (top) and 4 km further from RWNA (bottom).

coherence, as expected for nearby events. At a frequency of 8 Hz the mean coherence has dropped to a value near 0.7. This frequency of 8 Hz corresponds to a quarter-wavelength of around 100 m, assuming a shear-wave velocity of 3 km/sec. The Geller and Müller criterion suggests that this is the maximum distance between the events, which can be successfully correlated. The behaviour of the two events in the year 2000 is quite different, with a low-value of mean coherence at low frequencies. With increasing frequency the coherence rises to a very high value, and it drops subsequently. This curve shape is not consistent with waveform similarity depending on distance alone. Indeed, the character of the coherence is very different for the two stations. For one RWNA, the frequency dependence follows the expected decay with frequency, although with a surprisingly sharp decay, around 5 Hz. The other station, RSNA shows the unexpected

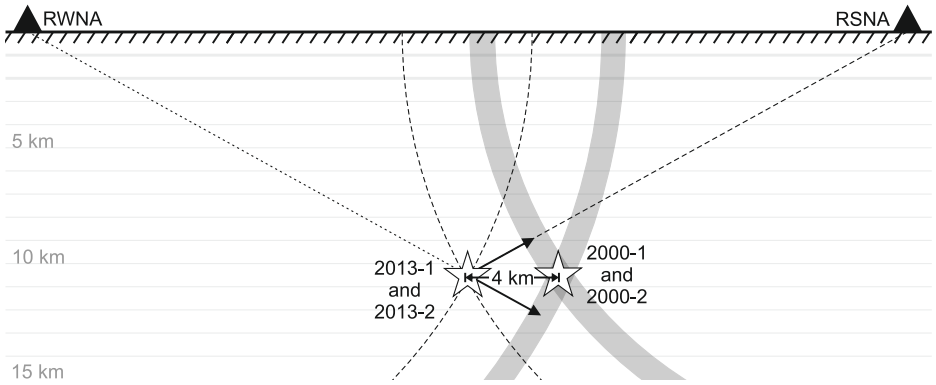

Figure 4.7.: Cross-section along the fault indicating the constraint on relative location, suggested in Figure 4.6.

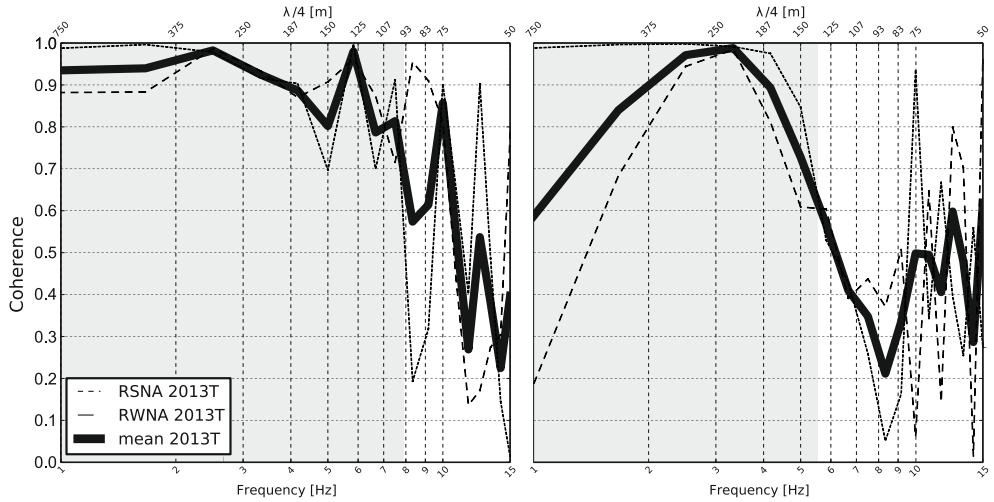

Figure 4.8.: Inter-event coherence for both pairs of main shocks on the transverse component, (left) for the 2013 series, and (right) for the 2000 series (see text). Top x-axes shows $\lambda/4$, as a criterium for inter-event distance, marked grey for coherences above 0.7.

behaviour of an increase with frequency. Why the characteristics are so different on the two stations, is not clear. However, the criterion should be used with caution in this circumstance. Applied as such, it implies that the maximum between the event, using the 5 Hz frequency is slightly larger, about 150 m. However, doubt remains whether the criterion may be applied for the 2000 series.

4.7. Discussion

Although, the 3-D velocity model used only approximates the rather heterogeneous underground structure in the area, it considerably enhances the number of phase observations usable for relocation, which in turn improves location accuracy. If no 3-D model is available, at least a locally adapted model like a 2-D crust model should be used for the Vienna Basin. If only one cluster of events is relocated, locations obtained with HypoDD are strongly dependent on the initial hypocentre location. Therefore, it is important to use high-quality initial locations like the ones calculated in the previous study. However, relative locations in the cluster are much less affected. Similar events, like the two main shocks, are always located close to each other, neither depending on velocity model used nor absolute position of the initial locations. The relative locations are at close range to those obtained using NonLinLoc. This results from the high quality of the NonLinLoc locations and also from the small number of events in the cluster. Due to the small number of links and to large inter-event distances, several events could not be relocated. After relocation, the earthquake series clusters on a smaller area and depth range, as can be seen in Figure 4.5. In particular the two main shocks are now less than 40 m apart. This study focuses only on one cluster of earthquakes which are located within a few kilometres. To extend this kind of study to the whole Vienna Basin, and therefore more clusters of earthquakes, either more accurate absolute locations or an improved velocity model of the Vienna Basin and its surroundings are needed.

A comparison with the 2000 series shows that the pairs of main shocks are 4 km apart and that both aftershock sequences have apparently occurred in between. Indeed, the (slightly) different S-P times indicate that the main shocks of 2000 are not collocated as closely as the main shocks in 2013. The bigger difference in source size is probably important. There may be further differences, e.g. in the source mechanism.. The notion of clustering of earthquakes along the Southern Vienna Basin fault segment appears to be less clear than thought before. The 2000 events, that were supposed to part of the "cluster" at Ebreichsdorf, are in reality about 4 km further to the North-east, and thus closer to a position between the villages of Unterwaltersdorf and Leithaprodersdorf. Furthermore, the new locations

of the main shocks from 2000 also indicate that the aftershock locations from Anonymous (2002) also need to be relocated to compare them to the data from 2013.

Coherence measurements at the two closest stations confirm also that the two 2013 events are collocated well within the length of the rupture, since coherence is very similar for both stations.The coherence constraint on collocation is weaker for the 2000 events, firstly by a faster decay of coherence with frequency, but more importantly by the unexpected increase of coherence with frequency. It shows that the 2000 events are less similar than the 2013 events, although its behaviour is not fully understood. Explanations may lie in the larger difference in magnitude, or by a different characteristic of the rupture. Changes in the wave propagation behaviour by the earlier event may play a role, and the radiation characteristics of the earthquakes. Station RWNA records higher frequencies than station RSNA for all four main shocks. This effect could be either caused by site effects or directivity of the rupture towards the South East. However, given to the relative large magnitude difference of the main shocks in 2000 and 2013 and similar subsurface conditions a directivity effects appears more likely.

For studies of seismicity in the area, it is important to have recordings, including the strong-motion stations available in real-time. If this had been the case in 2000, we could produce high-resolution relative locations now also for aftershocks in 2000, which were too weak to be recorded by the more distance regional network stations – and resolve the question of whether there is a significant migration between main shocks and aftershocks.

4.8. Conclusion

We have studied the spatial relation between the earthquakes that have occurred in the Ebreichsdorf area in 2013 and their aftershocks, and find that larger aftershocks have the tendency to occur at larger depth on the fault, and tend to migrate North-East. For the 2000 series, the spatial relation is less clear, since they have been recorded by different stations unfortunately – the national network for the main shocks, and the

temporary CTBTO network for the aftershocks. Continuous recordings at stations in the area would help to address such issues in the future.

There are interesting findings for rupture mechanisms resulting from this study: the two events in 2013 have occurred at the same place, apparently with overlapping rupture area, which is suggested by the relative location, but also by the high waveform correlation. We will address the question of stress transfer in a subsequent paper. This may help resolve the question of how rapidly repeated rupture is possible, even though the first event must have released (part of) the elastic strain already.

The relocated event from 2000 and 2013 show that the impression from the catalogue, that seismicity occurs only in separated clusters is misleading at least for the Ebreichsdorf area and originates from the incomplete seismic cycle used in the AEC (see Hinsch and Decker, 2010, for details). The 2000 earthquake series took place between the villages Unterwaltersdorf and Leithaprodersdorf.

This raises a very important question about the other parts of the fault that have not ruptured in historical times: will they release the mechanical stress aseismically by creep, or seismically and if the latter – with which magnitude? We do not know the answer to this question, but resolving it requires gaining more observations about the seismic and aseismic deformation in the Southern Vienna basin. This is a major question for understanding the regional seismic hazard, in particular for the city of Vienna.

4.9. Acknowledgements

We want to thank the team of the DMG for deploying the temporary stations around Ebreichsdorf. We thank all the persons in charge of the permanent networks in and around Austria, especially the ZAMG, the TU Vienna and GeoRisk Earthquake Engineering for making data fast and easy accessible

5. Earthquake interactions during the 2013 Ebreichsdorf aftershock sequence

This chapter is currently in press at the Austrian Journal of Earth Science as:

J.-B. Tary , M.-T. Apoloner and G. Bokelmann, Earthquake interactions during the 2013 Ebreichsdorf aftershock sequence

Thesis authors contribution:

M.-T. Apoloner participated in the definition of the objectives of the paper by calculating the double-difference earthquake relocations used in the study. She also helped with the determination of the main shock attributes that are necessary for Coulomb stress analysis (i.e., fault dimensions and slip) from focal mechanisms and corner frequencies. She contributed to the writing of the paper and the design of some of the figures. Finally, she helped correcting the paper after receiving the comments of the reviewers.

5.1. Abstract

The Vienna Basin Fault System (VBFS) is one of the most seismically active regions of Austria, delineating the southern part of the Vienna Basin. This sinistral, strike slip fault system, accommodates part of the deformation due to the northward push of the Adriatic microplate. In 2000 and 2013, two pairs of main shocks followed by a few tens of aftershocks occurred in the region of Ebreichsdorf, one of the clusters of seismicity along the

VBFS. The main shocks seem to be located closely in both cases, even though high-resolution double-difference locations are available only for the sequence in 2013.

Focusing on this sequence, we investigate the interactions between the two main shocks and their 18 aftershocks. The two main shocks are located almost at the same place, at a depth of 10.5 km, while the aftershocks constitute a shallower ellipsoid with its long axis parallel to the main trace of the VBFS. We use two Coulomb failure stress models to study possible static stress transfer between the main shocks and the aftershocks of this sequence, the apparent friction model and the isotropic poroelastic model. Both models yield Coulomb failure stress changes below 0.01 MPa at the aftershocks locations. Static stress transfer seems then unlikely to explain their occurrence, even though interactions between aftershocks could play a role in their triggering. Two other mechanisms are considered, namely pore pressure diffusion along an idealized fault plane, and aseismic creep.

A high hydraulic diffusivity of about $1 - 10 m^2/s$ would be however required to account for the spatial extent of the possible interactions($\sim 0.5 - 1 km$) and the inter-event times (hours to days). The shallower location of the aftershocks compared to both main shocks could also point to the migration of fluids toward the surface. The occurrence of collocated events of comparable sizes and focal mechanisms, also named seismic repeaters, is often attributed to the presence of aseismic creep. But without further observations it would be difficult to support or rule out this hypothesis. Either the presence of high pore pressure or aseismic slip has important implications for the present-day earthquake potential of the VBFS to produce large earthquakes.

5.2. German abstract

Das Wiener-Becken-Störungssystem (VBFS) ist eine der seismisch aktivsten Regionen Österreichs. Das VBFS ist eine sinistrale Blattverschiebung, welche den südlichen Teil des Wiener Beckens durchzieht. Damit ist es Teil eines größeren Systems von Verwerfungen, welches die Nordbewegung

der adriatischen Mikroplatte begleitet. Im Jahr 2000 und 2013 gab es jeweils zwei Erdbebenpaare an der VBFS, die von einer Serie an Nachbeben begleitet wurden. Die Hauptbeben ereigneten sich rund um Ebreichsdorf, einem Ort an dem schon mehrere Erdbebenserien aufgezeichnet wurden. Jedes der beiden Bebenpaare scheint praktisch am gleichen Ort stattgefunden zu haben, auch wenn hochauflösende "double-difference" Hypozentren nur für die Beben von 2013 zur Verfügung stehen. Diese Arbeit konzentriert sich daher auf die Serie von 2013.

Wir untersuchen die Wechselwirkungen zwischen den beiden Hauptbeben und ihrer 18 Nachbeben. Die beiden Hauptbeben fanden nahezu an der gleichen Stelle in einer Tiefe von 10.5 km statt, während die Nachbeben ein flaches Ellipsoid bilden, mit langer Achse parallel der Verwerfung. Wir verwenden zwei unterschiedliche Coulomb-Spannungsmodelle, um mögliche statische Spannungsübertragung zwischen den Hauptbeben und den Nachbeben zu untersuchen: das "apparent friction" Modell sowie ein isotropes poroelastisches Modell. Beide Modelle liefern Coulomb-Bruchspannungsänderungen unter 0,01 MPa an den Positionen der Nachbeben. Statische Spannungsübertragung scheint deswegen eine eher unwahrscheinliche Erklärung für das Nachbebenmuster zu sein, auch wenn Wechselwirkungen zwischen den Nachbeben eine Rolle bei ihrer Auslösung spielen könnten. Zwei weitere Mechanismen werden berücksichtigt: Porendruckdiffusion entlang einer idealisierten Verwerfungsfläche sowie aseismisches Kriechen.

Eine hohe hydraulische Diffusivität von etwa $1 - 10 m^2/s$ wäre jedoch im ersteren Fall erforderlich, um die räumliche Ausdehnung der möglichen Wechselwirkungen($\sim 0.5 - 1 km$) und den unterschiedlichen Intervallen (Stunden bis Tage) zu erklären. Die seichtere Lage hingegen der Nachbeben im Vergleich zu den beiden Hauptbeben steht im Einklang mit einer Migration von Fluiden in Richtung Oberfläche. Das Auftreten von Ereignissen vergleichbarer Größe und Herdmechanismus, welches als "seismic repeater" bezeichnet wird, wird oft auf das Vorhandensein von aseismischem Kriechen zurückgeführt. Ohne weitere Beobachtungen wäre es allerdings schwierig, diese Hypothese hier zu bestätigen oder auszuschließen. Die Anwesenheit von hohem Porendruck oder aseismischem Kriechen hätte wichtige Auswirkungen bzgl. des Auftretens größerer Erdbeben entlang des Störungssystems im Wiener Becken.

5.3. Introduction

The Vienna Basin is located at the intersection between the Eurasian plate in the North, the Pannonian Basin in the South, the Eastern Alps to the West, and the Western Carpathians to the East (e.g. Schmid et al., 2008). Considering the present-day kinematics, the Eurasian plate in this region is mainly constituted by the rigid Bohemian Massif which, together with the Adriatic microplate going northward, induce compressional stresses in the Alpine area (Grenerczy et al., 2005) . This leads to the eastward extrusion of part of both the Pannonian Basin and the Eastern Alps (Gutdeutsch et al., 1987; Ratschbacher et al., 1991; Grenerczy et al., 2000; Brückl et al., 2010).

The extrusion is largely accommodated on the northeastern part of the Eastern Alps by strike-slip faulting (Grenerczy et al., 2005), the fault system constituting the Vienna pull-apart Basin taking an active part in this process. The southern border of the Vienna Basin, the Vienna Basin Fault System (VBFS), is in the continuation of the Mur-Mürz-Linie (MML) fault, and then joins with the extension of the Steinberg fault to the northeast of the Vienna Basin (Decker et al., 2005). The basin is filled by about 3 to 8 km of Cenozoic sediments and underpinned by the rocks of the Bohemian Massif (Reinecker and Lenhardt, 1999; Decker et al., 2005).

GPS measurements show that the MML and VBFS, which the Ebreichsdorf area belongs to, accommodate approximately 0.5 mm of displacement per year (Umnig et al., 2015). These faults are among the most actives in Austria (Hausmann et al., 2010; Lenhardt et al., 2007), with known historical seismicity up to magnitude 6 (Lenhardt et al., 2007). The relatively linear fault trace of the MML gets more complicated as it enters the Vienna Basin pull-apart system. Specifically, the Ebreichsdorf area is located in a smaller-scale pull-apart basin called the Mitterndorf Basin involving both sinistral strike slip and normal faulting (Hinsch et al., 2005).

The seismicity along the VBFS seems to concentrate in clusters which are located approximately 20 km apart, and the Ebreichsdorf region is one of them (Apoloner et al., 2015). Recently, this region experienced four earthquakes with local magnitudes greater than 4: two earthquakes of local magnitudes 4.8 and 4.5 in July 2000 (Meurers et al., 2004), and

two earthquakes of local magnitudes 4.2 in September and October 2013 (Figs. 5.1, 5.2) (Apoloner et al., 2014). The focal mechanisms of these events, calculated by the ZAMG (Zentralanstalt für Meteorologie und Geodynamik), are consistent with local VBFS kinematics with mechanisms mainly sinistral strike slip and a quasi-vertical fault plane oriented WSW-ENE. Both pairs of main shocks generated about 20-30 aftershocks with local magnitudes between 0.5 and 3.4. Epicentres of these aftershocks form elongated ellipsoids close to the VBFS with long-axes parallel to the main fault trace (Apoloner et al., 2015).

In the case of the Ebreichsdorf sequence in 2013, high-precision double-difference locations show that the main shocks are collocated within the location uncertainties (Apoloner et al., 2015). Whether they share or not the same fault plane cannot be resolved due to the uncertainties in the locations and focal mechanisms. The occurrence of collocated pairs of main shocks of similar magnitudes is unexpected because the first main shock should have released the tectonic stresses that had build-up at its location. This raises the question of possible interactions between the earthquakes of this sequence, and if particular mechanisms such as high-pressured fluids or aseismic creep could be at play in this region. This in turn has some wider implications on the potential seismic hazard associated with the VBFS in Ebreichsdorf area.

After reviewing some observations from the Ebreichsdorf 2013 sequence, we will investigate possible earthquakes interactions using the Coulomb stress transfer model (e.g. King et al., 1994; Toda et al., 1998) using the apparent friction and isotropic poroelastic models (e.g. Harris, 1998; Cocco and Rice, 2002). We will then discuss observations and model results in terms of potential interpretations for the occurrence of these sequences in Ebreichsdorf area.

5.4. Ebreichsdorf sequence in 2013

The 1^{st} main shock of the Ebreichsdorf sequence in 2013 occurred on September 20, 2013. This event has a local magnitude of 4.2 and was widely felt throughout Eastern Austria, similarly to the 2000 earthquakes (Meurers et al., 2004). Its focal mechanism shows a sinistral strike-slip

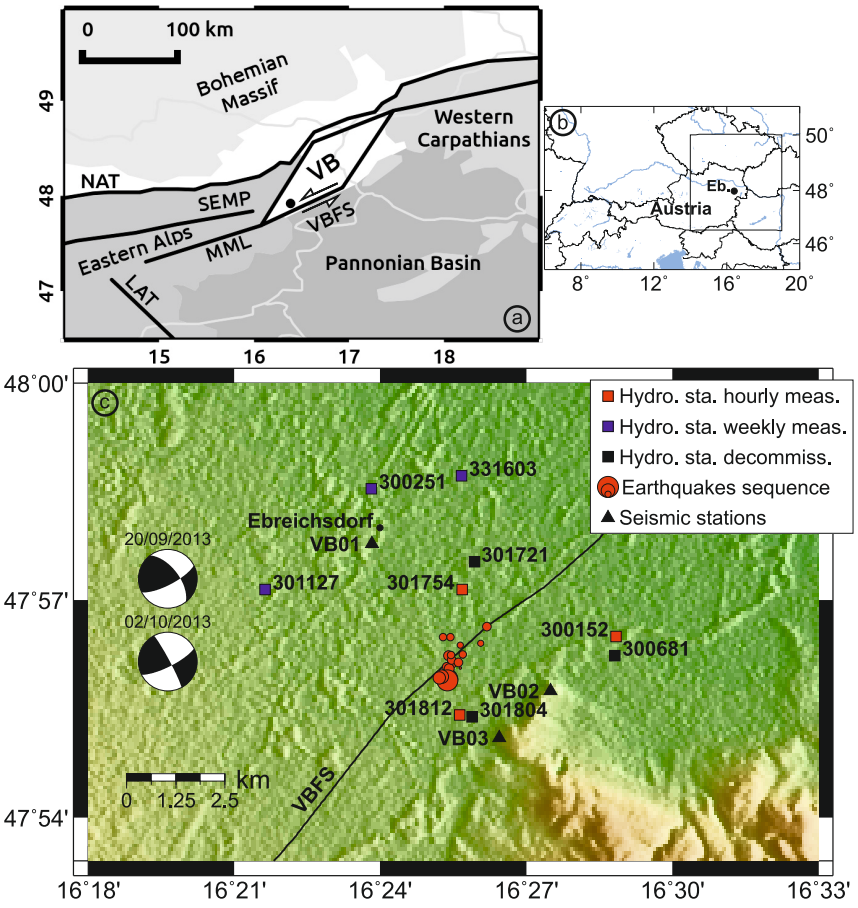

Figure 5.1.: (a) Schematic tectonic settings around the Vienna basin (VB) modified after Brückl et al. (2010), showing the main faults and tectonic units. Light gray lines indicate country borders, and the black dot the position of Ebreichsdorf area. The position of this map is shown by the inset (b). Abbreviations: NAT, North Alpine Thrust fault; SEMP, Salzachtal-Ennstal-Mariazell–Puchberg fault; MML, Mur-Mürz-Linie fault; LAT, Lavant fault; VBFS: Vienna Basin Fault System. (c) Zoom in the area of Ebreichsdorf, showing the aftershock sequence of 2013 (red dots with sizes proportional to their local magnitude), the three temporary seismic stations deployed close to the sequence to record the aftershock sequence after the second main shock (black triangles), and the location of hydrological stations used to investigate potential hydrological manifestations related to the earthquake sequence (squares, see Appendix 5.10). The focal mechanisms by Hausmann et al. (2010) of both main shocks are shown on the left, and the black line indicates the idealized trace of the VBFS.

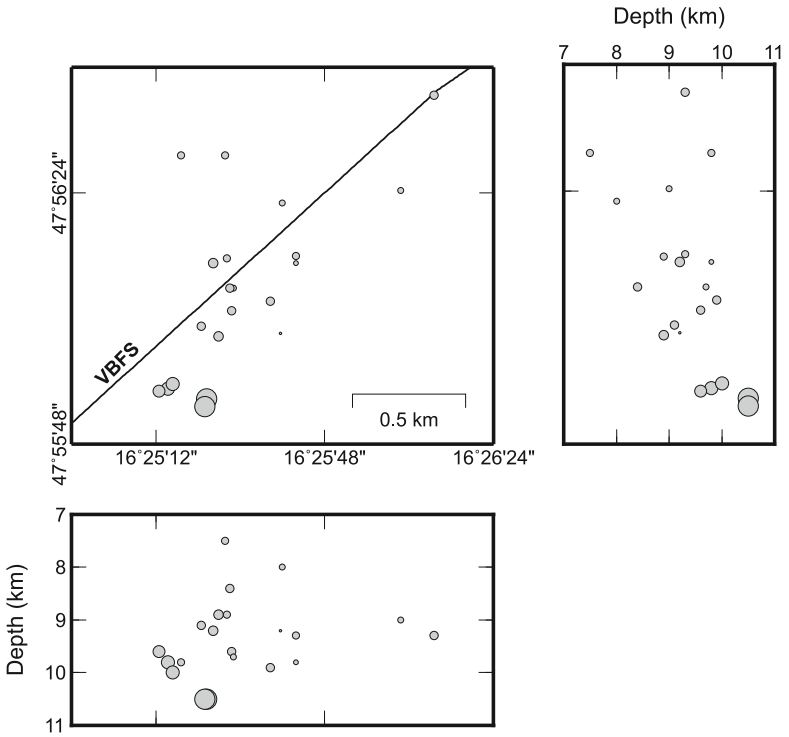

Figure 5.2.: Zoomed view of the 2013 Ebreichsdorf earthquakes sequence (grey dots with sizes proportional to their local magnitude). VBFS: Vienna Basin Fault System (black line).

fault oriented N63° and strongly dipping toward the SE (73°), which is consistent with the orientation of the VBFS in the area (Fig. 5.1). This event was followed by 3 events the same day, and by 10 in total before the 2nd main event.

The 2^{nd} main shock, which occurred on October 2^{nd}, 2013, has very similar local magnitude and focal mechanism compared to the 1^{st} main event (Fig. 5.1). This event was preceded by an acceleration of the seismicity rate with 4 events occurring earlier the same day. They could actually either correspond to aftershocks from the 1^{st}event or foreshocks to the 2nd, even though these events were located shallower and further to the northeast. The 2^{nd} event was then followed by 8 events with the last one occurring on September 23^{rd}, 2013. The complete aftershocks sequence consists of 18 events with local magnitudes between 1 and 3. These events seem to delineate a plane above the two main shocks which follows the presumed trace of the VBFS in this area (Figs. 5.1, 5.2).

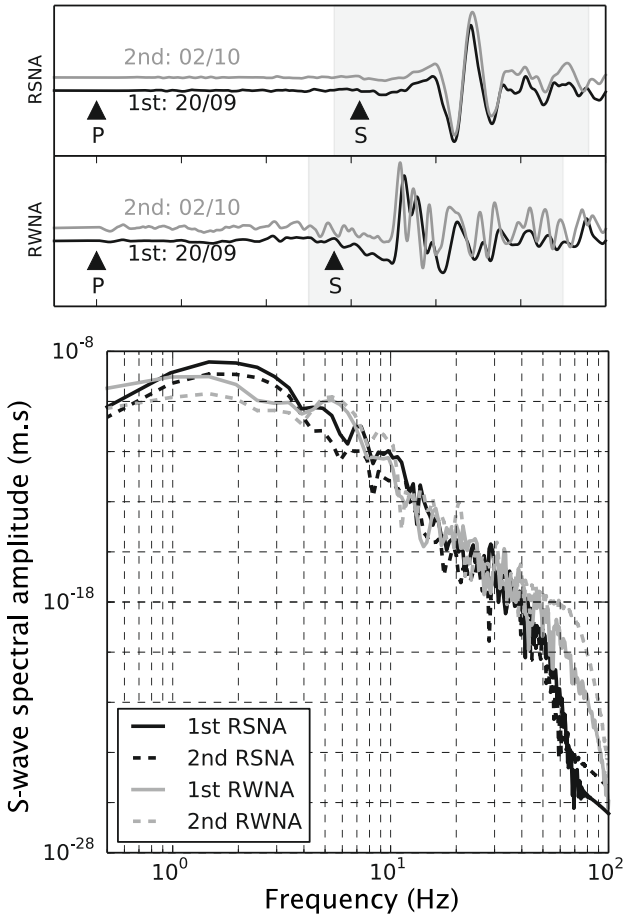

Figure 5.3.: Normalized seismic traces of the first and second main shock of the 2013 Ebreichsdorf sequence (top, instruments response removed), and displacement spectra corresponding to the part of the S-wave in these traces (bottom) indicated by the grey area, for two stations located approximately 20 km away from the two main shocks. RSNA is located 20 km to the NE, while RWNA is located 20 km to the SW. The seismic traces are aligned on the P-wave arrival times; P- and S-wave arrivals are indicated by black arrows. Note the high similarity in waveforms and frequency content of the two main events. At these stations, their corner frequencies are in the range 3-6 Hz.

Owing to the high waveforms similarity of the earthquakes of this sequence, Apoloner et al. (2015) relocated them using catalogue and cross-correlation data with the double-difference algorithm hypoDD (Waldhauser and Ellsworth, 2000). The velocity model used is a 3D velocity model for P-waves and S-waves of Eastern Austria (Behm et al., 2007a,b). In the following we use this relocated set of locations. Noticeably, the two main shocks are collocated within the location uncertainties (Fig. 5.2).

Their waveforms are indeed very similar (Fig. 5.3). The discrepancy in their spectra in Figure 5.3b is reversed whether we consider a station to the NE (RNSA) or SW (RWNA) of the events. This indicates that the difference in frequency between the two events most likely arises from directivity effects.

The reader is referred to Apoloner et al. (2014) and Apoloner et al. (2015) for more details on the location procedure, a complete list of the stations used to locate these events, as well as their exact timing and locations.

5.5. Coulomb stress interactions

Static stress changes calculated for large earthquakes seem to be correlated with the presence or absence of aftershocks (e.g. King et al., 1994; Toda et al., 1998). Areas exhibiting an increase in static stress are brought closer to failure and show higher aftershock activities, and the opposite for areas of static stress decrease (also called stress shadows). Static stress loading from previous earthquakes is also invoked to explain the triggering of nearby earthquakes, such as in the case of 20^{th} century sequence of large earthquakes along the North Anatolian fault in Turkey (Stein et al., 1997).

These calculations are based on the change in Coulomb failure stress on a predefined fault plane, incorporating the effective stress principle (e.g. Beeler et al., 2000; Jaeger et al., 2007), given by

$$\Delta\sigma_c = \Delta\tau_s - \mu(\Delta\sigma_n - \Delta p) \tag{5.1}$$

where $\Delta\sigma_c$ is the change in Coulomb failure stress, $\Delta\tau_s$ is the change in shear stress on the fault plane in the slip direction, μ is the friction coefficient, $\Delta\sigma_n$ is the change in fault-normal stress (positive for fault unclamping), and Δp is the change in pore pressure. Failure occurs on a given fault plane when $\Delta\sigma_c$ reaches a certain threshold which is unknown as in-situ background stresses on fault planes are generally also unknown. Strain, shear and normal stresses due to the earthquake are calculated using the dislocation model of Okada (1992).

Pore-pressure distribution prior to the earthquake will influence the change in Coulomb failure stress. Co-seismic stresses typically act on

timescales of seconds, generally much shorter than the timescale of pore-pressure diffusion in the medium (Cocco and Rice, 2002; Manga and Wang, 2007). In consequence, during co-seismic stresses variations, the medium is considered to be in "undrained" conditions which means that no fluid flow takes place (Rice and Cleary, 1976). In the case of an isotropic poroelastic material in undrained conditions, the pore-pressure variations Δp are related to the change in mean stress through the Skempton coefficient B as

$$\Delta p = B\frac{\Delta\sigma_{kk}}{3} \tag{5.2}$$

where $\Delta\sigma_{kk}$ is the sum of the changes in stress components corresponding to the trace of the stress tensor. Values for the Skempton coefficients range from 0.5 to 0.9 for consolidated rocks and up to 1 for unconsolidated materials (Cocco and Rice, 2002, and references therein). Using Eq.5.2, the Coulomb failure stress becomes

$$\Delta\sigma_c = \Delta\tau_s - \mu(\Delta\sigma_n - B\frac{\Delta\sigma_{kk}}{3}) \tag{5.3}$$

In the following, we refer to this equation as the isotropic model. Many authors assume that the mean stress can be replaced by the fault-normal stress (e.g. Stein et al., 1992; Harris et al., 1995; Toda et al., 1998), which would be appropriate for fault zones with strong fault-parallel anisotropy (Cocco and Rice, 2002), simplifying Equation 5.3 to

$$\Delta\sigma_c = \Delta\tau_s - \mu'\Delta\sigma_n \tag{5.4}$$

with the apparent friction coefficient $\mu' = \mu(1 - B)$.

These simple Coulomb failure stress models have some limitations in common. They consider a homogeneous medium with the fault zone having the same properties as the surrounding medium (Cocco and Rice, 2002). The static stress changes calculated are generally small, on the order of 0.1 MPa (Harris, 1998), compared to the stress drop of earthquakes ($\sim$ 1–10MPa Stein and Wysession, 2009). Interpretations based in these models are then mainly qualitative in terms of areas where failure is promoted or delayed. In addition, uncertainties in fault parameters typically coming from focal mechanisms (i.e. fault strike, dip and rake) and the complexity of slip patterns are not taken into account in most cases but could be essential (Kilb et al., 1997; Hardebeck et al., 1998). For the Coulomb stress modelling, we here consider undrained conditions where

the pore pressure diffusion is not taken into account, even though this might not be appropriate for the timescales of the Ebreichsdorf sequence (Jónsson et al., 2003).

5.6. Parameters and results

Calculations of Coulomb stress changes are made with the Coulomb 3.3 software (Lin and Stein, 2004; Toda et al., 2005) for both the apparent friction and isotropic models. The main parameters used are an apparent friction coefficient $\mu' = 0.35$, corresponding to a typical friction coefficient $\mu = 0.7$ (Byerlee, 1978) and a Skempton coefficient B of 0.5, a Young modulus of 75 GPa and a Poisson ratio of 0.25 (Stein and Wysession, 2009). Regional stresses correspond to a strike-slip system with the maximum and minimum compressive principal stresses being horizontal, and oriented N220 and N130, respectively (Bada et al., 2007).

The fault orientations of the first and second main event, which correspond to the source and receiver faults in the Coulomb failure stress calculations, are extracted from their focal mechanisms (Fig. 5.1). For the source and receiver faults, the strike/dip/rake sets are 62.5/73.3/31.2 and 63.3/76/5.3 degrees, respectively. Their geometries are estimated using their local magnitude (4.2), corner frequencies (1-6 Hz, Fig. 5.3) and scaling relationships (Geller, 1976; Madariaga, 1976; Stein and Wysession, 2009). Both faults have a length of 500 m and a width of 250 m, the second main event being approximately 40 m to the SE of the first main event. The source fault also has an average slip of 3.6 cm in the rake direction. The stress perturbations are calculated for the first main event, assuming receiver faults with the geometry of the second main event (Fig. 5.4). Calculations using receiver faults with the geometry of the first event gives similar results as both main events have similar local magnitudes and focal mechanisms.

Considering changes in shear and Coulomb stresses for the apparent friction model, the second main event is located within the stress shadow of the first event (Fig. 5.4a). It is however partially in the zone of normal stress increase (unclamping). The aftershocks are located above the two main shocks and, except for one, in areas of positive Coulomb failure stress changes mainly due to shear stress increase (Figs. 5.4, 5.5). However, for

most events these changes are very small, lower than 0.01 MPa (Fig. 5.5). In our configuration, the results using the isotropic model are relatively similar to those of the apparent friction model (Figs. 5.4, 5.5). The influence of the normal stress is more important in the isotropic model for most events, reducing the Coulomb failure stress changes.

Changes in Coulomb failure stress seem then insufficient to be the cause of the aftershocks, even though very small changes on the order of 0.01 MPa have sometimes been used to explain the triggering of aftershocks (e.g. King et al., 1994). One alternative hypothesis would be that the aftershocks triggered each other in a cascade-like fashion. We will discuss further potential mechanisms below.

5.7. Discussion

Static stress triggering of the aftershocks due to co-seismic static stress transfer from the first main event seems unlikely because of the small amplitude of Coulomb stress changes at the location of the aftershocks (Fig. 5.5). This is also unlikely for the second main event due to its occurrence in the stress shadow coming from the first main event. On the other hand, the first main event might have released only a part of the stress accumulated on this portion of the fault (Hinsch and Decker, 2003), leaving the possibility for this asperity to produce another event. This would be possible especially if dynamic stress effects have caused a reduction in fault strength (friction coefficient), for instance related to the weakening effects of earthquakes that can be observed seismologically (e.g. Baisch and Bokelmann, 2001). However, the recent geodetic measurements by Umnig et al. (2015) seem to indicate that the strain accumulated in the area is small in comparison with the cumulated co-seismic displacements. In addition, co-seismic slip and stress drop distributions on the rupture plane are not homogeneous, producing areas where stress is increased or decreased (Bouchon, 1997; Sammis et al., 1999). This complex pattern in Coulomb stress changes is not taken into account in our model which assumes a homogeneous slip on the fault plane.

The b-value is another interesting parameter corresponding to the slope of cumulative earthquake magnitude distributions expressed through

the Gutenberg-Richter power law (Gutenberg and Richter, 1944). This parameter seems correlated to the local differential stress state (Scholz, 2015) and could reveal potential highly stressed patches (Schorlemmer and Wiemer, 2005). This has implications for seismic hazard and the location of aftershocks, such as for those of the Ebreichsdorf sequence, as the seismicity would primarily be associated with these patches.

If the first main event caused the second one, then the response from the disturbance coming from the first main event would have been delayed by 12 days. This would imply some in-situ relaxation mechanism, potentially involving fluid diffusion in the surroundings of the first main event, as both events are located very close to each other. Co-seismic stress variations in the ground induce pore pressure re-adjustments on longer timescales (e.g. Nur and Booker, 1972; Roeloffs, 1998; Jónsson et al., 2003). For an isotropic poroelastic material, an order of magnitude of the timescale of pore pressure diffusion is given by $t \sim L^2/D$ (Manga and Wang, 2007), where L is the spatial scale of pore pressure diffusion and D is the hydraulic diffusivity.

During the Ebreichsdorf 2013 sequence, inter-event distances of few hundred meters to one kilometre and inter-event periods of hours to days would be compatible with an average hydraulic diffusivity of about 1-10 m2/s This would correspond to a highly permeable material (Roeloffs et al., 2003; Manga and Wang, 2007) and is few orders of magnitudes higher than values of hydraulic diffusivities found for fault gouges (10^{-2}–$10^{-7} m^2/s$ Wibberley, 2002; Doan et al., 2006).

Fluid overpressure at depth could also be the cause of this high diffusivity, due to the non-linear relationship between pore pressure and hydraulic diffusivity (Miller et al., 2004; Hummel and Müller, 2009). If pore pressure diffusion is the driving mechanisms of this sequence, it could explain the position of the aftershocks above the main shocks with the propagation of fluids toward the surface. The first part of the sequence, before the second main event, seems to migrate toward the surface, whereas the second part seems to envelope the area delimited by the events of the first part. However, no unambiguous correlation between hydrological measurements on the surface and the spatio-temporal distribution of this sequence has been found (see Appendix 5.10).

The near-collocation of two main events of similar magnitudes is essentially similar in character to seismic repeaters (e.g. Chen et al., 2013). Beside co-seismic stresses (Nadeau et al., 1995) and fluid overpressure (Daniel et al., 2011), a third alternative explanation is invoked with the presence of aseismic creep in the area surrounding these kind of events, re-loading the same asperity (Bouchon et al., 2011). Aseismic creep seems to take place also on portions of other continental strike-slip faults, such as the San Andreas fault (Gratier et al., 2011, and references therein) and the North Anatolian fault (Bouchon et al., 2011; Ḑakir et al., 2012). The actual presence of aseismic slip on the VBFS could be investigated using different kind of instrumentation, dense GPS network, InSAR and extensometers for surface deformation, and broad-band seismometers to better characterize the seismicity of this area. Comparison between long-term historical seismicity and the strain rate in the VBFS would also be helpful for detecting deficits in seismic strain in the area that could be accounted for by aseismic creep or forthcoming events (Hinsch and Decker, 2003). The presence or not of aseismic creep and over pressurized fluids in the VBFS has wider implications on potential seismic hazards in this region, i.e., on the timing of future ruptures and their spatial extension.

5.8. Conclusion

The Ebreichsdorf area is located along the VBFS, one of the most seismically active region of Austria. At this location, two sequences with similar characteristics occurred in 2000 and 2013: one main shock was followed by aftershocks, then by another main shock and further aftershocks. High-resolution locations are available for the sequence in 2013, showing that the two main shocks are collocated at depth within the uncertainties in locations, while the aftershocks are shallower and seem to follow the orientation of the VBFS in the area.

Using Coulomb failure stress modelling, we show that Coulomb stress transfer from the two main shocks seem insufficient to explain the triggering of the aftershocks. Both the apparent friction model and the isotropic model present co-seismic static stress changes of less than 0.01 MPa for most aftershocks. The sequence could then be driven by other mechanisms

such as dynamic effects reducing fault strength, high pore-pressure at depth, which could explain the spatio-temporal distribution of the events despite the necessity for a high hydraulic diffusivity, or aseismic creep, which is frequently invoked as a cause for seismic repeaters. The presence of some of these mechanisms along the VBFS would have important implications for the seismic hazard of this region; the VBFS having the potential of generating magnitude 6 earthquakes.

5.9. Acknowledgements

We thank the ZAMG, the Technical University of Vienna, ORFEUS and GeoRisk Earthquake Engineering for providing the seismic data and the focal mechanisms of the 2013 Ebreichsdorf sequence, the Hydrological Survey of Lower Austria for providing the time series of the hydrological stations around Ebreichsdorf, and M. Ristic and M. Dorninger for providing the precipitation data from the ZAMG. We thank Ewald Brückl and an anonymous reviewer for their useful comments which helped improve the original manuscript. The Generic Mapping Tools (GMT) software from Wessel et al. (2013) has been used to plot parts of Figs. 5.1 and 5.2 .

5.10. Appendix: Hydrological observations in Ebreichsdorf area

Co-seismic static stress due to earthquakes deforms the porous medium around them, generating changes in pore pressure (Manga and Wang, 2007). Some manifestations of this relationship include water-level changes in wells, variations in streamflows, or liquefaction(King et al., 1999; Roeloffs et al., 2003; Manga et al., 2012) . In order to investigate possible relationships between the Ebreichsdorf sequence in 2013 and fluids, we use 9 hydrologic stations at epicentral distances less than 5 km from the earthquake cluster (Fig. 5.1). The stations are operated by the Hydrological Survey of Lower Austria (Hydrographischer Dienst Niederösterreich, http://atlas.noe.gv.at). Of these stations, 6 were recording during the

sequence, half of them having weekly measurements and the other half hourly measurements (Fig. 5.6).

They are generally wells in towns or solid pipes, with perforations in the bottom part at about 3-5 m deep. The sensors themselves are submerged pressure sensors for stations with hourly measurements. In the case of stations with weekly measurements, readings are performed by an observer.

Before the time of the two main shocks, on September 16, 2013, the water-level is increasing at almost all 6 stations (Fig. 5.6). Four days later, the first main shock occurred. No variations in water-level are observed at the time of any of the main shocks. When compared with the rainfall data in Seibersdorf, a town located less than 10 km from Ebreichsdorf, and at towns of Eisenstadt, Schwechat and Wiener Neustadt, which are approximately 20-30 km away from Ebreichsdorf (data from the ZAMG), the increase of water-level is actually correlated with a heavy rainfall event on the same day.

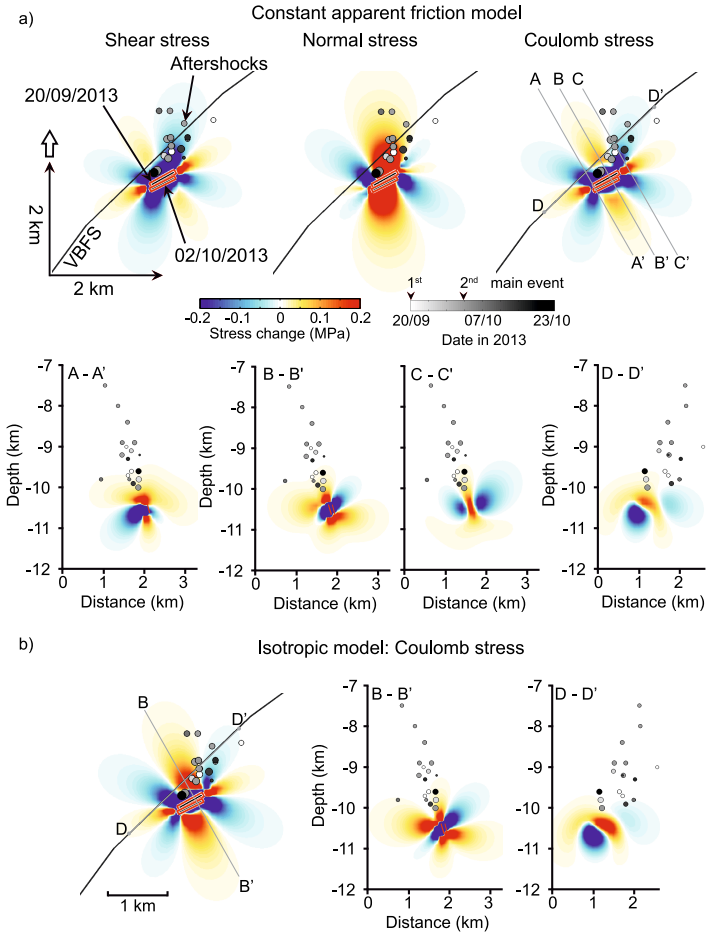

Figure 5.4.: a) Changes in Coulomb failure stress due to the first main event using the constant apparent friction model ($\mu' = 0.35$, see text for remaining parameters), calculated on faults with the orientation of the second main event. On top, changes in shear, normal and Coulomb stresses are shown on the left, middle and right, respectively (in map view). The locations of the four vertical cross-sections across the Coulomb stress change map are indicated by the gray lines. b) Changes in Coulomb failure stress due to the first main event using the isotropic model ($\mu' = 0.7$ and $B = 0.5$, see text for remaining parameters), calculated on faults with the orientation of the second main event (left). For comparison with the apparent friction model, two vertical cross-sections at the same locations are shown on the right. Positive stress changes are indicated by warm colors while negative changes are indicated by cold colours. Main shocks are indicated by red rectangles, aftershocks by dots with sizes proportional to their local magnitude and grey-coded depending on their occurrence time, and the VBFS by the black line.

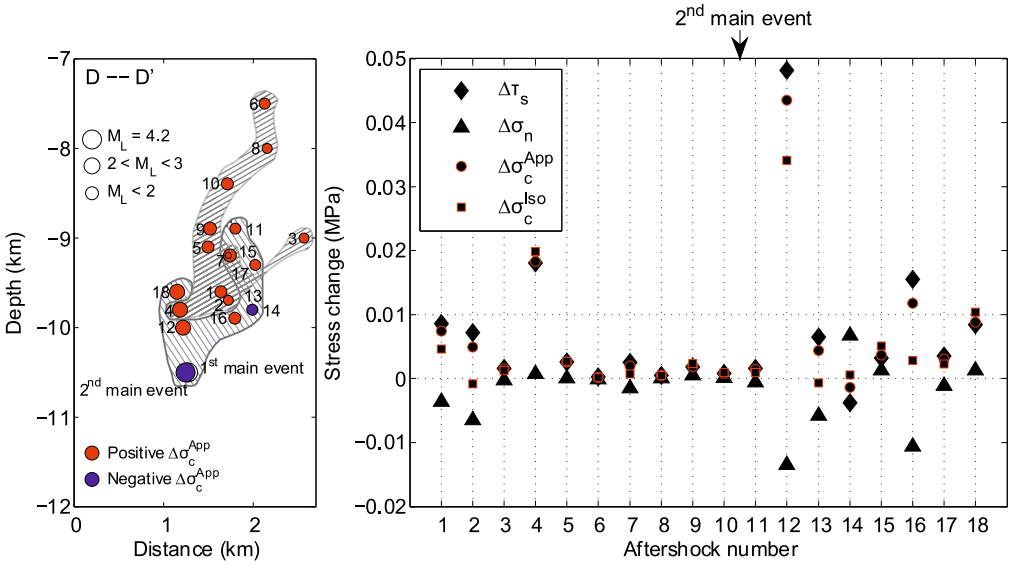

Figure 5.5.: (Right) Changes in shear $\Delta\tau_s$, normal $\Delta\sigma_n$ and Coulomb stress using the constant apparent friction $\Delta\sigma_c^{App}$ and isotropic $\Delta\sigma_c^{Iso}$ models, at the location of the aftershocks. The aftershocks are numbered in chronological order. (Left) Vertical cross-section along the strike of the VBFS with the complete aftershock sequence projected on it (see Fig. 5.4 for location of cross-section D-D'). The size of earthquake symbols is proportional to their local magnitude ML. They are colour-coded according to the polarity of the change in $\Delta\sigma_c^{App}$. The two grey hatched patches delimit the locations of the main shocks with the first 10 aftershocks, and the next 8 aftershocks.

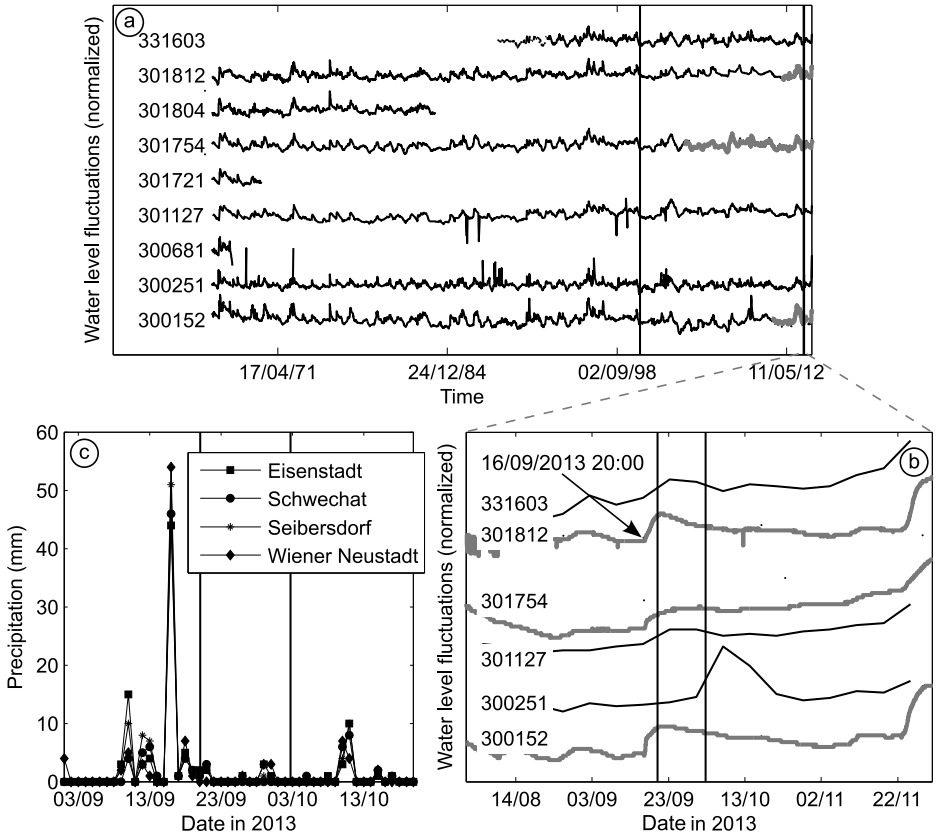

Figure 5.6.: a) Normalized time series of water level fluctuations recorded at 9 hydrological stations located in Ebreichsdorf area (Fig. 5.1) for the period 1966 - 2014. Black time series correspond to weekly measurements and grey time series to hourly measurements. Vertical lines correspond to the time of the main shocks in Ebreichsdorf sequences in 2000 and 2013. b) Zoom on the period 01/08/2013 – 31/11/2013. c) Precipitations (in mm) in the region of Ebreichsdorf, Seibersdorf being the closest station located less than 10 km away from Ebreichsdorf. Note the correlation between the increase in water level at almost all stations (except 300251) on September 16, 2013, and the peak in precipitations of approximately 50 mm on the same day.

6. Modeling and detection of regional depth phases at the GERES array

This chapter has been published as:

M.-T. Apoloner and G. Bokelmann, 2015, Modeling and detection of regional depth phases at the GERES array, Advances in Geosciences, 41, 5-10.

6.1. Abstract

The Vienna Basin in Eastern Austria is a region of low to moderate seismicity, and hence the seismological network coverage is relatively sparse. Nevertheless, the area is one of the most densely populated and most developed areas in Austria, so accurate earthquake location, including depth estimation and relation to faults is not only important for understanding tectonic processes, but also for estimating seismic hazard. Particularly depth estimation needs a dense seismic network around the anticipated epicentre. If the station coverage is not sufficient, the depth can only be estimated roughly. Regional Depth Phases (RDP) like sPg, sPmP and sPn have been already used successfully for calculating depth even if only observable from one station. However, especially in regions with sedimentary basins these phases prove difficult or impossible to recover from the seismic records.

For this study we use seismic array data from GERES. It is 220 km to the North West of the Vienna Basin, which - according to literature -

is a suitable distance to recover PmP and sPmP phases. We use array processing on recent earthquake data from the Vienna Basin with local magnitudes from 2.1 to 4.2 to reduce the SNR and to search for RDP. At the same time, we do similar processing on synthetic data specially modelled for this application. We compare real and synthetic results to assess which phases can be identified and to what extent depth estimation can be improved. Additionally, we calculate a map of lateral propagation behaviour of RDP for a typical strike-slip earthquake in our region of interest up to 400 km distance.

For our study case RDP propagation is strongly azimuthally dependent. Also, distance ranges differ from literature sources. Comparing with synthetic seismograms we identify PmP and PbP phases with array processing as strongest arrivals. Although the associated depth phases cannot be identified at this distance and azimuth, identification of the PbP phases limits possible depth to less than 20 km. Polarization analysis adds information on the first arriving Pn wave for local magnitudes above 2.5.

6.2. Introduction

Earthquake locations are fundamental for assessing seismic hazard. To provide these, areas with high seismicity rates and large magnitudes are instrumented with seismic stations. Particularly depth estimation requires a dense seismic network around the suspected epicentre. In contrast our study area, the Vienna Basin in Austria, a region of low to moderate seismicity with a largest instrumentally recorded magnitude around 5, is only covered sparsely with seismic stations. Nevertheless, the area is one of the most densely populated and most developed areas in Austria. In areas like these, estimation of seismic hazard has to be based on location of earthquakes with small magnitudes.

Regional Depth Phases (RDP) like sPg, sPmP and sPn are P phases converted to S at the surface. They develop at different regional distance ranges (Ma and Atkinson, 2006) and the time difference between direct and reflected phase is sensitive to epicentral depth. This property already has been successfully used for calculating depth even if an RDP is observable at least at one station. However, especially in regions with

sedimentary basins, these phases prove difficult or impossible to recover from the seismic records.

On the other hand, seismic arrays together with appropriate processing can be used to lower signal to noise ratio of seismic recordings and so help detect and identify phases as e.g., Rost and Thomas (2002) describes. The purpose of this study is to investigate the possibility of using a seismic array for identifying RDP in our region of interest.

In our study area we previously investigated a series of strike-slip earthquakes and relocated them (Apoloner and Bokelmann, 2015a) using local stations. From this dataset we select all earthquakes with local magnitudes from 2.0 to 4.2 and analyse the records at the 220 km distant seismological array GERES (Harjes, 1990). According to the literature (Ma and Atkinson, 2006) those events should have a suitable magnitude and distance to recover PmP and sPmP phases. We use array processing on the whole array and polarization analysis on the four 3-component stations. At the same time, we perform similar processing of synthetic data specially modelled for this application. We compare real and synthetic results to assert which phases can be identified.

6.3. Tectonic setting

Ongoing convergence between the Bohemian Massif on the European Plate in the north and the Adriatic Plate in the south lead to lateral extrusion of crustal blocks to the east (e.g. Brückl et al., 2010), into the Pannonian Basin as is shown in Figure 6.1. Two main sinistral strike-slip faults show this process: the Salzach-Enns-Mariazell-Puchberg (SEMP) fault and the seismically active Mur-Mürz-Lineament (MML). In the north-western extension of those faults a pull-apart basin, the Vienna Basin started forming and now is filled with sedimentary layers of a few kilometres. Beneath this basin the MML branches into the Vienna Basin Fault System (VBFS) which produces moderate seismic events with local magnitudes around 4.0. The Bohemian Massif extends beneath the Northern Alpine Transition (NAT) and forms the crystalline basement beneath the Vienna Basin (Wessely, 1983).

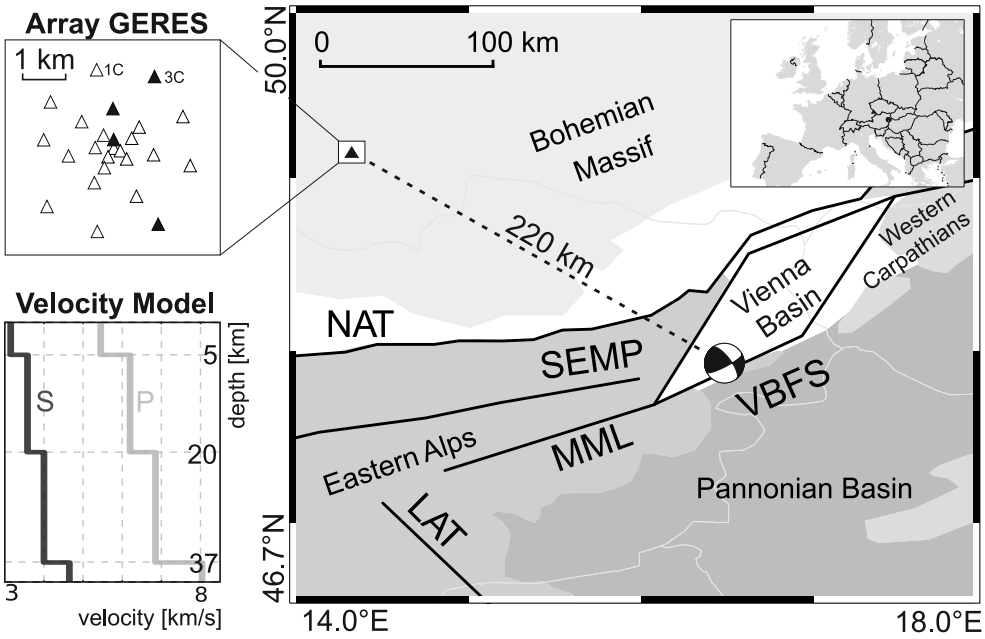

Figure 6.1.: Right panel: schematic map of the Vienna Basin with surrounding tectonic units and main faults shown together with the focal mechanism of the Ml 4.2 earthquake from 20/09/2013 in Ebreichsdorf by Hausmann et al. (2014). Top left: layout of seismic array GERES with 1-component stations (white triangles) and 3-component stations (black triangles). Bottom left: P and S velocity model for the area by Hausmann et al. (2010).

To approximate the underground between Ebreichsdorf and GERES we used the model proposed by Hausmann et al. (2010), which is a 4-layer simplification of the 3D model by Behm et al. (2007b).

6.4. Seismic data

For our research, we used the data from the Ebreichsdorf 2013 earthquake series, which was located by Apoloner and Bokelmann (2015a) with all available data within 230 km and the 3D velocity model by Behm et al. (2007b). For modelling the wave propagation we used the largest event with a local magnitude of 4.2 and a depth of 10.5 km. Also, this is one of the earthquakes in the Vienna Basin where a focal mechanism was published. From this dataset we selected the six earthquakes with local magnitudes above 2.0, which are listed in Table 1. Most important for

Table 6.1.: Hypocentral parameters of earthquakes with local magnitude above 2.0 from Apoloner and Bokelmann (2015a) sorted by focal depth.

ID	Origin Time (UTC)	Ml (ZAMG)	Longitude [deg]	Latitude [deg]	Depth [km]
A	20.09.2013 02:06	4.2	16.4230	47.9318	10.5
B	02.10.2013 17:17	4.2	16.4229	47.9315	10.5
C	02.10.2013 19:42	2.8	16.4210	47.9324	10.0
D	24.09.2013 13:53	2.7	16.4207	47.9322	9.8
E	23.10.2013 19:34	2.6	16.4202	47.9321	9.6
F	02.10.2013 05:26	2.1	16.4237	47.9343	8.9

this study the events were also recorded at the seismic array GERES in Germany . The array consists of 21 1-component and four 3-component seismic stations depicted in Figure 6.1 which have been continuously recording since 1991 (Harjes et al., 1993). The array is at a distance of approximately 220 km from our area of interest and has a backazimuth of 115° to the selected events.

6.5. Regional depth phase (RDP) propagation

Regional depth phases such as sPg, sPmP and sPn in combination with their reference phases Pg, PmP and Pn can be used to estimate focal depths of regional earthquakes, if they can be identified. Figure 6.2 sketches their wavepaths. In principle, a single station with one phase pair may be sufficient for accurately determining earthquake depth from the difference in their arrival times. Different studies, e.g., Ma and Eaton (2011) and Ma (2012) mention that regional depth phases depend mainly on epicentral distance: Between 200 and 300 km waveforms should be quite simple: a weak Pn is followed by a strong PmP and sPmP using a simple 2-layer model and a thrust type mechanism.

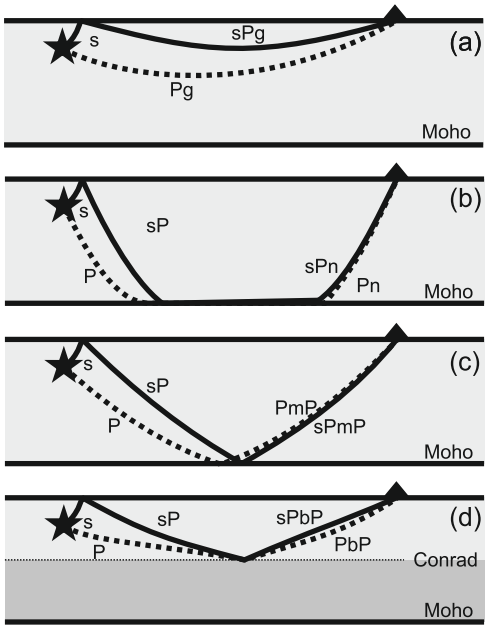

Figure 6.2.: Sketch figure for different RDP wavepaths adapted from Ma and Eaton (2011): (a) Pg and sPg, (b) Pn and sPn, (c) Moho reflection PmP and sPmP, augmented by (d) Mid crust reflection PbP and sPbP.

6.5.1. Waveform modeling

In the first part of this study we model RDP propagation for the tectonic setting and seismic data in our area of interest. Using the velocity model by Hausmann et al. (2010) and the focal mechanism by Hausmann et al. (2014), the source time function was estimated for both Ml 4.2 earthquakes with empirical Green functions and is approximated by a 0.2 second parabolic pulse. With those parameters synthetic seismograms were calculated using the wavenumber integration implemented by Herrmann (2013) for all stations of the array and for depths ranging from 0 to 25 km.

To gain an overview on lateral propagation behaviour of RDP, we additionally calculated synthetic seismograms in a regular spaced grid around Ebreichsdorf up to 400 km distance. However, Figure 6.3 shows the results for the closest grid point at an azimuth of 295° and 220 km distance, to facilitate comparison of the results to the next processing step.

To give an overview RDP propagation we processed the synthetic data as follows: we measure the maximum amplitude of arriving RDPs on

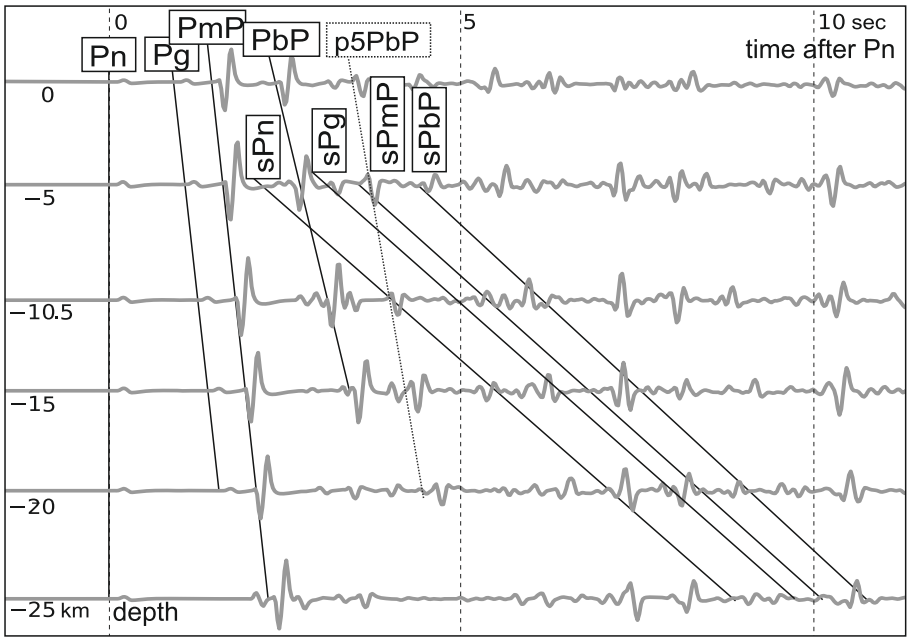

Figure 6.3.: Synthetic seismograms of the vertical component for the central array station GEAo for depths ranging from 0 to 25 km. Phases are arrivals annotated according to wave type. e.g. sPn seems to be visible, but is strongly overlapped by other phases. In addition to the RDPs, the p5PbP is recognizable.

the horizontal component velocity record envelope for each grid point. Afterwards, we multiply those values for each phase pair at each grid point and normalize their power by extracting the square root. The interpolated results are shown in Figure 6.4 superimposed on our area of interest. Dark coloring indicates high amplitudes for at least one phase of a depth

However, for depth estimation it is advantageous, though not necessary, to identify both. For this reason, we extract the area where both phases of a pair should have a significant amplitude. Based on the synthetic traces and real data from GERES, we know that we can identify PmP and PbP. Therefore, we assume that half the amplitude of PmP should be still visible. We draw a contour line around the area where each phase is above this minimum value and intersect the contours for each phase pair. The result for PmP and sPmP is shown in Figure 6.4 in the right panel. Figure 6.5 puts together the contour lines for different depth phase pairs.

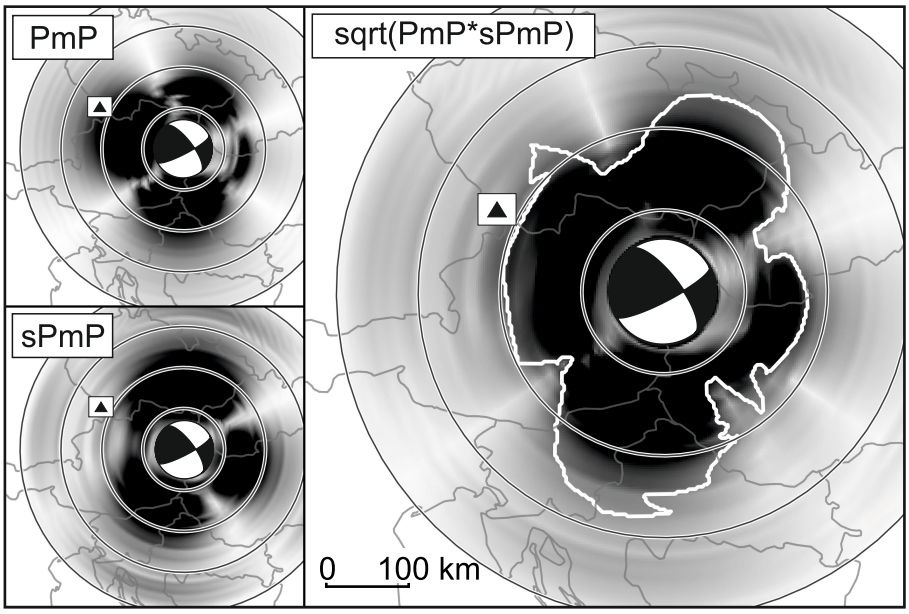

Figure 6.4.: Lateral propagation of PmP (top left panel) and sPmP (bottom left panel) for a strike-slip earthquake in Ebreichsdorf at 10.5 km depth from synthetic traces: right panel shows combined strength of phases (grey shades) and area of minimal visible amplitude for both phases (white line).

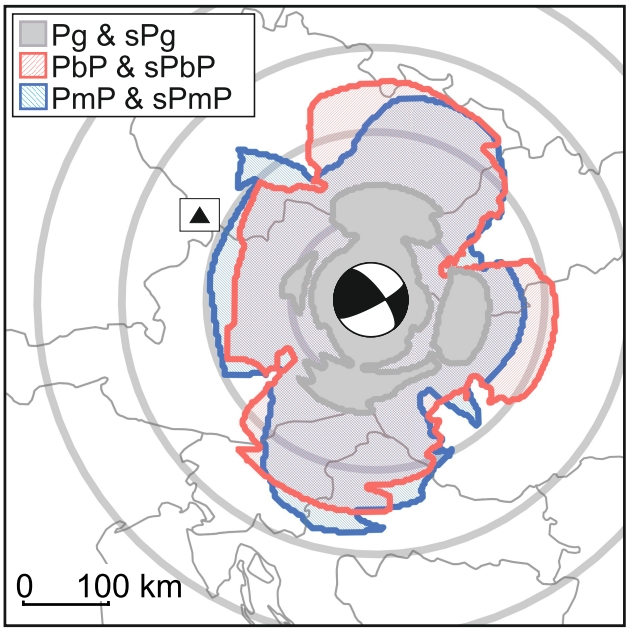

Figure 6.5.: Areas of visibility for both phases of a depth phase pair derived from synthetic seismograms.

6.6. Array analysis with vespagrams

The synthetic traces in Figure 6.3 as well as the spreading maps in Figure 6.4 and 6.5 show, that PmP and PbP should be visible clearly because of their high amplitudes at GERES. However, S to P conversions like sPmP and sPbP are not visible. As mentioned before array processing can be used to improve SNR of time series by, e.g. creating vespagrams. Figure 6.6 shows the results for all earthquakes in our dataset in colour and for the synthetics of the first earthquake A.

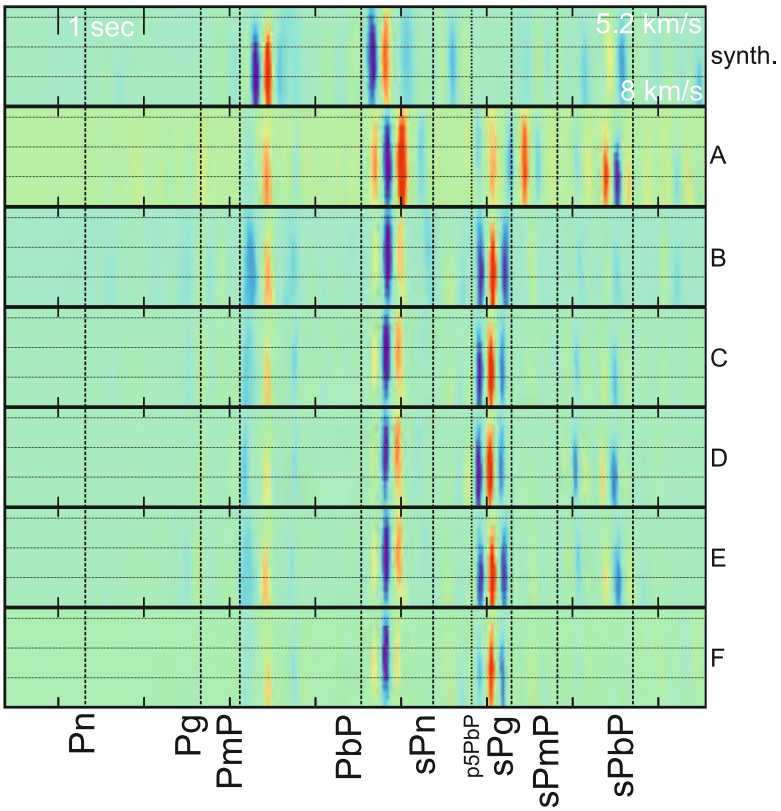

Figure 6.6.: Vespagrams for synthetic data for the first earthquake at GERES and real data for all selected earthquakes from Table 1. Vespagrams are aligned on PmP arrival and phases were calculated with TauP of Crotwell et al. (1999).

6.7. Polarization analysis of 3-component stations

Most elements of GERES are only recording the vertical movement. This is sufficient to identify backazimuth and slowness by array processing. However, GERES does also have four 3-component sensors, which are shown in the top left panel in Figure 6.1. In the next step we try to use those stations to identify the phases visible in the vespagrams, using their polarization. For polarization analysis we used the method introduced by Vidale (1986). Figure 6.7 shows the results for earthquakes A to E in grey and for the synthetics of the first event in black. Earthquake F was not used because of low SNR due to the small magnitude.

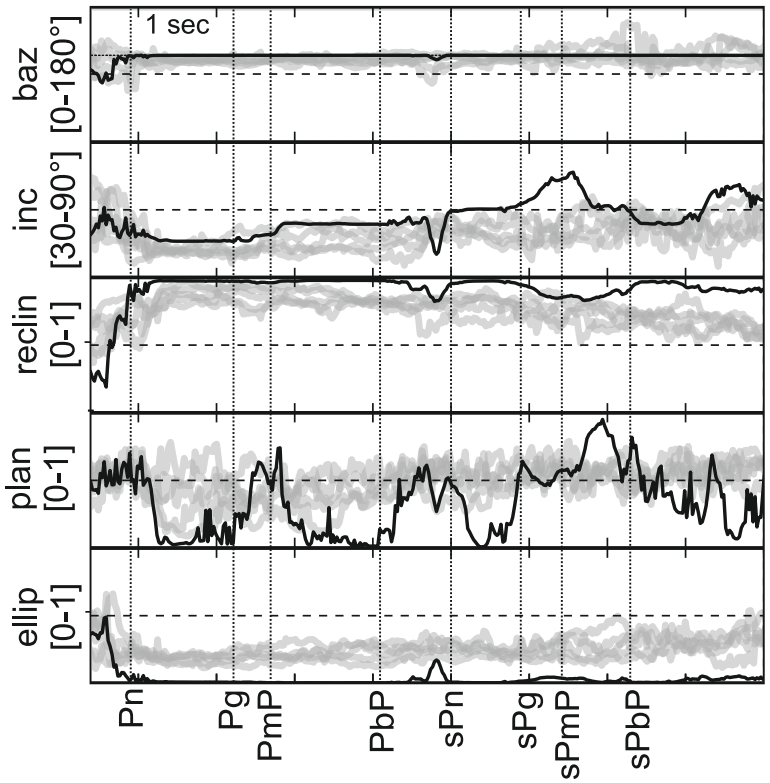

Figure 6.7.: Polarization analysis for synthetic data (black) and earthquakes (grey). From top to bottom: backazimuth, incidence angle, rectilinearity, planarity and ellipticity.

6.8. Results

6.8.1. Regional depth phase spreading

The different propagation patterns for PmP and sPmP are shown in Figure 6.4, together with the combination of both. Wave propagation for our dataset with a four layer model and a strike-slip mechanism is more complex than anticipated from literature, which, among other factors assumes that the mechanism is not relevant. The PmP phase has propagation pattern like a P wave with four lobes with strong amplitudes between 100 and 200 km. On the other hand, the sPmP propagates like a S wave but is stronger at up to 90° azimuth to the PmP and a similar distance range. The areas where both phases are likely to be identified are depicted in the right panel in Figure 6.4. Depending on the azimuth distances between 50 and 250 km can have strong amplitudes.

Figure 6.5 shows the outlines of three different depth phase combinations for our area of interest. Interestingly also the PbP and sPbP phase pair, which has not been used for depth estimations, shows a similar pattern to PmP and sPmP phases. Pg and sPg also show strong azimuth dependence.

6.8.2. Array analysis

The vespagrams for our data in Figure 6.6 show a clear pattern for all earthquakes, which is also visible in the synthetics: A strong PmP with an apparent velocity of 7 km/s is followed by an even stronger PbP at 6.2 km/s even for our smallest used magnitudes. PbP arrives later than calculated, which indicated either a deeper Conrad discontinuity or higher velocities above it.

However, another strong phase follows with a high amplitude in the real data, shortly before the sPg. In the synthetics this phase is also visible and the most likely wavepath is an upward going P wave which reflects at the 5 km interface in the model and then propagates as PbP (p5PbP). The high amplitude indicates a depth below this interface and above the Conrad discontinuity. Also, the downwards reflection happens very close

to the earthquakes, which would relate to a downward reflection from the bottom of the Vienna Basin.

Converted depth phases like sPg, sPmP and sPbP are not visible. Although we could not identify depth phases, depth is restricted since we know from modelling that a strong PbP is only possible for sources above the Conrad.

Furthermore, it is important to notice that PmP is the by far strongest phase arriving at GERES. This can lead to errors in location if it is mistaken for the Pn phase, which is the first arrival, but has much less energy.

The figures above show the results of the vespagrams of an event at GERES. The top figure shows the result for the recorded data, the bottom one for the synthetics. Although the Pn onset is clearly visible after processing, other phases cannot be identified because they occur very close to each other.

6.8.3. Polarization analysis

In the last step we analysed the polarization of data and compared it to the synthetic results (see Figure 7). For the beginning of the P coda analysed by us the backazimuth stays stable at the estimated 115.5°. Inclination changes with the different phases arriving, in clear steps for the synthetic data and slowly for the real data. Planarity and ellipticity do not show a clear signal.

The Pn onset is clearly visible in backazimuth, incidence and rectilinearity down to a local magnitude of 2.6. Earthquake F with a Ml of 2.1 does not even show this feature and therefore was excluded.

6.9. Conclusions

Lateral analysis of synthetic data shows that regional depth phase propagation is strongly dependent not only on depth but also on the focal mechanism. Therefore, the knowledge of focal mechanism is important and a typical mechanism for the area needs to be used. Also, additional

layers in the underground can produce strong reflections not reported by literature like PbP or p5PbP. Although no RDP pair could be identified, the visible regional phases restrict depth of the events in our dataset between a layer above and below the earthquakes, which relate to the bottom of the Vienna Basin and the Conrad discontinuity.

From comparison of the afore mentioned results to our dataset, we conclude that earthquakes from the Vienna Basin develop clear PmP and PbP arrivals at GERES. However, the converted depth phases sPn, sPg, sPmP and sPbP are not visible, not even with the improved SNR of the array. Yet, vespagram analysis can be used to identify phases in the P-coda by their slowness even down to magnitudes of 2.1.

Further research will analyse RDP propagation around the Vienna Basin in more detail. One important feature that needs to be addressed is the low-velocity sediment layer, which is reported to weaken converted phases we are looking for. Also, we will investigate data from our dataset recorded at stations, which are in areas where the synthetics indicate high amplitudes for RDPs. Since time difference between RDP pairs is mainly affected by depth, as stated in Ma (2010), it should be possible to use phase readings of single phases at varying distances to estimate depth.

With newly deployed dense seismic network like the AlpArray presented in Fuchs et al. (2015) or profiles like EASI (see Plomerova et al. (2015) wave propagation could be monitored and maybe even tracked across the region. This extended knowledge of RDP behaviour can then be used to locate even small earthquakes more accurately as more information than first picks is available.

6.10. Acknowledgements

We thank the Zentralanstalt für Meteorologie und Geodynamik (ZAMG) and the Bundesanstalt für Geowissenschaften und Rohstoffe (BGR) for making available seismic data for this study. Plots were created with ObsPy (Beyreuther et al., 2010) and maps with QGIS (QGIS, 2009). Synthetics were generated with Computer Programs in Seismology by Herrmann (2013). Travel Times were calculated with TauP (Crotwell et al., 1999).

7. Influences on regional depth phase identification

Currently regional depth phases are rarely used in standard localization procedures, not because those additional arrival times are not useful, but because they are not identified. Multiple studies focus on depth phases. Most, however, focus on events with magnitudes above 5 (e.g. Stroujkova et al., 2007; Alinaghi and Krüger, 2014; Bonner et al., 2001; Sipkin, 2000; Heyburn et al., 2013) at teleseismic ranges to detect either pP or sP. At smaller distances, regional depth phases (Pg and sPg, PmP and sPmP, Pn and sPn) are used. These studies (e.g. Bock, 1993; Langston, 1987; Ma and Atkinson, 2006; Kastrup et al., 2007; Husebye et al., 2013) utilise earthquakes with magnitudes above 2 to detect either PmP and sPmP or Pn and sPn for selected sets of events.

Another fact common to many studies, is that the earthquakes investigated mostly of thrust-type (Gamage et al., 2009; Uski et al., 2003; Ma and Atkinson, 2006; Warren and Shearer, 2005; Langston, 1987; Bock, 1993; Ebel and Bonjer, 1990). Less studies detect RDP also from strike-slip earthquakes (Bock, 1993; Bock et al., 1996; Kim et al., 2006; Kastrup et al., 2007).

Furthermore, multiple studies focus only on the areas with stable continental lithosphere: Eastern Canada (Bent and Perry, 2002; Kim et al., 2006; Ma and Atkinson, 2006; Ma, 2010; Ma and Eaton, 2011), Alaska (Bonner et al., 2001; Langston, 1996) and Australia (Bock, 1993; Langston, 1987). For areas with more complex subsurface structure, like the Alpine Foreland (Ebel and Bonjer, 1990; Kastrup et al., 2007), Western Bohemia (Bock et al., 1996), Turkey (Stroujkova et al., 2007) or the Japanese subduction zone (Gamage et al., 2009), less studies exist.

For detection of depth phases different methods were already used: polarization filtering Husebye et al. (2013), travel time curves (Uski et al., 2003), regional depth phase modelling (e.g. Ma, 2012), frequency analysis (Murphy and Barker, 2006), frequency change with depth (Warren and Shearer, 2005), envelopes (Sipkin, 2000), autocorrelation (Zhang et al., 2014) and array processing (Alinaghi and Krüger, 2014). Yet, in the literature different problems with identification are also mentioned, i.e., complicated source time functions (Zhu et al., 1997), sedimentary basins (Ma, 2012) and influence of the source mechanism on the radiation pattern (Ebel and Bonjer, 1990).

This chapter investigates in which distances and azimuths regional depth phases are likely to be identified in the region around the Vienna Basin. To investigate this I use different approaches: In the first part arrival times are considered, in the second part amplitudes and the adjacent waveform.

As the focus of this thesis is on the Ebreichsdorf 2013 series, source parameters usual in this area are used, as given in Section 2.4.2. For this research the focal mechanism of the Ml 4.2 earthquake from 20/09/2013 by Hausmann et al. (2014) is taken. Also a simple source time function, a paraboloid, is assumed due its moderate magnitude. The velocity model (see Figure 7.4 for details) is adapted to this area, to reflect the sediments of the Vienna Basin. In addition to the phases mentioned in the literature (Pg and sPg, PmP and sPmP, Pn and sPn) I investigate PbP and sPbP, which show strong amplitudes in this setting (see Chapter 6). The simplified wave paths are illustrated in Figure 7.1.

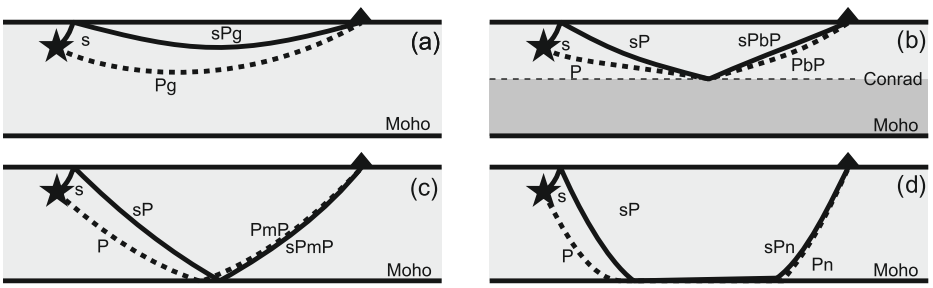

Figure 7.1.: Regional depth phases and their reference phases, adapted from Ma and Eaton (2011): (a) Pg and sPg, (b) PbP and sPbP, (c) PmP and sPmP, (d) Pn and sPn.

7.1. Travel times

Usually only primary direct arrivals are used for standard location procedures. They can be distinguished comparatively easily, either because of the stronger amplitude, polarization or a clear change in frequency. RDP are more difficult to identify as they are either reflections, refractions, conversions or combinations of the aforementioned, and have smaller amplitudes. The first part of this chapter looks into calculated arrival times to see if and at which distances and depths, those phases can be distinguished due to their arrival time difference to other phases.

7.1.1. Phase overlaps

To analyse this question I first look into possible phase overlaps in time. With the software TauP by Crotwell et al. (1999), the velocity model by Hausmann et al. (2010) and a source depth of 10.5 km I calculate travel times for the phases mentioned in the introduction of this chapter as well as for the first arriving S wave up to distances up to 400 km. The results are jointly plotted in Figure 7.2. Figure 7.2 shows clearly that:

- at distances up to 70 km from the source RDP are often superimposed by S waves
- around 150 km all direct RDP arrive simultaneously, also their converted counterparts arrive simultaneously
- some phases like (Pn and sPn) need a minimum distance to emerge.

7.1.2. Minimum time difference between RDP pairs

To estimate depths with RDP is favourable to be able to identify both phases of a pair e.g. Pg and sPg. This section focuses on investigating at which depths and distances RDP pairs do not overlap. Therefore, I compute the travel times for depths from 0 to 25 km at distances between 0 and 400 km. Afterwards, I calculate the difference in arrival time for each pair and plot the result to Figure 7.3.

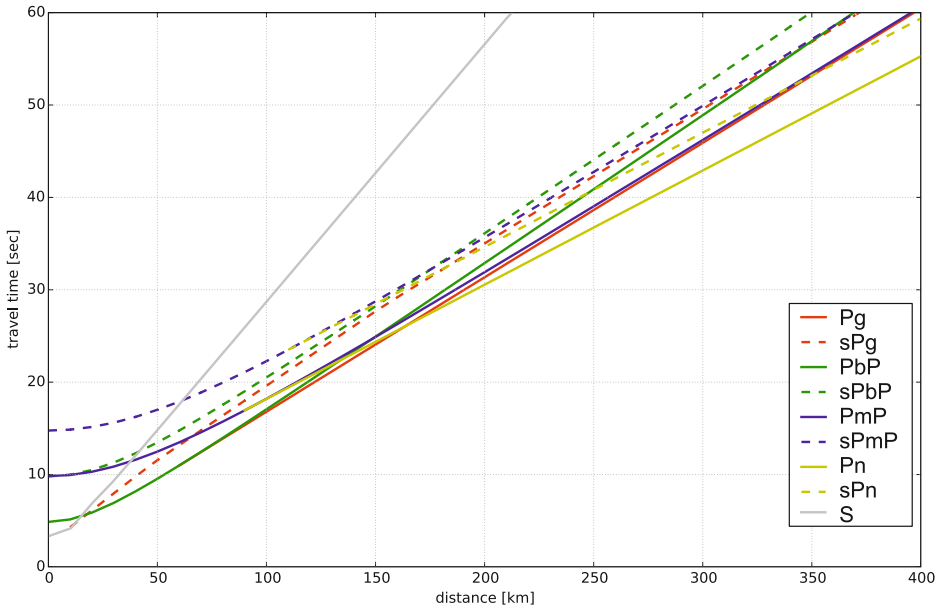

Figure 7.2.: Travel times for P waves, their corresponend depth phases and fastest pure S wave for an event at 10.5 km depth at distances from 0 to 400 km.

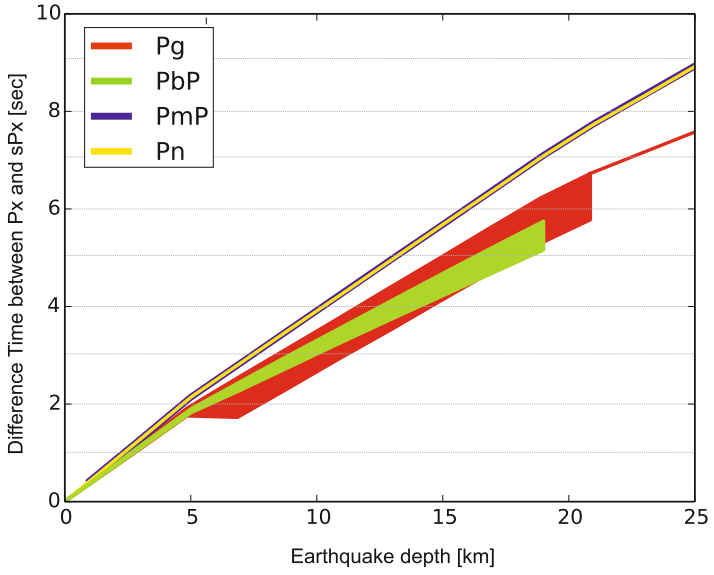

Figure 7.3.: Travel time difference between all P wave (Pg, PbP, PmP and Pn) and converted wave (sPg, sPbP, sPmP and sPn) for an event at 10.5 depth at distances from 0 to 400 km.

As known from literature, e.g. Ma (2012), time difference of RDP is strongly dependent on earthquake depth, which makes theses phases useful for

depth estimation. Only Pg and PbP are influenced by epicentral distance, however a location error of 100 km only results in 1 km of error in depth. Another important observation is that very shallow events above 3 km only have a time difference below 1 second, which will probably be covered by the conversions in the P coda.

7.2. Amplitudes and waveforms

Two other important aspects for identifying phases are the RDP amplitudes and the amplitudes of the surrounding arrivals thus the waveform. To investigate this I calculated synthetic seismograms with the Computer Programs in Seismology by Herrmann (2013) using the waveform integration and the 1-D velocity model based on Hausmann et al. (2010).

Initially I simulate a low velocity layer as top layer above the earthquakes, to investigate the effects e.g. a sedimentary basin would have. Afterwards I investigate the effects of different focal mechanisms on RDP propagation.

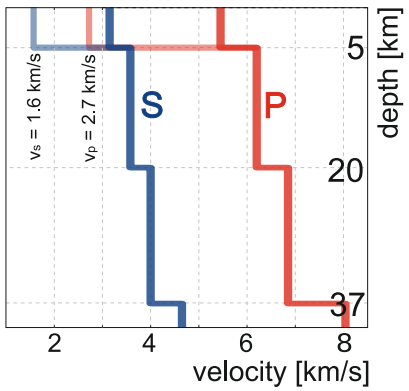

Figure 7.4.: Velocity model from Hausmann et al. (2010) and same model with the top layer velocity reduced by half. Figure adapted from Apoloner and Bokelmann (2015b).

7.2.1. Influence of low-velocity surface layer

To simulate and compare a low-velocity layer I use the model by Hausmann et al. (2010) and reduce the velocity in the topmost layer by half. The resulting and the original model are shown in Figure 7.4. For the calculation of synthetic seismograms additional information is needed: the focal mechanism from the Ebreichsdorf 2013 series by Hausmann et al. (2014), which is shown in Figure 7.10 on panel (a). The source time function length was estimated with 0.4 seconds, for further details see Chapter 5.

I calculated the waveforms for distances from 0 to 400 km and azimuths in 5° steps. The computed vertical component seismograms are shown together for both models at 0° azimuth, which equates to the north direction. Additionally, phase arrivals have been calculated with TauP and the corresponding velocity models. To facilitate interpretation, traces are plotted separately for each phase pair: Figure 7.5 shows Pg and sPg, Figure 7.8 PbP and sPbP, Figure 7.6 PmP and sPmP and Figure 7.7 Pn and sPn. The traces are normalized at each distance separately to facilitate inspection of the waveform, otherwise only traces < 100 km would show any signal at all. Figure 7.9 shows the time window around the arrivals of PbP and sPbP for better amplitude comparison.

The most obvious difference is the more complex waveform generated by the slower top velocity layer. In the original model sPg is the first strong phase to arrive after Pg. With the changed model other phases arrive earlier with strong amplitudes and make sPg undetectable (see Figure 7.5 last trace). PmP and Pg arrive almost simultaneously and can be easily mistaken for each other. In the distance range selected Pn and sPn have very low amplitudes. However, at distances bigger than 150 km they are the first arrivals, not overlapping with any other phase.

Because PbP and its corresponding phase sPbP are clearly strongest, this phase is shown in more detail in Figure 7.9. PbP does not change much between the different models. However, it gets slightly more complicated by distance. Although, the converted phase sPbP shows almost the same amplitude for both models, it is much harder to identify in the second

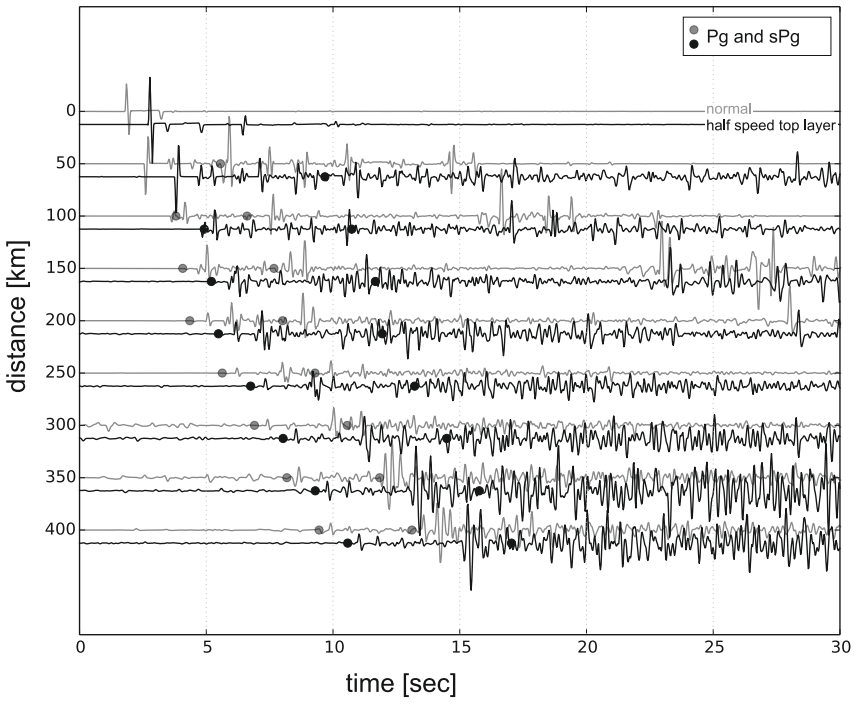

Figure 7.5.: Synthetic seismograms with calculated Pg and sPg arrivals for a strike-slip source at 10.5 km depth at epicentral distances up to 400 km calculated with the velocity models from Figure 7.4.

model, as the surrounding arrivals show higher amplitudes (see Figure 7.9 right panel).

7.2.2. Influence of focal mechanism

After modelling the wave propagation for the Ebreichsdorf series at the array GERES it was clear that RDP show a complex pattern, related mainly to the focal mechanism. To examine the effect of the focal mechanism three different focal mechanisms were used. They are shown jointly in Figure 7.10 and were selected for different purposes:

- from Ebreichsdorf 2013 series by Hausmann et al. (2014) as it is a representative strike-slip mechanism for the area investigated,
- an explosion source which does not show any direct S waves, so the panels with the converted waves show only artefacts produced by the processing and

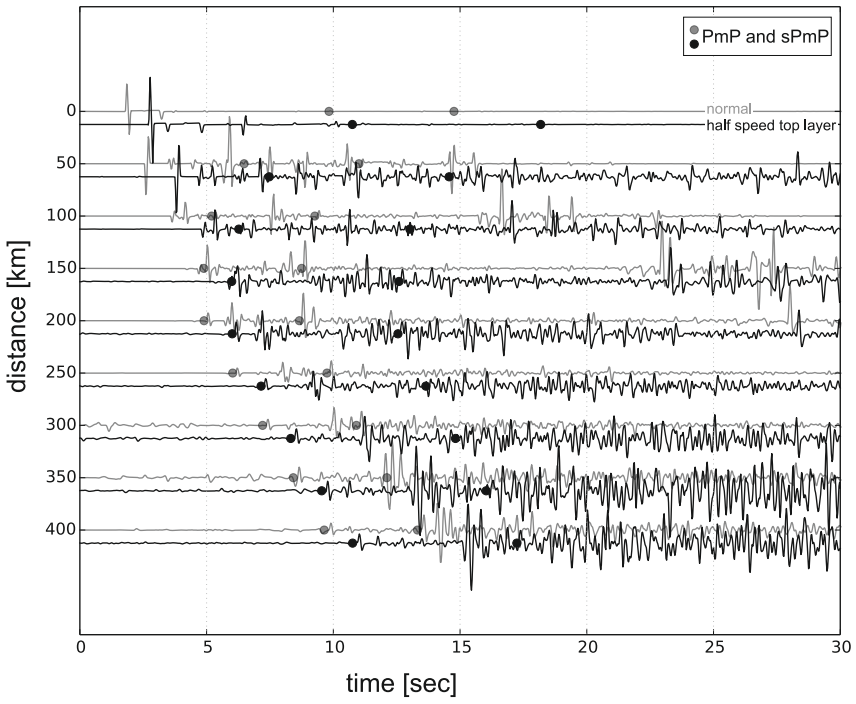

Figure 7.6.: Synthetic seismograms with calculated PmP and sPmP arrivals for a strike-slip source at 10.5 km depth at epicentral distances up to 400 km calculated with the velocity models from Figure 7.4.

- the focal mechanism from Ma (2012), which is a thrust-type mechanism where RDP have been already successfully identified.

Processing

The propagation maps shown in the Figures 7.11, 7.12 and 7.13 were calculated with the model from Hausmann et al. (2010), source time function length of 0.4 seconds and the according focal mechanism. A grid spacing of 5° in azimuth and 10 km epicentral distance up to 400 km was used. The source was fixed at 10.5 km. Subsequent to trace calculation the maximum of a time window with 0.4 seconds length around the phase of interest was taken. The resulting points for each phase were interpolated with inverse distance weighting implemented in the QGIS Software package by QGIS (2009). In the last step the maximum amplitudes of a pair were multiplied and the square root was drawn to be able to use the same scaling for all panels. Additionally, range rings in 50 km steps

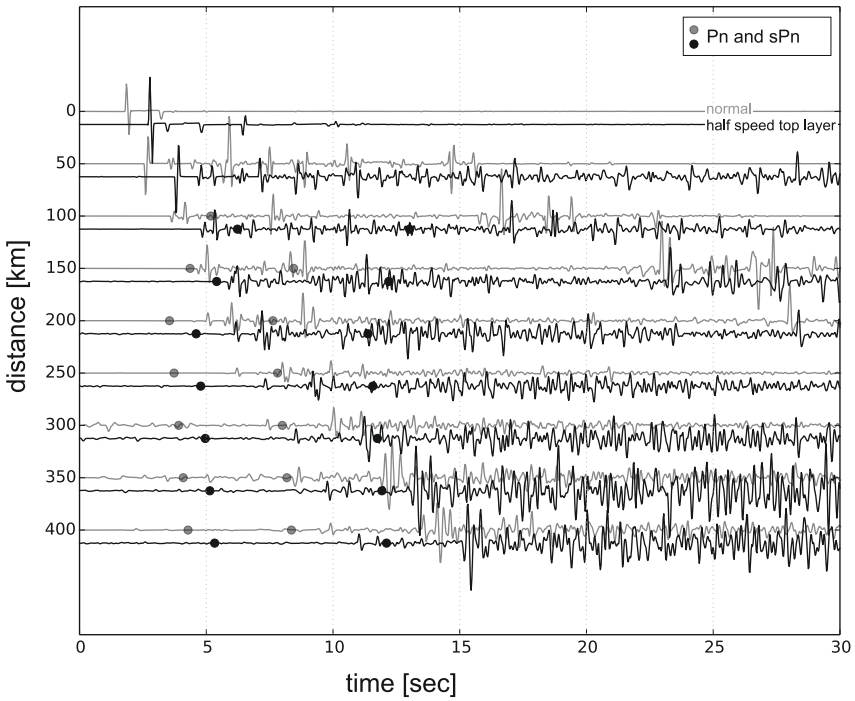

Figure 7.7.: Synthetic seismograms with calculated Pn and sPn arrivals for a strike-slip source at 10.5 km depth at epicentral distances up to 400 km calculated with the velocity models from Figure 7.4.

were superimposed on each map.

Propagation pattern for strike-slip focal mechanism

Figure 7.11 was computed with the strike-slip focal mechanism. In general RDP have high amplitudes within 200 km of the event. Direct RDP are strongest at 280° azimuth between 50 and 150 km (see panels a, d, g and j). Converted RDP are strongest in the North only at distances between 100 and 150 km (see panel b, e, h and k). This complicates identification of a connected phase pair: it is possible only at selected distances and azimuths e.g. 80-120 km at 10° or 190° azimuth for Pg and sPg (see panel c). The phase pair best visible is PbP with sPbP.

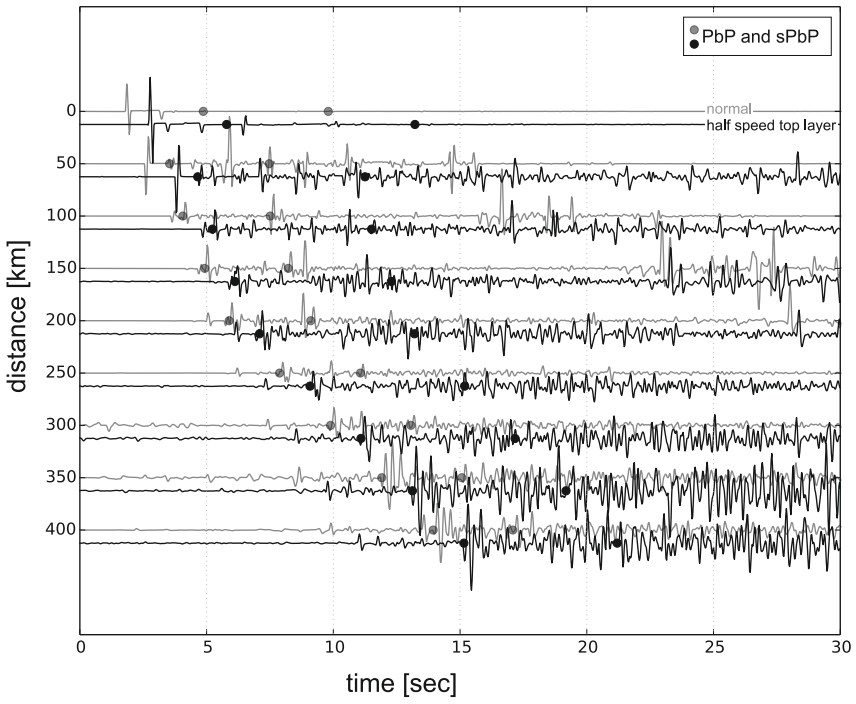

Figure 7.8.: Synthetic seismograms with calculated PbP and sPbP arrivals for a strike-slip source at 10.5 km depth at epicentral distances up to 400 km calculated with the velocity models from Figure 7.4.

Propagation pattern for explosion focal mechanism

The next Figure 7.12 shows the results for an explosion. This is beneficial for this study, because it does not produce S waves. This means neither sPg, sPbP, sPmP nor sPn develop. The same computation routine was used as before.

One immediately notices that the nodes typically for strike-slip do not exist here. The result is not azimuth-dependent. In theory, the second column with the panels b, e, h and k should not show any signal. However, the maps are not blank because phases which occur in the same time window as the converted phase are measured.

This information can be used to estimate the error made by using the processing described above: Compared to the direct phases, the amplitudes of other phases (not RDP) are very low and can be neglected.

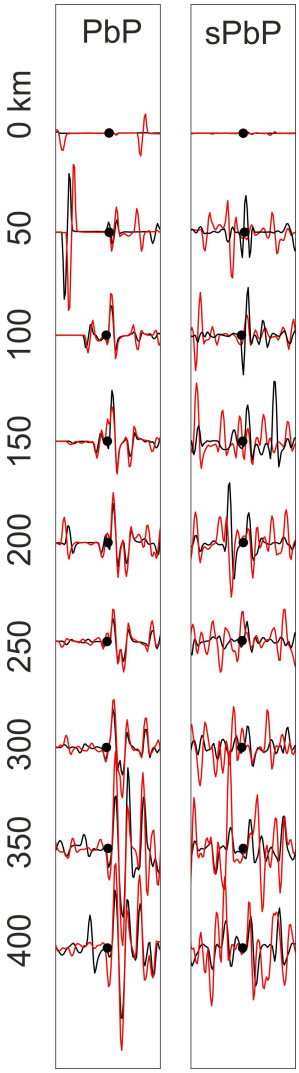

Figure 7.9.: Sections from Figure 7.8 aligned along arrival of PbP and sPbP. Synthetic seismograms calculated with velocity model from Hausmann et al. (2010) in black and with half velocity in the top layer to simulate sedimentary basin in red.

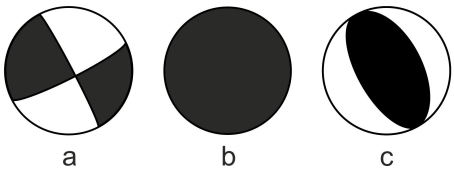

Figure 7.10.: a) Strike-slip focal mechanism from Ebreichsdorf 2013 from Hausmann et al. (2014) b) Explosion c) Thrust-type focal mechanism from Ma (2012).

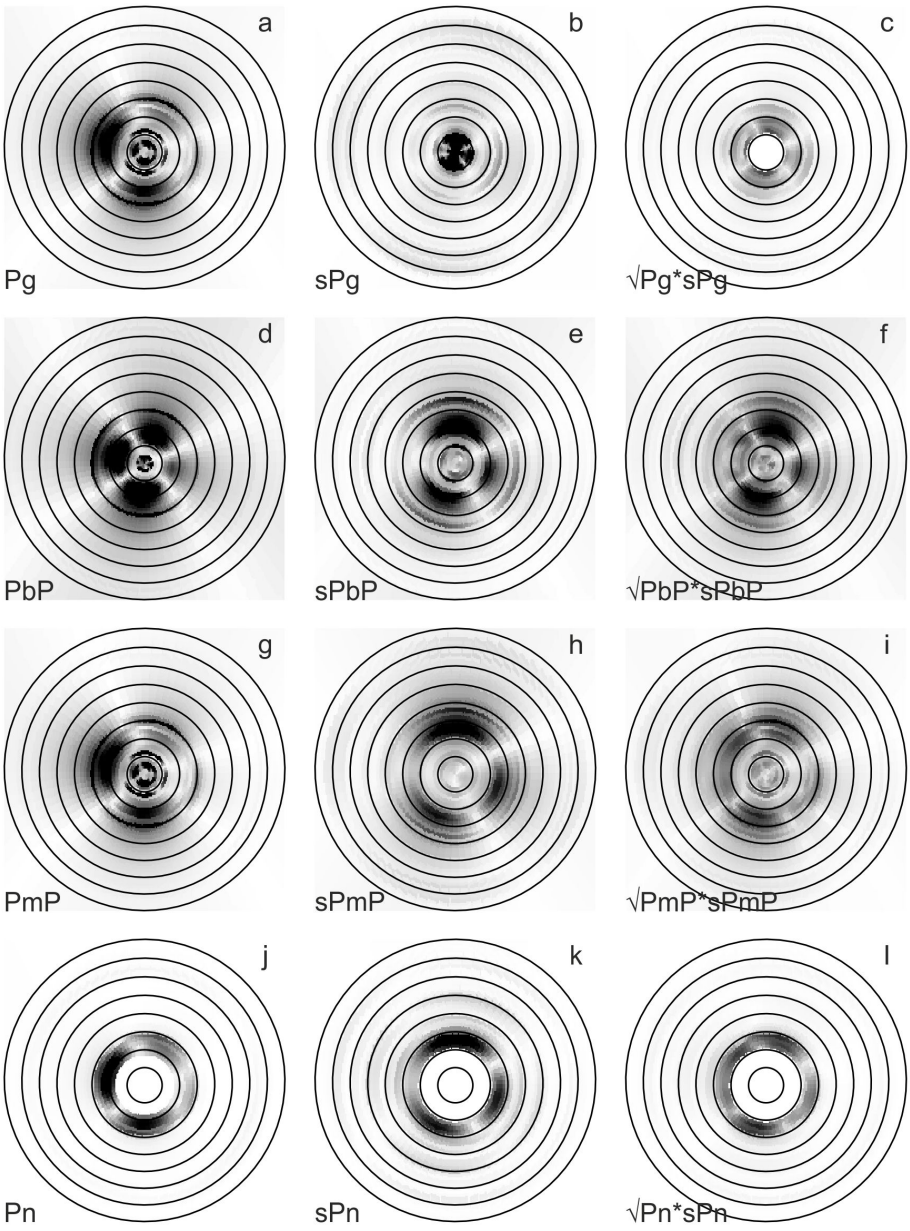

Figure 7.11.: Wave propagation for focal mechanism (a) from Figure 7.10 (strike-slip). Each row shows the maximum amplitude of each phase of a pair and their combined amplitude. Range rings from 50 - 400 km in 50 km steps.

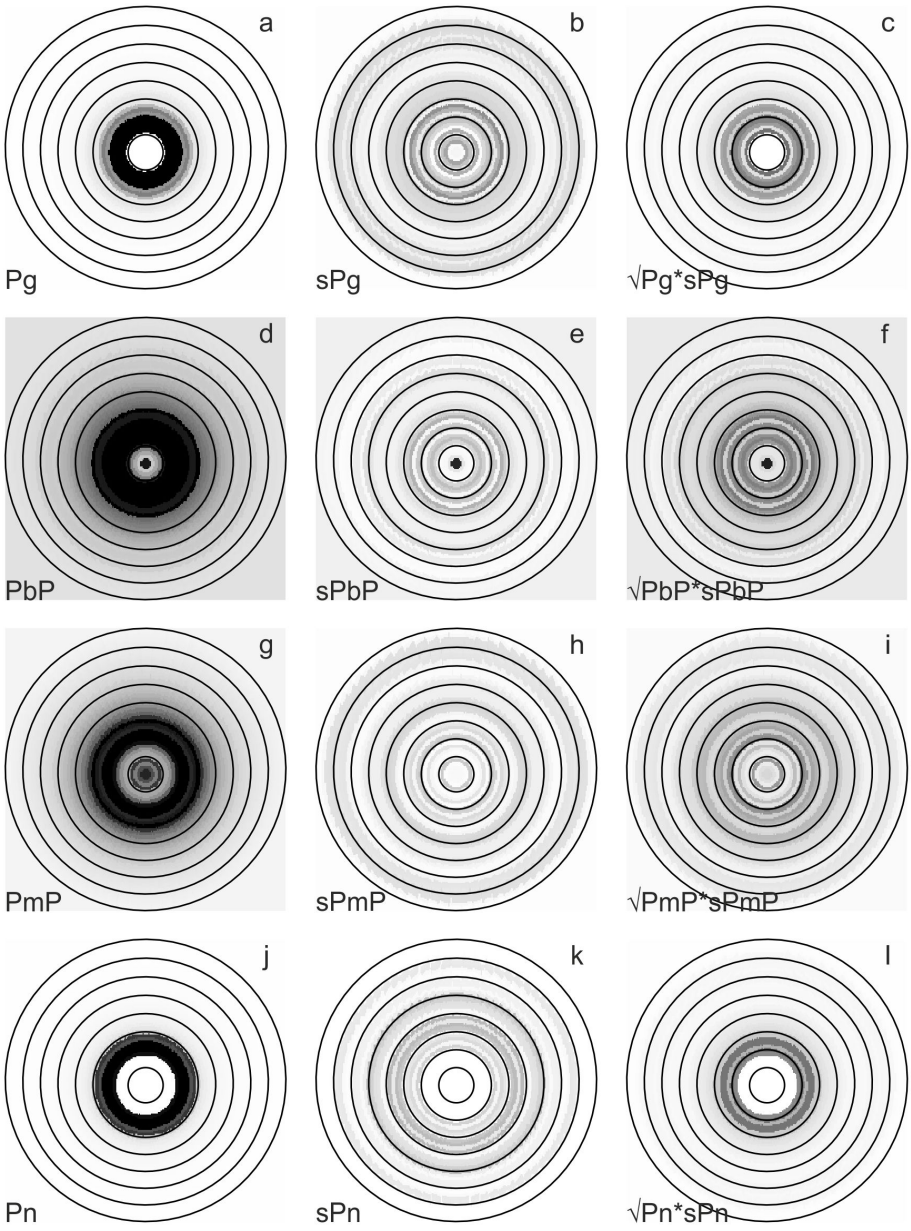

Figure 7.12.: Wave propagation for focal mechanism (b) from Figure 7.10 (explosion). Each row shows the maximum amplitude of each phase of a pair and their combined amplitude. Range rings from 50 - 400 km in 50 km steps.

Propagation pattern for thrust-type focal mechanism

The last figure, Figure 7.13, gives the result for a thrust-type mechanism. The pattern looks simpler than for the strike-slip mechanism. Fault parallel directions show higher amplitudes. The distances with strong amplitudes vary stronger though. Areas with high amplitudes for both phases are even smaller than for the strike-slip focal mechanism (see panel c, f, i and l). Converted phases like sPmP or sPbP are stronger developed yet (see panel e and h).

7.3. Summary

In this chapter I investigated influences on regional depth phase development and identification. Modelling of travel time indicated that accurate knowledge of location is not important for using RDP. Slow surface layers, like a sedimentary basin, complicate phase identification to a point where it is not possible to see some phases, especially the converted ones, at all. When looking for RDP it is important to have knowledge of the focal mechanism, as it severely reduces areas/stations where one can expect those phases.

Calculation of synthetic waveform is a prerequisite to identify phases in settings with multiple layers above the Moho. Additionally, it is important to have knowledge of the approximate depth of the earthquake investigated, as very shallow earthquake depths make usage of RDP impossible.

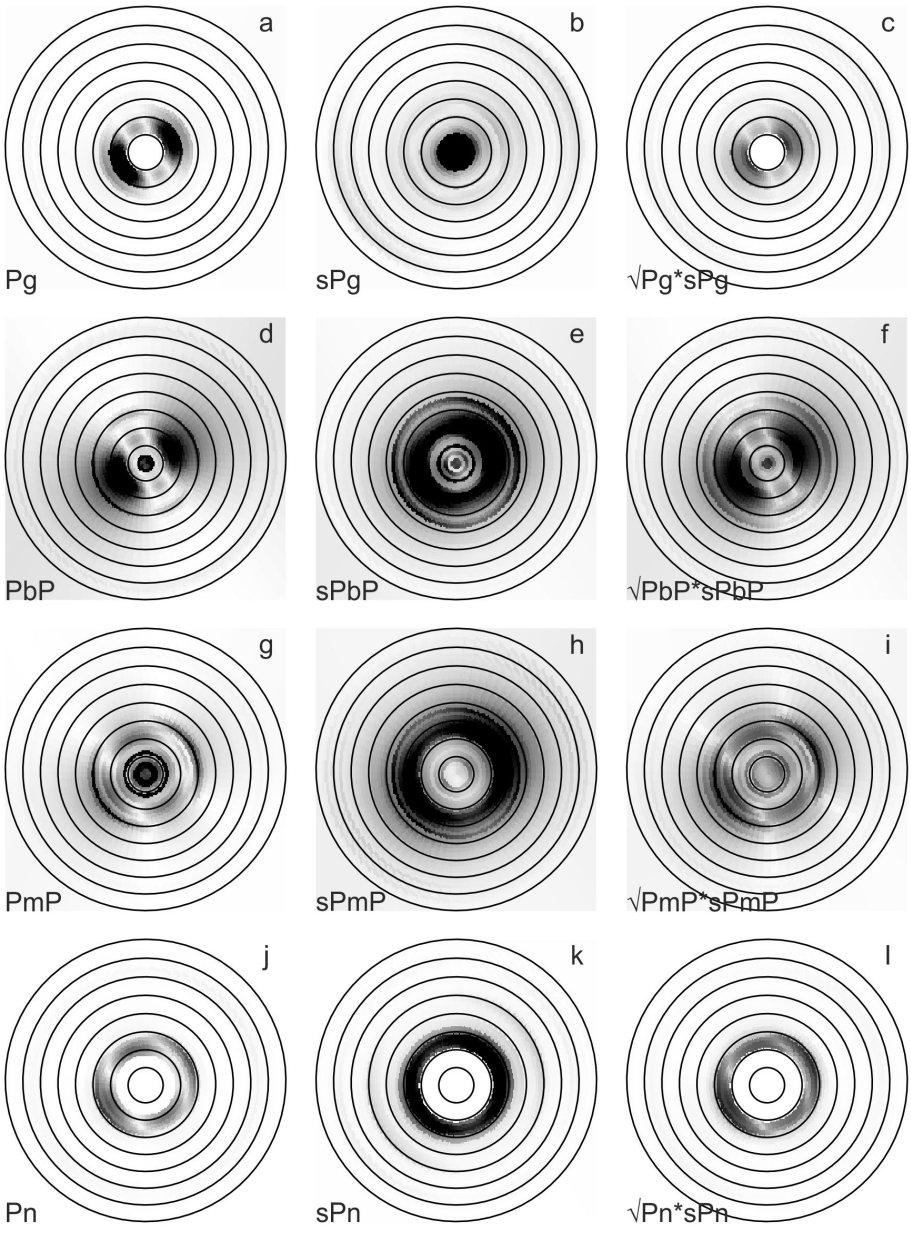

Figure 7.13.: Wave propagation for focal mechanism (c) from Figure 7.10 (thrust-type). Each row shows the maximum amplitude of each phase of a pair and their combined amplitude. Range rings from 50 - 400 km in 50 km steps.

8. Summary and conclusions

In this thesis, I have explored the benefits of using additional data, different methods and multiple processing methods in the Vienna Basin. This research, based on recent earthquakes in the vicinity of Ebreichsdorf, started with the compilation of a dataset. Most obviously, more and especially local seismic stations observe more seismicity. Moreover, comparison with earlier research shows that previously recorded earthquakes are similar to more recent ones: all calculated focal mechanisms are strike-slip with similar orientations. Also, all macroseismic intensity distributions that are currently available show the same patterns.

As anticipated, the higher network density around the epicentre improves the quality of earthquake locations, even with a 1D velocity model. Nevertheless, the use of NonLinLoc, 3D velocity model, and station corrections is necessary to give stable epicentres in station configurations that are sparse and changing with time, like in Ebreichsdorf. With this location technique and the additional seismic data and station correction parameters used, the epicentres can be associated with the nearby Vienna Basin Fault System. Anyhow, no systematic space-time pattern of the main shocks and their aftershocks can be seen with this combination of method and the available data.

However, localisation with NonLinLoc moves the events closer together for this dataset. The consequential investigation of waveforms, showed that they were highly correlated. The cross-correlation between the traces was fundamental to improving the relative location of the events with HypoDD. Relocation revealed a certain space-time organisation: larger aftershocks tend to occur at larger depth on the fault, and to migrate North-East in the 2013 series.

Also, the main shocks are collocated at depth within the uncertainties in locations and within the rupture area. Building on these results the

spatial relation between the main shocks of the 2000 and the 2013 series was analysed. With lower cross-correlation values and S-P-travel time differences, the events from 2000 are not collocated, but probably broke a different fault patch, 4 km to the North-East of the 2013 series.

Due to their collocation the earthquakes from 2013 analysis continued: Can stress transfer lead to this repeated rupture in the same location? Modelling of Coulomb failure stress and stress transfer shows that the main shocks were insufficient to trigger the aftershocks. Possible mechanisms could be dynamic effects reducing fault strength or high pore-pressure at depth.

Subsequent array and polarization analysis of the 2013 earthquake series as well as synthetic data shows that earthquakes from the Vienna Basin develop clear PmP and PbP arrivals at GERES. However, the converted depth phases are not visible, not even with the improved SNR of the array. Yet, vespagram analysis can be used to identify phases in the P-coda.

Concluding analysis of synthetic data shows that the regional depth phase propagation is strongly dependent not only on depth but also on the focal mechanism. Therefore, the knowledge of focal mechanism is important. A low-velocity sediment layer above the epicentre is also an important feature to consider: it complicates RDP identification to a point where it may not be possible to see them at all.

This thesis shows that much more seismic information is available than currently used in standard procedures. However, that knowledge is usually not collected, but needs to be discovered for each earthquake scenario. Also access is sometimes complicated and has to conform to different regulations. Easier and streamlined access to these data would simplify future analysis in this area.

Processing of data with different methods and additional background data improves the location accuracy, and thereby knowledge about an area. Regardless of the methods available, resolution and accuracy of the results always depends on the quality and density of data. Deploying seismic stations for short time periods of high seismicity is helpful to gain insight, but for long-term studies to assess the earthquake hazard continuous recording with a dense network, at least medium-quality is a prerequisite.

This thesis only used a selected set of methods, assuming that the given earthquake catalogue contains all earthquakes. Techniques like template or subspace-matching could be used to extend this catalogue to a lower magnitude of completeness for the area. However, with only one remaining local station, and thereof resulting bad localisation accuracy, this was not attempted in this thesis. With denser networks like the AlpArray (Fuchs et al., 2015), this could be a possibility for the future.

Another issue that needs to be considered is that adding stations or using different stations for processing, not only improves the results, but may bias them (e.g. events from 2000 located by Anonymous, 2002, are moved closer to the network). So while adding data and information may create better estimates, the results are not coherent and need to be considered carefully, like the relative locations between the main shocks of 2000 and 2013.

Appendix

Appendix A.

Improving identification of regional depth phases in sparse networks

This chapter has been presented as a poster at PanGEO2012, Salzburg, Austria:

M.-T. Apoloner and G. Bokelmann, 2012, Improving identification of regional depth phases in sparse networks.

A.1. Overview

Regional depth phases such as sPg and sPmP in combination with their reference phases Pg and PmP can be used to estimate focal depths of regional earthquakes, if they can be identified. In principle, a single station with one phase pair may be sufficient for accurately determining earthquake depth from the difference in their arrival times. Different studies, e.g. Ma and Eaton (2011) show that regional depth phases develop differently well depending on epicentral distance and magnitude:

Phases	Distance	Magnitude
Pg & sPg	$<$ 100 km	$>$ 1.5
PmP & sPmP	200 -300 km	$>$ 2.0

Ray paths of the regional depth can be seen in Figure A.1 The challenge lies in robustly detecting and identifying the phases, within the coda of the P-phase. Sedimentary basins, for example, may render these phases complex (Ma, 2010), and it may prove complicated to recover them from the seismic records.

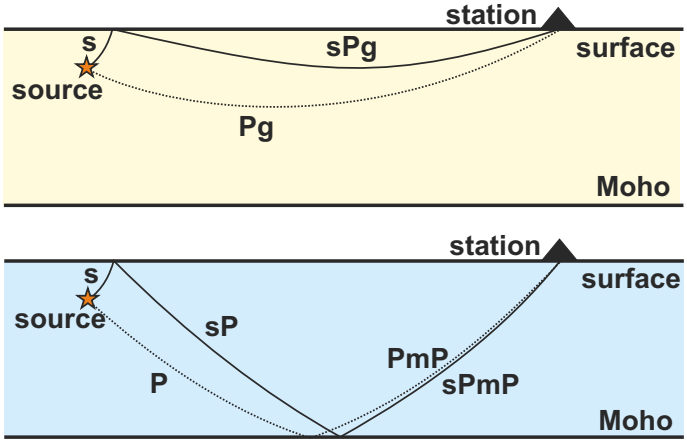

Figure A.1.: Regional Depth Phases adapted from Ma and Eaton (2011).

A.2. Region and seismic data

The study area is situated at the transition of the Eastern Alps to the Pannonian Basin and the Western Carpathians. The Vienna Basin is, due to its vicinity to Vienna, one of the most densely populated and developed areas in the region. Instrumentally recorded seismicity in the area is weak, with a maximum instrumentally recorded magnitude of around 5. There are historical records of stronger earthquakes though, and even larger events have been suggested based on paleoseismicity (Hintersberger et al., 2010).

The Austrian seismological network is built of very-high quality stations, but their station density is relatively sparse. For our research we added data from surrounding international observatories as well as from the ALPAACT network (Mertl and Brückl, 2010), which continuously recorded broadband data at additional 17 locations, shown in Figure A.2.

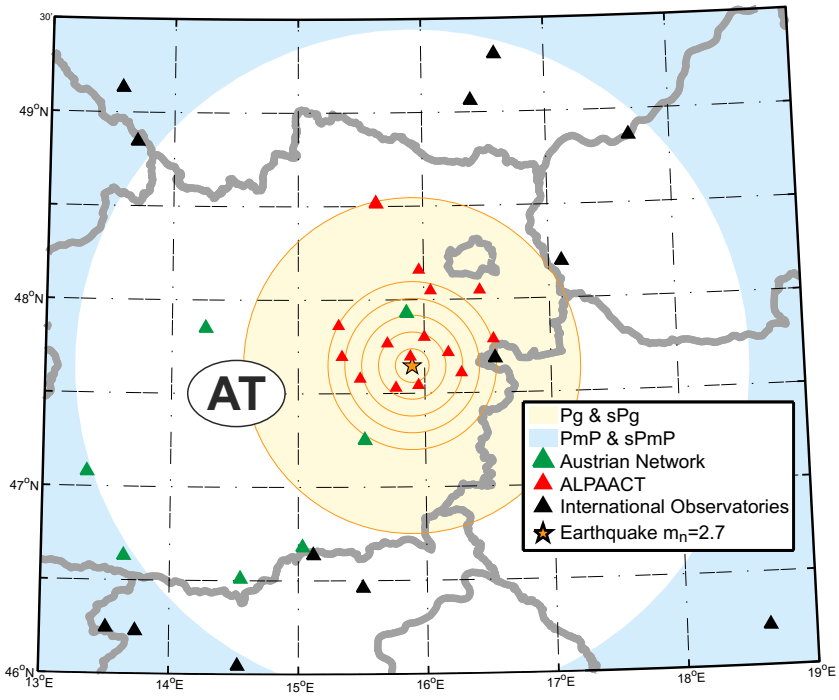

Figure A.2.: Areas of well developed regional depth phases.

A.3. Polarization filtering

We use a polarization filter presented by Schimmel and Gallart (2004), which was shown to increase signal-noise-ratio substantially in refraction data. The filter is based on the assumption that noise is less polarized than the signal; polarization weighing can thus increase the number of identifiable phases. Figure A.3 shows how this filter works on earthquake data. The first part shows the time and frequency dependent filter which is calculated from the original ZNE-traces. Part 2 to 4 show the original trace compared to the filtered trace. Phase onsets calculated with TauP Toolkit by Crotwell et al. (1999) are shown as reference.

A.4. Depth phase stacking

The time difference between depth phases and their reference phases changes with distance and with depth. If the distance is given one can

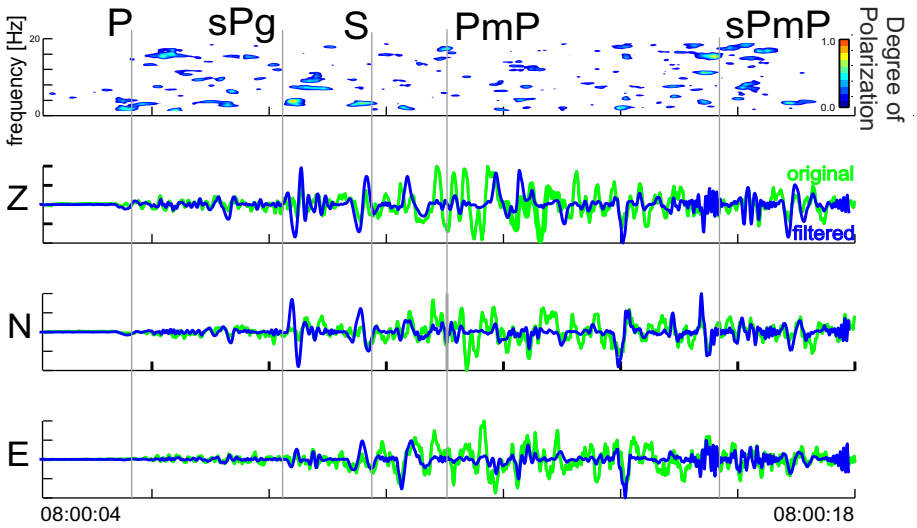

Figure A.3.: Polarization filter.

estimate depth from the arrival time of depth phases or calculate the arrival time for a given depth e.g. with the TauP Toolkit by Crotwell et al. (1999). As depth phases are hard to identify in our data set, we try to get depth information without picking the phases themselves. At first we resample all data to the same frequency, rotate the traces to the ray coordinate system (ZNE to LQT) and calculate the envelope as can be seen in Figure A.4(a). Then we determine earthquake depth by stacking along predicted travel times for different depths and in the end search for the maximum.

The result is shown in Figure A.4(b). The grey line shows the result for the 4 stations given in Figure A.4(a). The coloured lines show the result of the same calculation but with all stations in a distance of less than 100 km. At first one notices, that the energy in the trace grows with depth. For longer time windows the result gets smoother. For all time windows there is a maximum around 15 km which would indicate the earthquake being at this depth. At the depth of 10.3 given by the bulletin there is only a local maximum which can not be seen at all time window lengths.

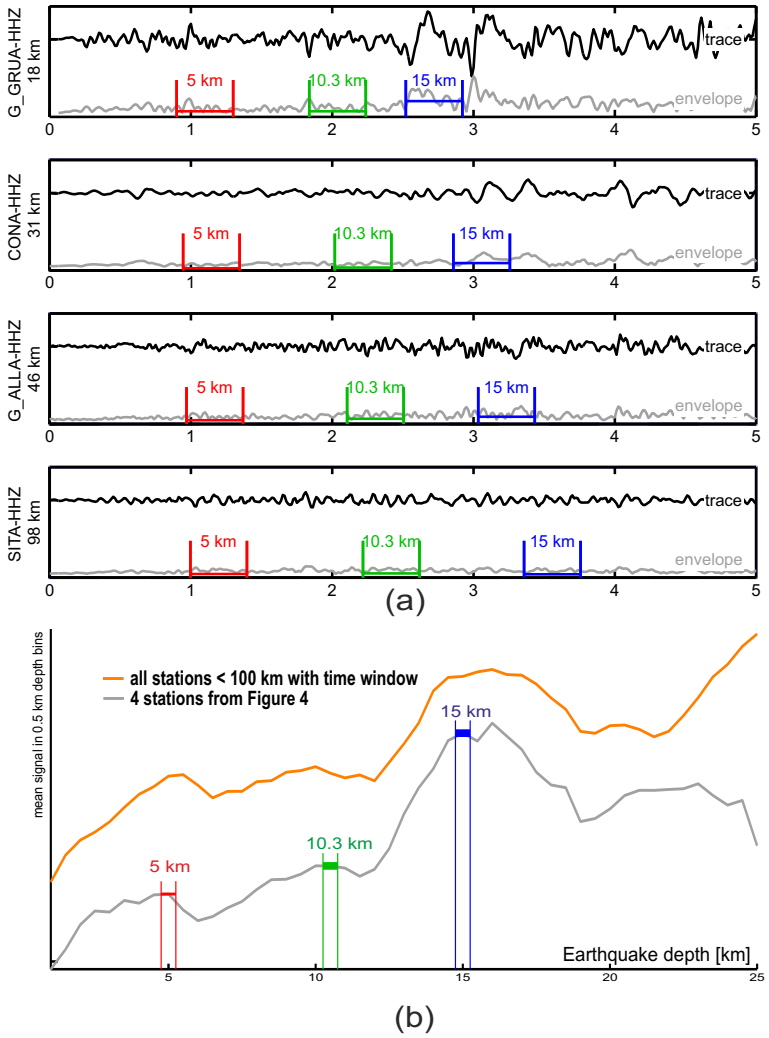

Figure A.4.: (a) Z-Traces (b) Stack.

A.5. Current research - Northern California

The San Andreas fault in Northern California is one of the most studied areas in seismology worldwide. Due to its numerous earthquakes and a very dense seismic station network it is a well suited area for testing.

To confirm our result from Austria, we selected 9 earthquakes between magnitude 2 to 4 with depths between 5 and 15 km recorded by the Northern California Seismic Network. One example is shown in Figure A.5.

Results from depth phase stacking in Northern California are encouraging.

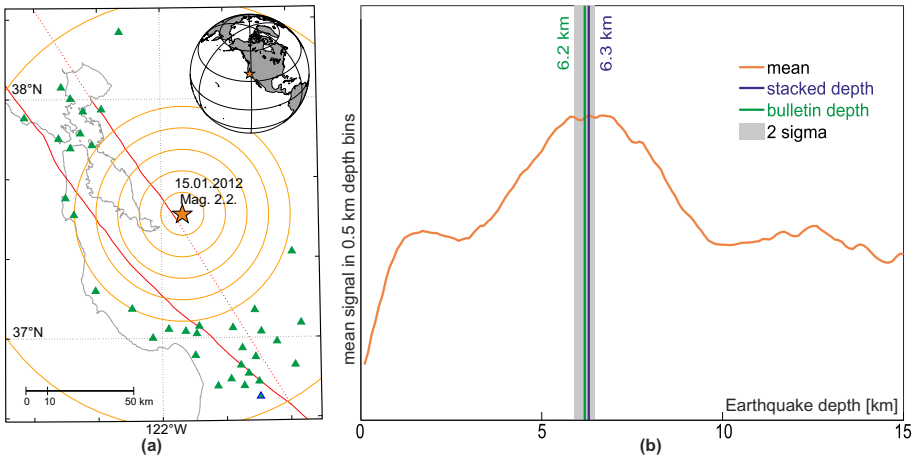

Figure A.5.: (a) Area and Stations (b) Depth Phase Stack.

Most events show approximately the depth given in the bulletin, although less stations than for the localisation are used.

Analysis with an even bigger catalogue of events from this area, containing more and smaller earthquakes, remains to be done still.

A.6. Summary and further research

Regional depth phases allow to estimate earthquake depth even if only a single depth phase with corresponding reference phase can be identified. The data used in this research do not let us identify any depth phases directly. Different methods for enhancing the depth phases were applied. One method was to stack the depth phases corresponding to their calculated move out. Preliminary results show that this method could also work in sparser networks than the one used, at least for the sPg phases tested.

The signal-to-noise ratio can be further enhanced by a polarization filter. This technique can be very useful for regional network processing. The Zentralanstalt für Meteorologie und Geodynamik (ZAMG) can not always derive earthquake depth from seismometer data, and has to set the earthquake depths in the bulletin from a priori knowledge.

Efforts have been made to get a better picture of earthquake depths in Austria e.g. by Lenhardt et al. (2007) where the depths were estimated from macroseismic data. Nevertheless the method used in that paper is not suitable for automated determination of earthquake parameters.

To improve the identification of depth phases, further research has to be done. The depth phase stacking has to be improved, possibly in combination with other techniques, and tested thoroughly on a larger dataset.

Appendix B.

Modeling local and regional wave propagation

This chapter has been presented as a poster at DGG 2013, Leipzig, Germany:

M.-T. Apoloner and G. Bokelmann, 2013, Modeling local and regional wave propagation

B.1. Overview

Seismograms reflect the combined effects of the source, recording instrument, ambient noise, and the propagation path. Especially at distances smaller than 10° the appearance of seismograms varies strongly because of the underlying crustal structure. This complicates record interpretation and phase identification severely. However, for earthquakes with small magnitudes, close distance records are the only ones available with sufficient signal.

Due to sparse seismic station coverage and the use of only Pg and Sg, localization cannot always be ensured. Using additional regional phases, also for depth estimation, can improve the result. At local and regional distances the challenge lies in robustly detecting and identifying these phases correctly, which are usually superimposed by the coda of the P- and S-phase and sometimes even arrive simultaneously. Synthetic seismograms can support our understanding how and when those phases can be used.

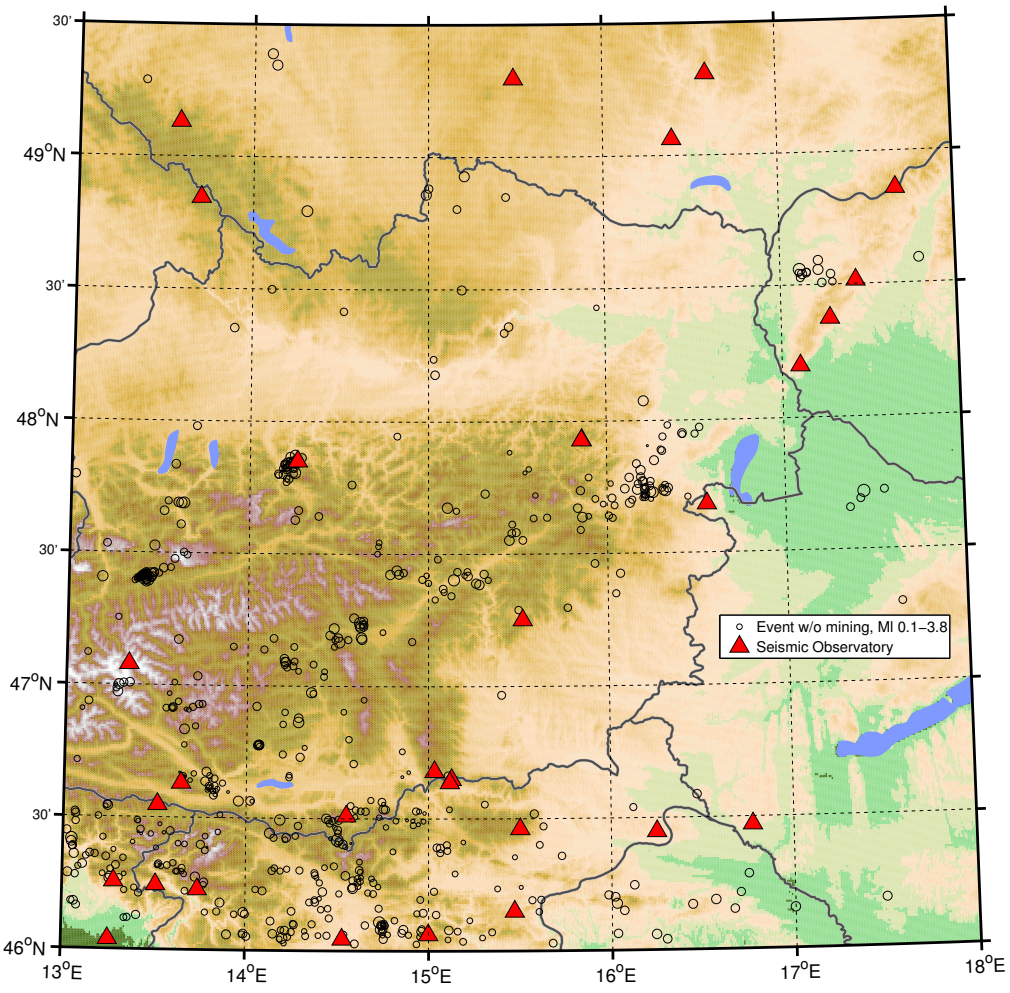

Figure B.1.: Observatories and Events in 2012 from ZAMG Bulletin.

B.2. Local and regional phases

Beyond direct phases normally used for localization, there are other useful phases according to literature: Pg with its reflection sPg (e.g. Ma and Eaton, 2011) as well as PvmP[1] with sPvmP, the so called regional depth phases. Amongst others, Ma and Motazedian (2012) mention that events at very shallow depths also generate strong Rayleigh waves.

[1]Naming convention according to TauP-Software by Crotwell et al. (1999), e.g. PmP is equal to PvmP and sPmP is equal to sPvmP

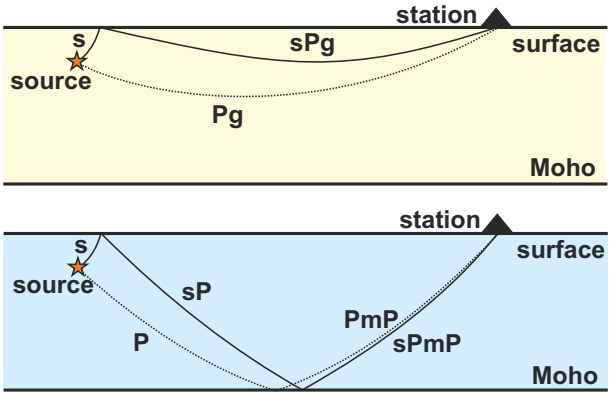

Figure B.2.: Regional depth phases adapted from Ma and Eaton (2011).

B.3. Synthetic Seismograms

B.3.1. Model and methods

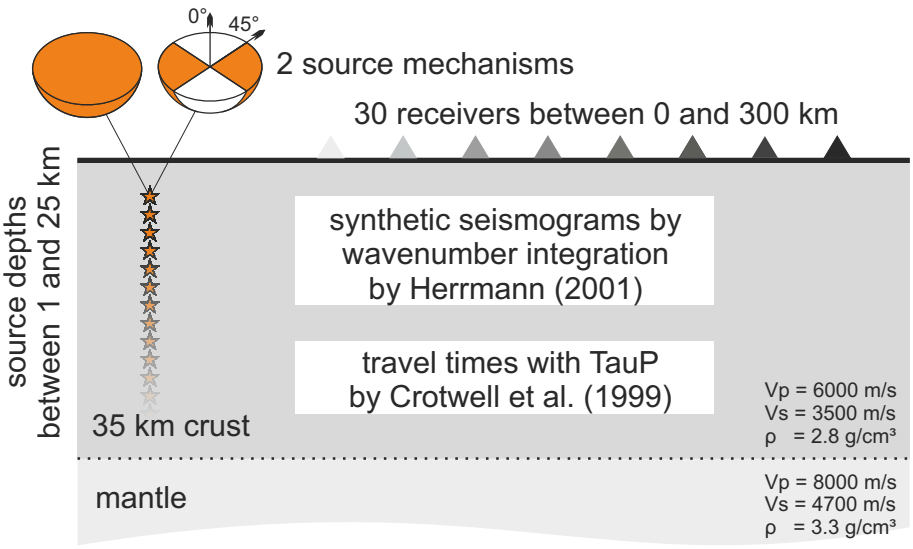

Figure B.3.: Model and methods.

B.3.2. Explosion source

Both figures above[2] show the synthetic seismograms of the vertical component calculated for an explosion source at different depths (Fig. B.4) and different distances (Fig. B.5). All traces are normalised to the lowest trace in each plot. The by far strongest phase visible is a regional Rayleigh phase at shallow depths. For shallow depths the time difference between the first arriving Pg phase and the later arriving PvmP (PmP) and Pn permits identification. However, PvmP and Pn arrive almost simultaneously at 100 km distance and are not separable. But comparison with the distance plot clearly shows that the PvmP phase is stronger developed by far. Regional depth phases like sPg, sPn and sPvmP are not generated as an explosion source does not emit S waves.

B.3.3. Strike slip source at at 0° and 45° azimuth

The figures above[3] show synthetic seismograms for a strike slip source with 45° strike and 90° dip at 2 different azimuths for the vertical component. All four plots are normalised to their respective lowest trace. The signals at 0° (Fig. B.6 and B.7) are generally stronger than at 45° azimuth (Fig. B.8 and B.9) and are scaled separately for better visibility.

Again the most prominent feature for shallow depths is the Rayleigh phase which attenuates with depth. As can be expected with the source mechanism used P arrivals are better visible at 0° azimuth and S arrivals at 45° azimuth. Interestingly there is almost no difference in the PvmP arrival.

B.4. Results and outlook

Although the model used for seismogram calculation is rather simple, identification of phases can be already quite complicated if the station is at an unfavourable distance or azimuth. In the real crust seismograms

[2]Figure B.4 and Figure B.5
[3]Figure B.6, B.7,B.8 and Figure B.10

get even harder to read. Figure B.10 shows a data example from Austria with calculated arrivals for the assumed strongest phases. If you compare synthetic with real seismograms, it becomes clear that the real seismograms show a more complex signal, where single phases are even harder to identify.

Further research will explore the possible usage of additional local phases for localization especially source depth. Also different ways to improve phase identification will be evaluated.

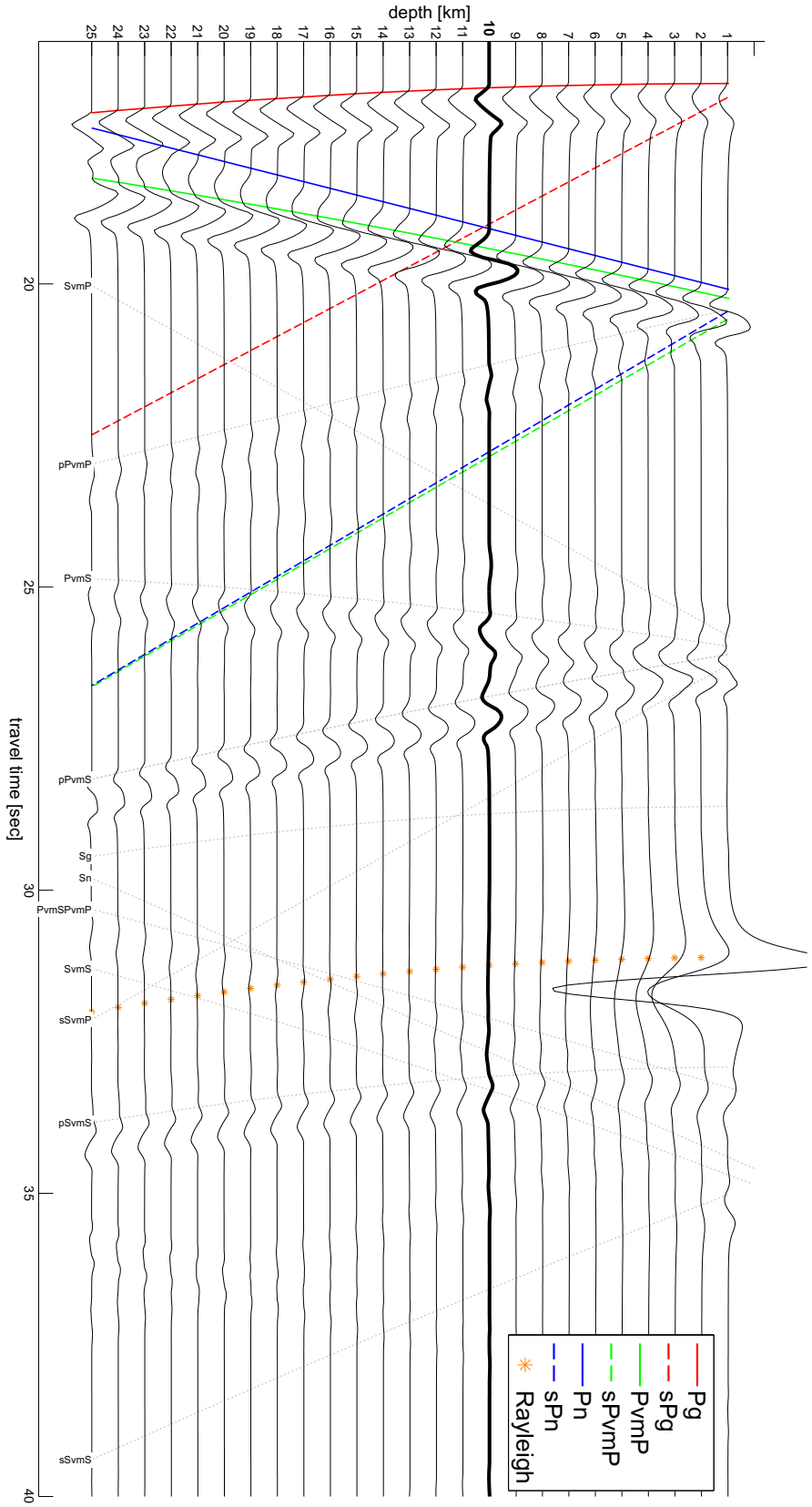

Figure B.4.: Synthetic seismograms at 100 km distance.

Figure B.5.: Synthetic seismograms for 10 km depth.

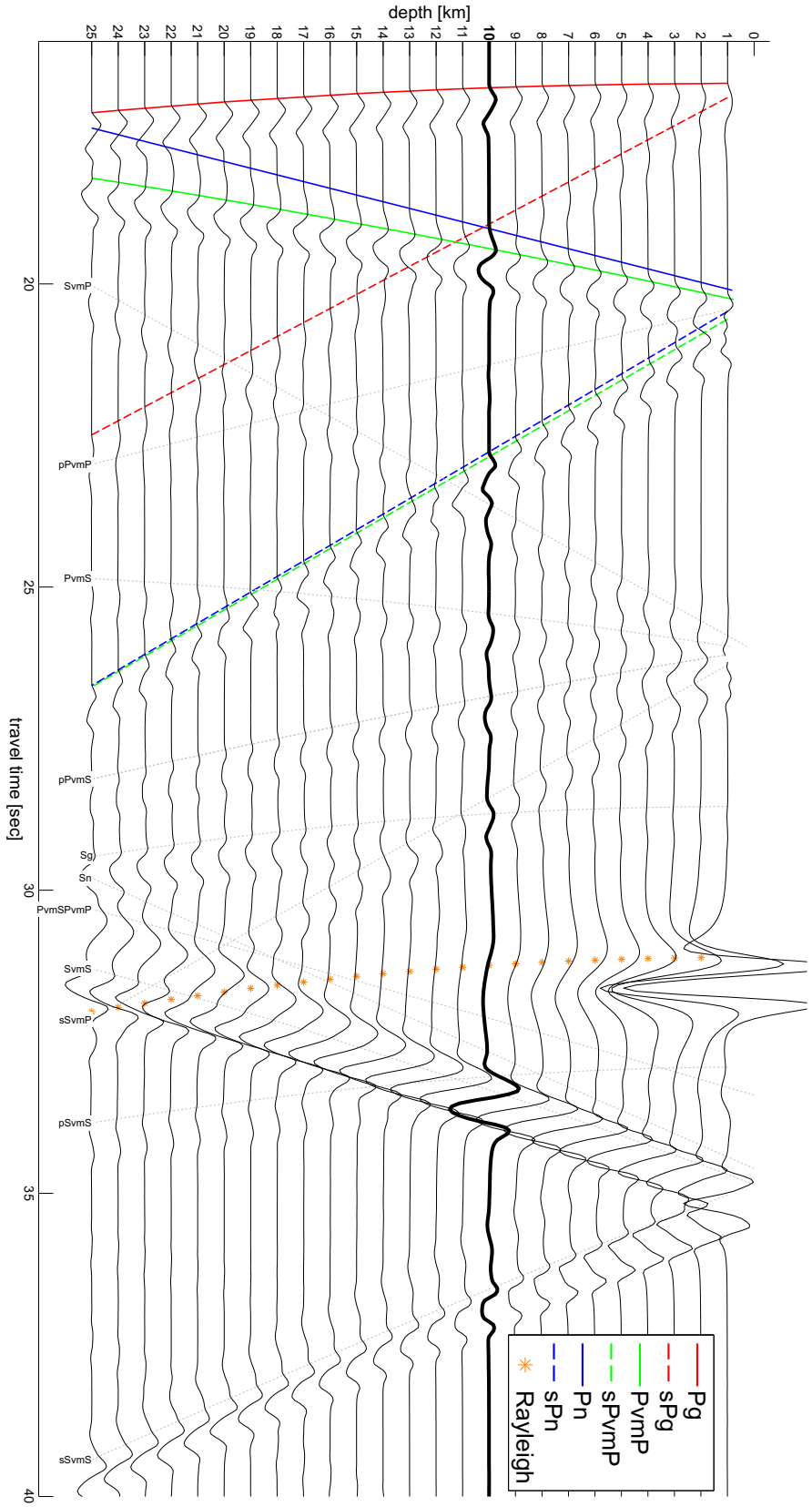

Figure B.6.: Synthetic seismograms at 100 km distance at 0°.

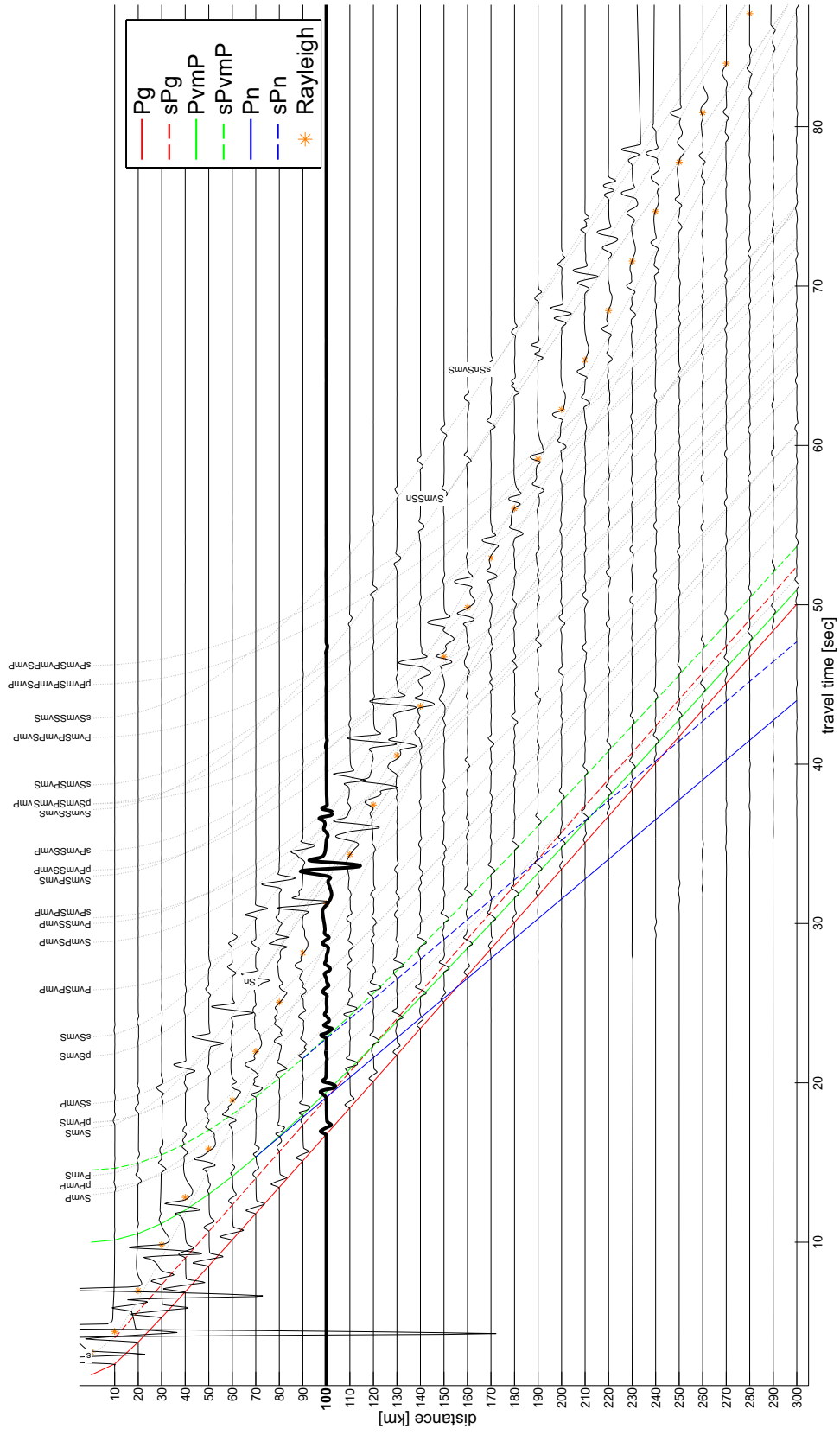

Figure B.7.: Synthetic seismograms for 10 km depth at 0°.

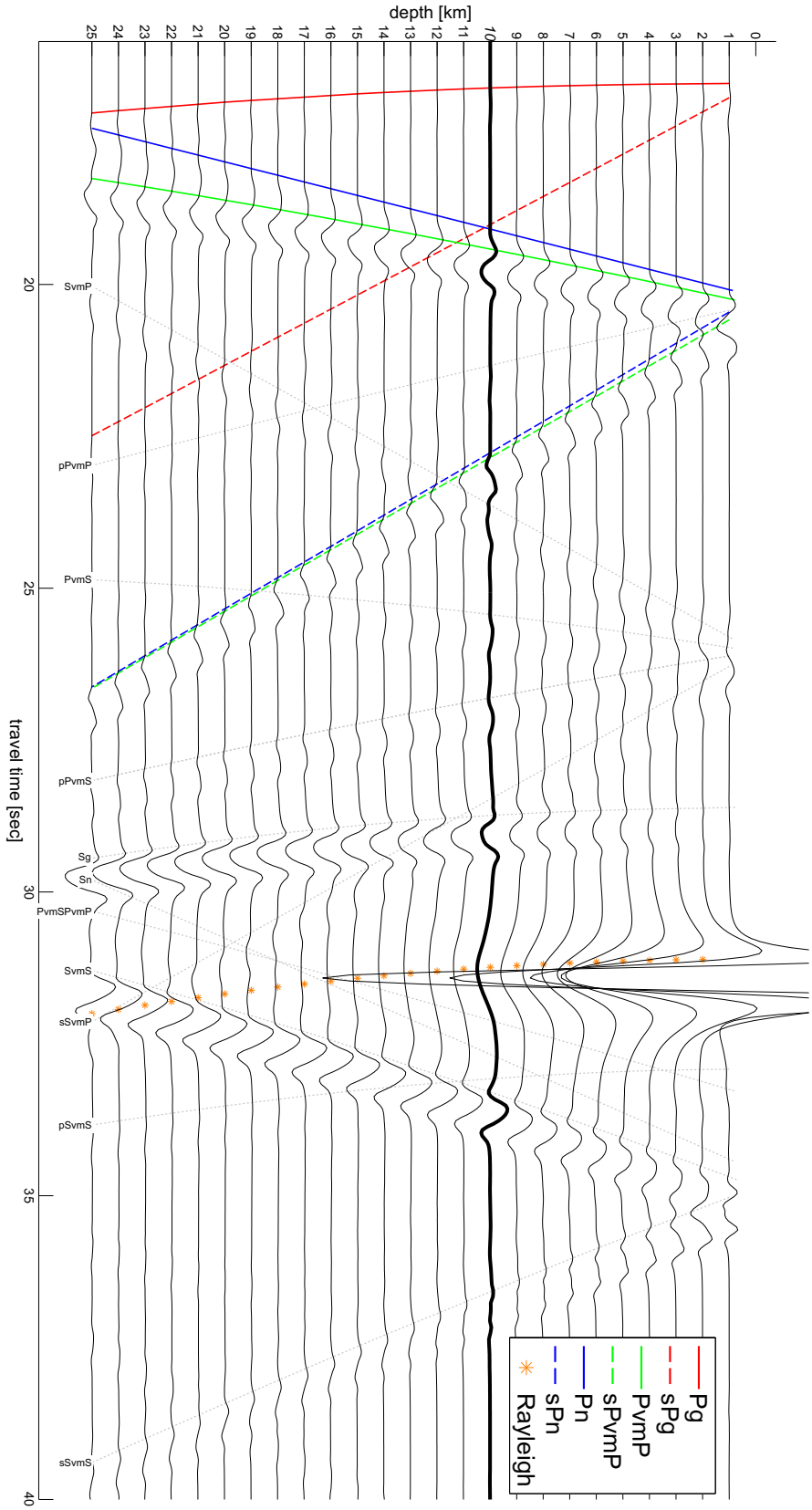

Figure B.8.: Synthetic seismograms at 100 km distance at 45°.

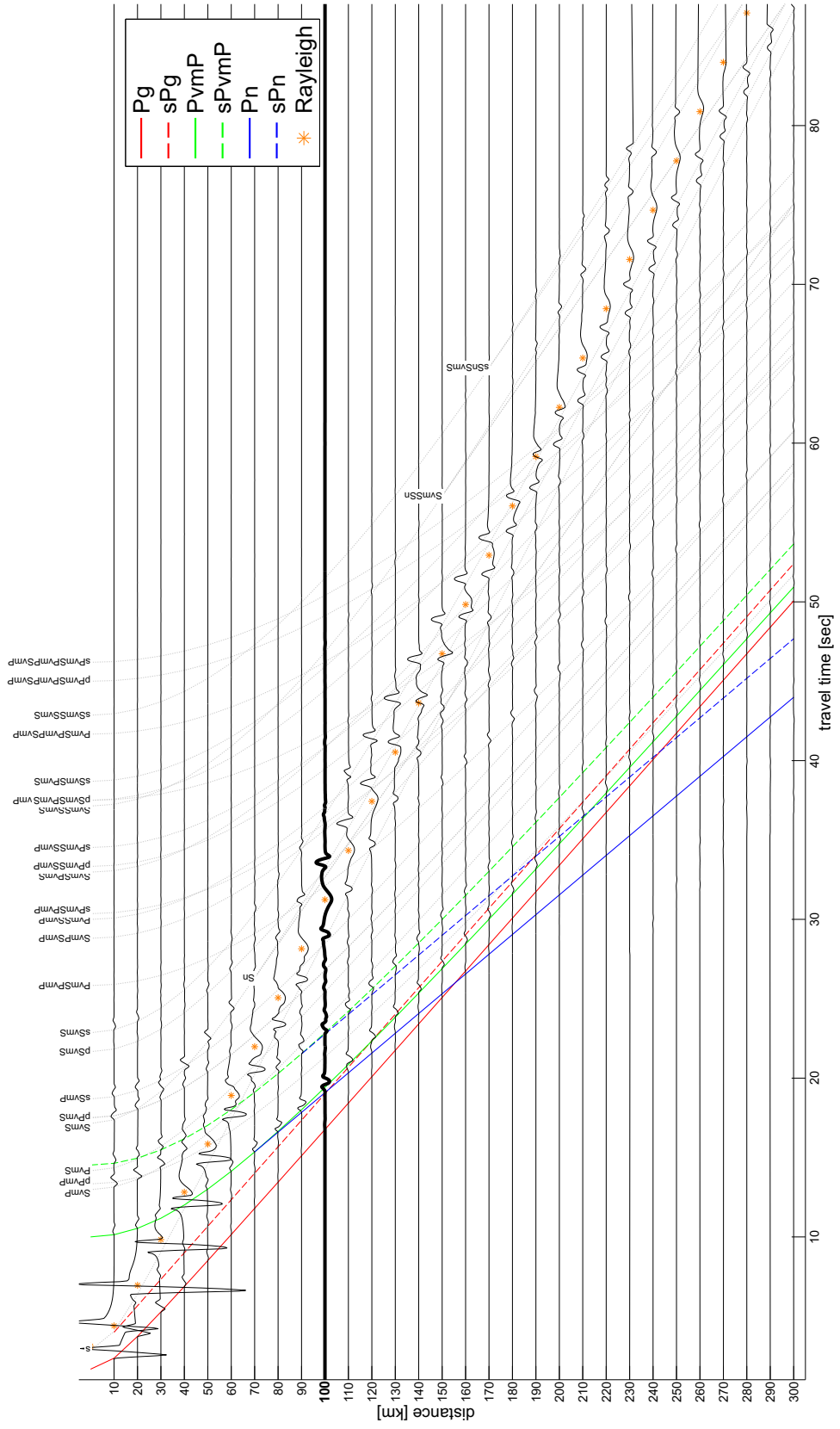

Figure B.9.: Synthetic seismograms for 10 km depth at 45°.

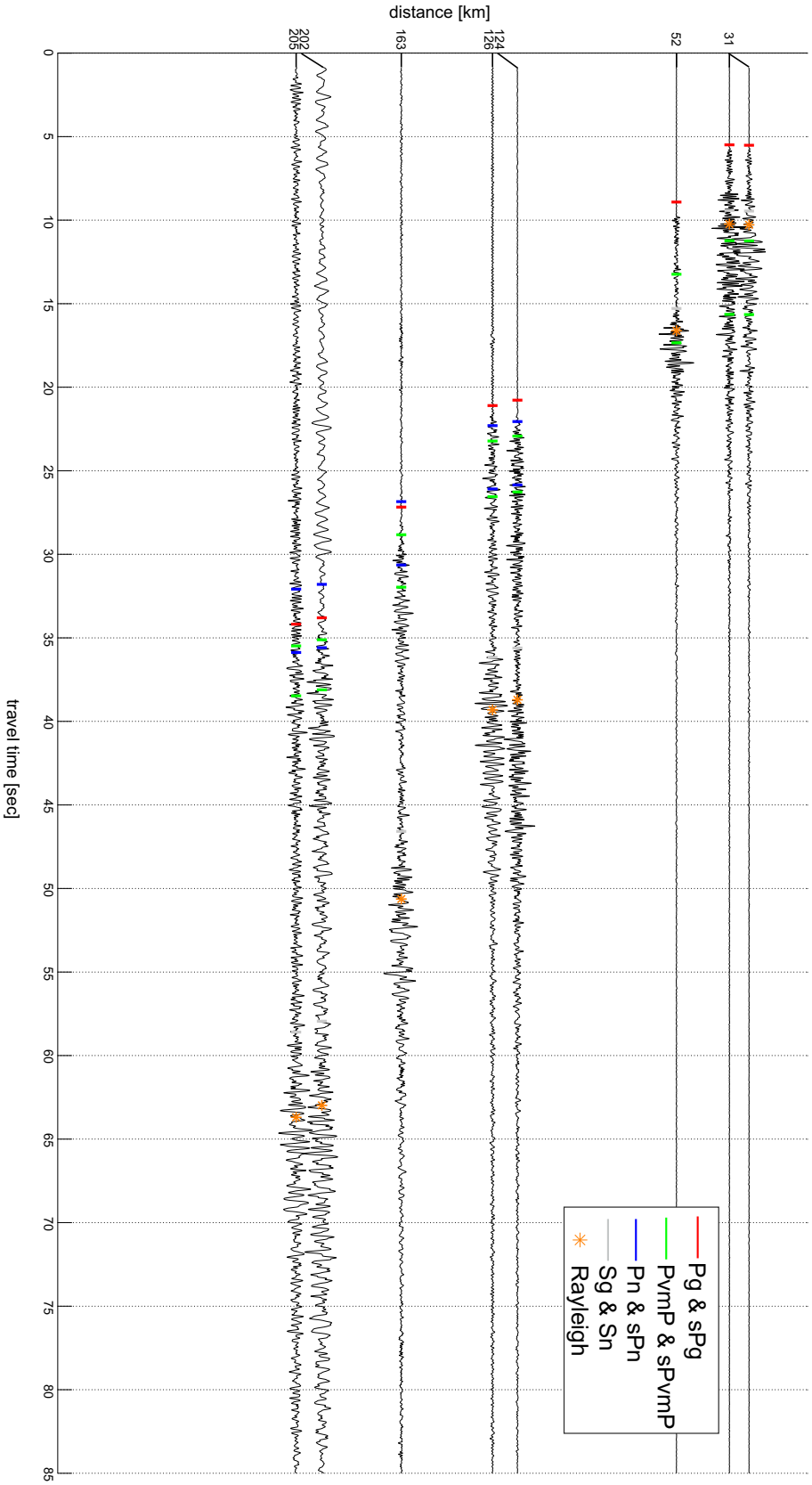

Figure B.10.: Earthquake at 10.3 km depth, Ml 2.7 recorded by ZAMG 31-08-2010.

Appendix C.

Academic curriculum vitae

Name: Dipl.-Ing. Maria-Theresia Apoloner, BSc.

Date of Birth: May 5, 1986

Academic employment

- June 2015 - November 2015: University of Vienna, Department of Meteorology and Geophysics, project assistent for geophysics
- June 2011 - May 2015: University of Vienna, Department of Meteorology and Geophysics, assistent "prae doc" for geophysics
- March 2011 – May 2011: Vienna University of Technology, Department for Geodesy and Geophysics, project assistent for geophysics
- October 2010 – March 2011: Vienna University of Technology, Department for Geodesy and Geophysics, study assistent for geophysics

Academic achievements

- **PhD studies** (Doctor of Philosopy) at University of Vienna, Topic: "The Ebreichsdorf 2013 earthquake series: location, interaction and wave propagation", Supervisor: Götz Bokelmann
- **MSc / Dipl.-Ing.** (Master of Science / Diplom-Ingenieurin) at Vienna University of Technology, Topic: "Einflüsse der Netzwerkkonfiguration auf Erdbebelokalisierungen", Supervisor: Ewald Brückl
- **BSc** (Bachelor of Science) at Vienna University of Technology, Topic: "Interpretation von Georadarmessungen in Eishöhlen", Supervisor: Michael Behm

Publications in peer reviewed journals

- Fuchs, F., Kolínský, P., Gröschl, G., **Apoloner, M.-T.**, Qorbani, E., Schneider, F. and Bokelmann, G., Site selection for a countrywide temporary network in Austria: noise analysis and preliminary performance, Advances in Geosciences, 41, 25-33, 2015, doi: 10.5194/adgeo-41-25-2015

- Tary, J.B., **Apoloner, M.-T.** and Bokelmann, G., 2015, Earthquake interactions during the 2013 Ebreichsdorf aftershock sequence, Austrian Journal of Earth Sciences, in press

- **Apoloner, M.-T.**, Tary, J.B. and Bokelmann, G., 2015, Ebreichsdorf 2014 earthquake series: relative location, Austrian Journal of Earth Sciences, in press

- Bianchi, I., Anselmi, M., **Apoloner, M.-T.**, Qorbani, E., Gribovszki, K. and Bokelmann, G., The installation campaign of 9 seismic stations around the KTB site to test anisotropy detection by the receiver function technique, Advances in Geosciences, 41, 11-23, 2015, doi: 10.5194/adgeo-41-11-2015

- **Apoloner, M.-T.** and Bokelman, G., Modelling and detection of regional depth phases at the GERES array, Adv. Geosci, 42, 5-10, 2015, doi: 10.5194/adgeo-41-5-2015

- **Apoloner, M.-T.**, Bokelmann, G., Bianchi, I., Brückl, E., Hausmann, H., Mertl, S. and Meurers, R., The 2013 earthquake series in the Southern Vienna Basin: location, Advances in Geosciences, 36, 77-80, doi: 10.5194/adgeo-36-77-2014, 2014

Conference contributions

- **AG Seismologie 2015**: AlpArray in Austria and Slovakia: The network and current status, Fuchs, F., Bokelmann, G., Kolinsky, P., Gröschl, G., Apoloner, M.-T. and AlpArray Working Group

- **TIDES Advanced Training School 2015**:

  - AlpArray Austria: The network and current status, Fuchs, F., Bokelmann, G., Bianchi, I., Apoloner, M.-T., Kolinsky, P. and AlpArray Working Group

  - Modelling Regional Depth Phases for Eastern Austria, Apoloner, M.-T. and Bokelmann, G.

- **SnT 2015**: Modeling Regional Depth Phases for Eastern Austria, Apoloner, M.-T. and Bokelmann, G.

- **EGU 2015**:

  - Implications of mainshock-aftershocks interactions during the 2013 Ebreichsdorf sequence, Austria, Tary, J. B., Apoloner, M.-T. and Bokelmann, G.

  - Working Group, AlpArray Austia - Illuminating the subsurface of Austria and understanding of Alpine geodynamics, Fuchs, F., Bokelmann, G., Bianchi, I., Apoloner, M.-T. and AlpArray Working Group

  - Modelling and Detection of Regional Depth Phases at the GERES Array, Apoloner, M.-T. and Bokelmann, G.

  - Ebreichsdorf 2013 Earthquake Series: Relative Location, Apoloner, M.-T. and Bokelmann, G.

  - Ground Truth and Application for the Anisotropic Receiver Functions Technique - Test site KTB: the installation campaign, Bianchi, I., Anselmi, M., Apoloner, M.-T., Qorbani, E., Gribovszki, K. and Bokelmann, G.

- **AGU 2014**: Crustal Anisotropy from Receiver Functions, Bianchi, I., Apoloner, M.-T., Qorbani, E., Lloyd, S., Gribovszki, K., Gerner, A., Arneitz, P., Jordakiev, P. and Bokelmann, G.

- **Earthquakes: nucleation, triggering, and relationship with aseismic processes, Cargese, Corsica, 2014**: Seismotectonic Analysis of an Earthquake Cluster in the Southern Vienna Basin, Apoloner, M.-T., Tary, J. B. and Bokelmann, G.

- **EGU 2014**: The 2013 Earthquake Series in the Southern Vienna Basin: Location, Apoloner, M.-T., Bianchi, I., Bokelmann, G., Brückl, E., Hausmann, H., Mertl, S. and Meurers, R.

- **SnT 2013, EGU 2013, DGG 2013**: Modelling Local and Regional Wave Propagation, Apoloner, M.-T. and Bokelmann, G.

- **PanGEO 2012**

  - Improving identification of regional depth phases in sparse networks, Apoloner, M.-T. and Bokelmann, G.

  - ALPAACT - Zielsetzung und Stand des Projektes, Brückl, E, Weber, R., Apoloner, M.-T., Gottwald, C., Mertl, S., Möller, G., Schurr, B., Umnig, E. and Weginger, S.

- **EGU 2012**: Improving identification of regional depth phases in sparse networks, Apoloner, M.-T. and Bokelmann, G.

- **EGU 2011**: Location performance of the ALPAACT seismic network, Apoloner, M.-T., Brückl, E., Brückl, J., Loderer, W., Mertl, S. and Schurr, B.

Participation in projects

- "EASI-13.4", (07/2014-07/2015), funded by the Austrian Academy of Science

- "AlpArray Austria", (2014-2017), FWF-Project: P26391 (Austrian Science Fund)

- "Ground Truth and Application for the Anisotropic Receiver Functions Technique", (2012-2014), FWF-Project: P 24218-N24 (Austrian Science Fund)

- "ALPAACT, Seismological and Geodetic Monitoring of Alpine-PAnnonian Active Tectonics", (2008-2013), funded by the Austrian Academy of Science."

Technical reports

ALPAACT, Seismological and Geodetic Monitoring of Alpine-PAnnonian Active Tectonics Final Report, 2008-2013, Brückl, E., Weber, R., Apoloner, M.T., Brückl, J., Loder, W., Maras, J., Mertl, S., Moeller, G., Schurr, B., Weginger, S. and Umnig, E.

List of Figures

1.1. Seismotectonic overview of the Vienna Basin: main tectonic units and generalized faults from GBA (2010) combined with earthquakes from the Austrian Earthquake Catalogue scaled by magnitude (ZAMG, 2014). Triangles indicate the positions of seismic stations available for this thesis. 2
1.2. Schematic RDP wavepaths adapted from Ma and Eaton (2011). 6
1.3. Regions with zones of detectable regional depth phases after Ma (2010) around Ebreichsdorf. 7
1.4. Stations of the seismic array GERES. White triangles mark seismic station positions with one component, black with three components. 8
1.5. Maximum power Rg/ Sg spectral ratio by Ma and Motazedian (2012). 9

2.1. Historical and recent seismicity in a 10 km radius around station VB01 at Ebreichsdorf Castle: Data until 12/2009 from Hammerl and Lenhardt (2013), 01/2010 - 09/2013 from ZAMG (2014), 10/2013 - 09/2015 from AutoDRM Bulletin using station VB01. 12
2.2. Seismic stations in and around Eastern Austria used in this thesis (ALPAACT, Ebreichsdorf 2000 and 2013) and from deployments starting afterwards (EASI in 2014 and AlpArrray in 2015). Permanent stations are marked in white, temporary ones in blue colour. 14
2.3. Isoseists available for earthquakes close to Ebreichsdorf: 1938 by Mifka and Trapp (1941) (top left), 2000 by Meurers et al. (2004) (top right), 2013 by ZAMG (bottom left), all intensity 5 isoseists (bottom right). 17

2.4. Beachballs of available focal mechanisms in the vicinity of Ebreichsdorf (for a complete list of references see Table 2.2. 18

3.1. Local station networks and earthquake distribution. 24

3.2. Comparison of epicentral locations calculated with different approaches. Profile A parallel to fault direction by Peresson and Decker (1997). 25

3.3. Earthquake depth distribution along profile A (see Figure 3.2 for details). 26

4.1. Seismotectonic overview of the Vienna Basin: main tectonic units and generalized faults from GBA (2010). Earthquakes from the Austrian Earthquake Catalog scaled by Magnitude (ZAMG, 2014). Triangles indicate the positions of seismic stations used in this study. 32

4.2. Seismotectonic overview of the area around the VBFS close the Ebreichsdorf. Micone faults (Hinsch and Decker, 2010) as solid grey lines. Earthquakes from the Austrian Earthquake Catalogue scaled by Magnitude (ZAMG, 2014), events mentioned in the text are labelled with year of occurrence. Triangles indicate the positions of seismic stations used in this study. Profile A – A' parallel to VBFS is used in Figure 4.4. 33

4.3. Focal mechanisms from left to right: main shocks in 2000 around Ebreichsdorf from SED (2006) and for the two main shocks in 2013 from Hausmann et al. (2014). 35

4.4. (a) The principle of double-difference calculation: Two earthquakes (star 1 and 2) with close-by location produce similar arrivals at a station (triangle), as they are affected nearly equally by small-scale velocity inhomogeneities. Using double-differences between the observed and calculated arrival times for the events reduces the effect of unmodeled velocity changes. (b) Seismograms (P-phases) of two events at station VRAC, showing a sub-sample shift that can be resolved using cross-correlation. 37

4.5. (left) Map of earthquakes near Ebreichsdorf area from 2000 and 2013. Initial locations for 2013 (grey) by Apoloner et al. (2014) with NonLinLoc, relocations with HypoDD (blue). Red dots show aftershocks of the earthquakes in 2000 (Anonymous, 2002). The red star indicates the location of main shocks in 2000 relative to the two 2013 main shocks, determined with S-P-differences (right) .Vertical profile along the VBFS with events projected on a vertical fault plane. 42

4.6. S-arrivals of main shocks of 2000 (1^{st}: 2000-1, 2^{nd}: 2000-2) and 2013 (1^{st}: 2013-1, 2^{nd}: 2013-2) earthquake series aligned at the P-arrival. S-arrival on 2013-1 is marked by a continuous grey line (picked using all three components). Dashed lines show 5 km distance difference to the station, based on S-P-time difference with respect to 2013-1 suggested S pick. Main shocks from the 2000 series are 4 km closer to station RSNA (top) and 4 km further from RWNA (bottom). 43

4.7. Cross-section along the fault indicating the constraint on relative location, suggested in Figure 4.6. 44

4.8. Inter-event coherence for both pairs of main shocks on the transverse component, (left) for the 2013 series, and (right) for the 2000 series (see text). Top x-axes shows $\lambda/4$, as a criterium for inter-event distance, marked grey for coherences above 0.7. 44

5.1. (a) Schematic tectonic settings around the Vienna basin (VB) modified after Brückl et al. (2010), showing the main faults and tectonic units. Light gray lines indicate country borders, and the black dot the position of Ebreichsdorf area. The position of this map is shown by the inset (b). Abbreviations: NAT, North Alpine Thrust fault; SEMP, Salzachtal-Ennstal-Mariazell–Puchberg fault; MML, Mur-Mürz-Linie fault; LAT, Lavant fault; VBFS: Vienna Basin Fault System. (c) Zoom in the area of Ebreichsdorf, showing the aftershock sequence of 2013 (red dots with sizes proportional to their local magnitude), the three temporary seismic stations deployed close to the sequence to record the aftershock sequence after the second main shock (black triangles), and the location of hydrological stations used to investigate potential hydrological manifestations related to the earthquake sequence (squares, see Appendix 5.10). The focal mechanisms by Hausmann et al. (2010) of both main shocks are shown on the left, and the black line indicates the idealized trace of the VBFS. 54

5.2. Zoomed view of the 2013 Ebreichsdorf earthquakes sequence (grey dots with sizes proportional to their local magnitude). VBFS: Vienna Basin Fault System (black line). . 55

5.3. Normalized seismic traces of the first and second main shock of the 2013 Ebreichsdorf sequence (top, instruments response removed), and displacement spectra corresponding to the part of the S-wave in these traces (bottom) indicated by the grey area, for two stations located approximately 20 km away from the two main shocks. RSNA is located 20 km to the NE, while RWNA is located 20 km to the SW. The seismic traces are aligned on the P-wave arrival times; P- and S-wave arrivals are indicated by black arrows. Note the high similarity in waveforms and frequency content of the two main events. At these stations, their corner frequencies are in the range 3-6 Hz. 56

5.4. a) Changes in Coulomb failure stress due to the first main event using the constant apparent friction model ($\mu' = 0.35$, see text for remaining parameters), calculated on faults with the orientation of the second main event. On top, changes in shear, normal and Coulomb stresses are shown on the left, middle and right, respectively (in map view). The locations of the four vertical cross-sections across the Coulomb stress change map are indicated by the gray lines. b) Changes in Coulomb failure stress due to the first main event using the isotropic model ($\mu' = 0.7$ and $B = 0.5$, see text for remaining parameters), calculated on faults with the orientation of the second main event (left). For comparison with the apparent friction model, two vertical cross-sections at the same locations are shown on the right. Positive stress changes are indicated by warm colors while negative changes are indicated by cold colours. Main shocks are indicated by red rectangles, aftershocks by dots with sizes proportional to their local magnitude and grey-coded depending on their occurrence time, and the VBFS by the black line. 65

5.5. (Right) Changes in shear $\Delta\tau_s$, normal $\Delta\sigma_n$ and Coulomb stress using the constant apparent friction $\Delta\sigma_c^{App}$ and isotropic $\Delta\sigma_c^{Iso}$ models, at the location of the aftershocks. The aftershocks are numbered in chronological order. (Left) Vertical cross-section along the strike of the VBFS with the complete aftershock sequence projected on it (see Fig. 5.4 for location of cross-section D-D'). The size of earthquake symbols is proportional to their local magnitude ML. They are colour-coded according to the polarity of the change in $\Delta\sigma_c^{App}$. The two grey hatched patches delimit the locations of the main shocks with the first 10 aftershocks, and the next 8 aftershocks. 66

5.6. a) Normalized time series of water level fluctuations recorded at 9 hydrological stations located in Ebreichsdorf area (Fig. 5.1) for the period 1966 - 2014. Black time series correspond to weekly measurements and grey time series to hourly measurements. Vertical lines correspond to the time of the main shocks in Ebreichsdorf sequences in 2000 and 2013. b) Zoom on the period 01/08/2013 – 31/11/2013. c) Precipitations (in mm) in the region of Ebreichsdorf, Seibersdorf being the closest station located less than 10 km away from Ebreichsdorf. Note the correlation between the increase in water level at almost all stations (except 300251) on September 16, 2013, and the peak in precipitations of approximately 50 mm on the same day. 67

6.1. Right panel: schematic map of the Vienna Basin with surrounding tectonic units and main faults shown together with the focal mechanism of the Ml 4.2 earthquake from 20/09/2013 in Ebreichsdorf by Hausmann et al. (2014). Top left: layout of seismic array GERES with 1-component stations (white triangles) and 3-component stations (black triangles). Bottom left: P and S velocity model for the area by Hausmann et al. (2010). 72

6.2. Sketch figure for different RDP wavepaths adapted from Ma and Eaton (2011): (a) Pg and sPg, (b) Pn and sPn, (c) Moho reflection PmP and sPmP, augmented by (d) Mid crust reflection PbP and sPbP. 74

6.3. Synthetic seismograms of the vertical component for the central array station GEA0 for depths ranging from 0 to 25 km. Phases are arrivals annotated ackording to wave type. e.g. sPn seems to be visible, but is strongly overlapped by other phases. In addition to the RDPs, the p5PbP is recognizable. 75

6.4. Lateral propagation of PmP (top left panel) and sPmP (bottom left panel) for a strike-slip earthquake in Ebreichsdorf at 10.5 km depth from synthetic traces: right panel shows combined strength of phases (grey shades) and area of minimal visible amplitude for both phases (white line). 76

6.5. Areas of visibility for both phases of a depth phase pair derived from synthetic seismograms. 76

6.6. Vespagrams for synthetic data for the first earthquake at GERES and real data for all selected earthquakes from Table 1. Vespagrams are aligned on PmP arrival and phases were calculated with TauP of Crotwell et al. (1999). 77

6.7. Polarization analysis for synthetic data (black) and earthquakes (grey). From top to bottom: backazimuth, incidence angle, rectilinearity, planarity and ellipticity. 78

7.1. Regional depth phases and their reference phases, adapted from Ma and Eaton (2011): (a) Pg and sPg, (b) PbP and sPbP, (c) PmP and sPmP, (d) Pn and sPn. 84

7.2. Travel times for P waves, their corresponend depth phases and fastest pure S wave for an event at 10.5 km depth at distances from 0 to 400 km. 86

7.3. Travel time difference between all P wave (Pg, PbP, PmP and Pn) and converted wave (sPg, sPbP, sPmP and sPn) for an event at 10.5 depth at distances from 0 to 400 km. 86

7.4. Velocity model from Hausmann et al. (2010) and same model with the top layer velocity reduced by half. Figure adapted from Apoloner and Bokelmann (2015b). 87

7.5. Synthetic seismograms with calculated Pg and sPg arrivals for a strike-slip source at 10.5 km depth at epicentral distances up to 400 km calculated with the velocity models from Figure 7.4. 89

7.6. Synthetic seismograms with calculated PmP and sPmP arrivals for a strike-slip source at 10.5 km depth at epicentral distances up to 400 km calculated with the velocity models from Figure 7.4. 90

7.7. Synthetic seismograms with calculated Pn and sPn arrivals for a strike-slip source at 10.5 km depth at epicentral distances up to 400 km calculated with the velocity models from Figure 7.4. 91

7.8. Synthetic seismograms with calculated PbP and sPbP arrivals for a strike-slip source at 10.5 km depth at epicentral distances up to 400 km calculated with the velocity models from Figure 7.4. 92
7.9. Sections from Figure 7.8 aligned along arrival of PbP and sPbP. Synthetic seismograms calculated with velocity model from Hausmann et al. (2010) in black and with half velocity in the top layer to simulate sedimentary basin in red. 93
7.10. a) Strike-slip focal mechanism from Ebreichsdorf 2013 from Hausmann et al. (2014) b) Explosion c) Thrust-type focal mechanism from Ma (2012). 93
7.11. Wave propagation for focal mechanism (a) from Figure 7.10 (strike-slip). Each row shows the maximum amplitude of each phase of a pair and their combined amplitude. Range rings from 50 - 400 km in 50 km steps. 94
7.12. Wave propagation for focal mechanism (b) from Figure 7.10 (explosion). Each row shows the maximum amplitude of each phase of a pair and their combined amplitude. Range rings from 50 - 400 km in 50 km steps. 95
7.13. Wave propagation for focal mechanism (c) from Figure 7.10 (thrust-type). Each row shows the maximum amplitude of each phase of a pair and their combined amplitude. Range rings from 50 - 400 km in 50 km steps. 97

A.1. Regional Depth Phases adapted from Ma and Eaton (2011). 106
A.2. Areas of well developed regional depth phases. 107
A.3. Polarization filter. 108
A.4. (a) Z-Traces (b) Stack. 109
A.5. (a) Area and Stations (b) Depth Phase Stack. 110

B.1. Observatories and Events in 2012 from ZAMG Bulletin. . . 114
B.2. Regional depth phases adapted from Ma and Eaton (2011). 115
B.3. Model and methods. 115
B.4. Synthetic seismograms at 100 km distance. 118
B.5. Synthetic seismograms for 10 km depth. 119
B.6. Synthetic seismograms at 100 km distance at 0°. 120
B.7. Synthetic seismograms for 10 km depth at 0°. 121
B.8. Synthetic seismograms at 100 km distance at 45°. 122

B.9. Synthetic seismograms for 10 km depth at 45°. 123
B.10. Earthquake at 10.3 km depth, Ml 2.7 recorded by ZAMG 31-08-2010. 124

List of Tables

1.1. RDP detectability adapted from Ma (2010). 6

2.1. Earthquakes from the revised Earthquake Catalog for Lower Austria by Hammerl and Lenhardt (2013) with intensity $\geq$ 5.0 in a 10 km radius around Ebreichsdorf, supplemented by the main shocks from 2013. 13
2.2. Nodal planes and sources of focal mechanisms in the vicinity of Ebreichsdorf. 18

3.1. Hypocentral parameters with LOCSAT and NonLinLoc, events located with LOCSAT using VB01, VB02 and VB03 are marked with * at the beginning of the line. 28

4.1. Location of temporary seismic stations deployed on 03/10/2013 around Ebreichsdorf for recording of aftershocks. 34
4.2. Location with different velocity models (initial locations are from Apoloner et al. (2014); see text. 39
4.3. Initial locations used for relative location calculation with HypoDD. 40
4.4. Relocated earthquakes from 2013 around Ebreichsdorf. Ml taken from ZAMG Bulletin. CC and Cat DT give the number of cross-correlation and catalogue double-difference times used for location. 41

6.1. Hypocentral parameters of earthquakes with local magnitude above 2.0 from Apoloner and Bokelmann (2015a) sorted by focal depth. 73

Bibliography

A. Alinaghi and F. Krüger. Seismic array analysis and redetermination of depths of earthquakes in Tien-Shan: implications for strength of the crust and lithosphere. *Geophysical Journal International*, 198(2):1111–1129, 2014. doi: 10.1093/gji/ggu141. URL http://gji.oxfordjournals.org/content/198/2/1111.abstract.

Anonymous. Investigation the aftershocks of the eartquake of Ebreichsdorf from 11th July, 2000 near Vienna. Report of the on site inspection group of the CTBTO, Comprehensive Test Ban Treaty Organization, Vienna, Austria, 2002.

M.-T. Apoloner and G. Bokelmann. Improving identification of regional depth phases in sparse networks. In *PanGEO Austria*, PanGEO, Salzburg, Austria, 2012.

M.-T. Apoloner and G. Bokelmann. Ebreichsdorf 2013 earthquake series: relative location. In *EGU General Assembly*, EGU General Assembly Conference Abstracts, Vienna, Austria, 2015a.

M.-T. Apoloner and G. Bokelmann. Modeling and detection of regional depth phases at the GERES array. *Advances in Geosciences*, 41:5–10, 2015b. doi: 10.5194/adgeo-41-5-2015. URL http://www.adv-geosci.net/41/5/2015/.

M.-T. Apoloner, G. Bokelmann, I. Bianchi, E. Brückl, H. Hausmann, S. Mertl, and R. Meurers. The 2013 earthquake series in the Southern Vienna Basin: location. *Advances in Geosciences*, 36:77–80, 2014. doi: 10.5194/adgeo-36-77-2014.

M.-T. Apoloner, J. B. Tary, and G. Bokelmann. The Ebreichsdorf 2013 earthquake series: relative location. *Austrian Journal of Earth Sciences*, 108/2(108), 2015.

G. Bada, F. Horváth, P. Dövényi, P. Szafián, G. Windhoffer, and S. Cloetingh. Present-day stress field and tectonic inversion in the Pannonian basin. *Global and Planetary Change*, 58(1–4):165 – 180, 2007. ISSN 0921-8181. doi: http://dx.doi.org/10.1016/j.gloplacha.2007.01.007. URL http://www.sciencedirect.com/science/article/pii/S0921818107000616. TOPO-EUROPE: the Geoscience of Coupled Deep Earth-Surface Processes.

S. Baisch and G. Bokelmann. Seismic waveform attributes before and after the Loma Prieta earthquake: Scattering change near the earthquake and temporal recovery. *Journal of Geophysical Research: Solid Earth*, 106(B8): 16323–16337, 2001. ISSN 2156-2202. doi: 10.1029/2001JB000151. URL http://dx.doi.org/10.1029/2001JB000151.

N. M. Beeler, R. W. Simpson, S. H. Hickman, and D. A. Lockner. Pore fluid pressure, apparent friction, and Coulomb failure. *Journal of Geophysical Research: Solid Earth*, 105(B11):25533–25542, 2000. ISSN 2156-2202. doi: 10.1029/2000JB900119. URL http://dx.doi.org/10.1029/2000JB900119.

M. Behm, E. Brückl, W. Chwatal, and H. Thybo. Application of stacking and inversion techniques to three-dimensional wide-angle reflection and refraction seismic data of the Eastern Alps. *Geophysical Journal International*, 170:275–298, 2007a.

M. Behm, E. Brückl, and U. Mitterbauer. A new seismic model of the Eastern Alps and its relevance for geodesy and geodynamics. *VGI Österrreichische Zeitschrift für Vermessung & Geoinformation*, 2:121–133, 2007b.

A. Beidinger and K. Decker. 3d geometry and kinematics of the Lassee flower structure: Implications for segmentation ans seismotectonics of the Vienna Basin strike-slip fault, Austria. *Tectonophysics*, 499:22–40, 2011.

A. Bent and H. Perry. Depths of Eastern Canadian earthquakes from regional datas. *Seismological Research Letters*, 73(2):273–284, 2002. doi: 10.1785/gssrl.73.2.273. URL http://srl.geoscienceworld.org/content/73/2/273.abstract.

M. Beyreuther, R. Barsch, L. Krischer, T. Megies, Y. Behr, and J. Wassermann. ObsPy: A python toolbox for seismology. *Seismological Research Letters*, 81(3):530–533, 2010.

I. Bianchi, M. Behm, E. M. Rumpfhuber, and G. Bokelmann. A new seismic data set on the depth of the Moho in the alps. *Pure and Applied Geophysics*, 172:295–308, 2015. doi: 10.1007/s00024-014-0953-1.

G. Bock. Depth phases from local earthquakes. *BMR Journal of Australian Geology & Geophysics*, 13:275–279, 1993.

G. Bock, G. Grünthal, and K. Wylegalla. The 1985/86 Western Bohemia earthquakes: Modelling source parameters with synthetic seismograms. *Tectonophysics*, 261:139–146, 1996.

J. L. Bonner, D. T. Reiter, A. M. Roscal, and R. H. Shumwal. Cepstral f-statistic performance at regional distances. In *23rd Seismic Research Review: Worldwide Monitoring of Nuclear Explosions*, 2001.

P. Bormann, B. Engdahl, and R. Kind. Seismic wave propagation and earth models. In Peter Bormann, editor, *New Manual of Seismological Observatory Practice 2 (NMSOP2)*, chapter 2, pages 1–105. Potsdam: Deutsches GeoForschungsZentrum GFZ, 2012. doi: 10.2312/GFZ.NMSOP-2_ch2.

M. Bouchon. The state of stress on some faults of the San Andreas system as inferred from near-field strong motion data. *Journal of Geophysical Research: Solid Earth*, 102(B6):11731–11744, 1997. ISSN 2156-2202. doi: 10.1029/97JB00623. URL http://dx.doi.org/10.1029/97JB00623.

M. Bouchon, H. Karabulut, M. Aktar, S. Özalaybey, J. Schmittbuhl, and M.-P. Bouin. Extended nucleation of the 1999 Mw 7.6 Izmit earthquake. *Science*, 331(6019):877–880, 2011. doi: 10.1126/science.1197341. URL http://www.sciencemag.org/content/331/6019/877.abstract.

E. Brückl, M. Behm, K. Decker, M. Grad, A. Guterch, G. R. Keller, and H. Thybo. Crustal structure and active tectonics in the Eastern Alps. *Tectonics*, 29(2), 2010. ISSN 1944-9194. doi: 10.1029/2009TC002491. URL http://dx.doi.org/10.1029/2009TC002491.

E. Brückl, R. Weber, M.-T. Apoloner, C. Gottwald, S. Mertl, G. Möller, B. Schurr, E. Umnig, and S. Weginger. ALPAACT - zielsetzung und stand des projektes. In *PanGEO Austria*, Salzburg, Austria, 2012.

E. Brückl, R. Weber, M.-T. Apoloner, J. Brückl, W. Loder, J. Maras, S. Mertl, G. Möller, B. Schurr, S. Weginger, and E. Umnig. Seismological and geodetic monitoring of Alpine-PAnnonian Active Tectonics - final report. Technical report, Österreichische Akademie der Wissenschaften, Vienna, Austria, 2014.

J. Byerlee. Friction of rocks. *Pure and Applied Geophysics*, 116(4-5):615–626, 1978. ISSN 0033-4553. doi: 10.1007/BF00876528. URL http://dx.doi.org/10.1007/BF00876528.

K. H. Chen, R. Bürgmann, and R. M. Nadeau. Do earthquakes talk to each other? triggering and interaction of repeating sequences at Parkfield. *Journal of Geophysical Research: Solid Earth*, 118(1):165–182, 2013. ISSN 2169-9356. doi: 10.1029/2012JB009486. URL http://dx.doi.org/10.1029/2012JB009486.

M. Cocco and J. R. Rice. Pore pressure and poroelasticity effects in Coulomb stress analysis of earthquake interactions. *Journal of Geophysical Research: Solid Earth*, 107(B2):ESE 2–1–ESE 2–17, 2002. ISSN 2156-2202. doi: 10.1029/2000JB000138. URL http://dx.doi.org/10.1029/2000JB000138.

H. P. Crotwell, T. J. Owens, and J. Ritsema. The TauP toolkit: Flexible seismic travel-time and ray-path utilities. *Seismological Research Letters*, 70:154–160, 1999.

Z. Ḉakir, S. Ergintav, H. Özener, U. Dogan, A. M. Akoglu, M. Meghraoui, and R. Reilinger. Onset of aseismic creep on major strike-slip faults. *Geology*, 40(12):1115–1118, 2012. doi: 10.1130/G33522.1. URL http://geology.gsapubs.org/content/40/12/1115.abstract.

B. D. E. Dando, G. W. Stuart, G. A. Houseman, E. Hegedues, E. Brückl, and S. Radovanovic. Teleseismic tomography of the mantle in the Carpathian–Pannonian region of Central Europe. *Geophysical Journal International*, 186(1):11–31, 2011. ISSN 1365-246X. doi: 10.1111/j.1365-246X.2011.04998.x. URL http://dx.doi.org/10.1111/j.1365-246X.2011.04998.x.

G. Daniel, E. Prono, F. Renard, F. Thouvenot, S. Hainzl, D. Marsan, A. Helmstetter, P. Traversa, J. L. Got, L. Jenatton, and R. Guiguet.

Changes in effective stress during the 2003-2004 Ubaye seismic swarm, France. *Journal of Geophysical Research: Solid Earth*, 116(B1), 2011. ISSN 2156-2202. doi: 10.1029/2010JB007551. URL http://dx.doi.org/10.1029/2010JB007551. B01309.

K. Decker, H. Peresson, and R. Hinsch. Active tectonics and Quaternary basin formation along the Vienna Basin transform fault. *Quaternary Science Reviews*, 24(3,Äì4):305–320, 2005. ISSN 0277-3791. doi: http://dx.doi.org/10.1016/j.quascirev.2004.04.012. URL http://www.sciencedirect.com/science/article/pii/S0277379104002033. Neotectonics and Quaternary fault-reactivation in Europe's intrap late lithosphere.

N. Deichmann and M. Garcia-Fernandez. Rupture geometry from high-precision relative hypocentre locations of microearthquake clusters. *Geophysical Journal International*, 110:501–517, 1992.

M. L. Doan, E. E. Brodsky, Y. Kano, and K. F. Ma. In situ measurement of the hydraulic diffusivity of the active Chelungpu Fault, Taiwan. *Geophysical Research Letters*, 33(16), 2006. ISSN 1944-8007. doi: 10.1029/2006GL026889. URL http://dx.doi.org/10.1029/2006GL026889. L16317.

J. E. Ebel and K.-P. Bonjer. Moment tensor inversion of small earthquakes in southwestern Germany for the fault plane solution. *Geophysical Journal International*, 101(1):133–146, 1990. doi: 10.1111/j.1365-246X.1990.tb00763.x. URL http://gji.oxfordjournals.org/content/101/1/133.abstract.

F. Fuchs, G. Bokelmann, I. Bianchi, M.-T. Apoloner, and "AlpArray Working Group". AlpArray Austria - Illuminating the subsurface of Austria and understanding of Alpine geodynamics. In *EGU General Assembly*, EGU General Assembly Conference Abstracts, Vienna, Austria, 2015.

S. S. N. Gamage, N. Umino, A. Hasegawa, and S. H. Kirby. Offshore double-planed shallow seismic zone in the NE Japan forearc region revealed by sP depth phases recorded by regional networks. *Geophysical Journal International*, 178(1):195–214, 2009. doi: 10.1111/j.1365-246X.2009.04048.x. URL http://gji.oxfordjournals.org/content/178/1/195.abstract.

GBA. Die Energieausbreitung ostalpiner Beben. In Geologische Bundesanstalt, editor, *Der Geologische Aufbau Österreichs*, pages 510–512. Springer Vienna, 1980. ISBN 978-3-7091-3745-1. doi: 10.1007/978-3-7091-3744-4_25. URL http://dx.doi.org/10.1007/978-3-7091-3744-4_25.

GBA. Datensatz KM500 Austria – Geologie. Technical report, Geologische Bundesanstalt, Vienna, 2010.

R. J. Geller. Scaling relations for earthquake source parameters and magnitudes. *Bulletin of the Seismological Society of America*, 66:1501–1523, 1976.

R. J. Geller and C. S. Müller. Four similar earthquakes in central California. *Geophysical Research Letters*, 7(10):821–824, 1980. ISSN 1944-8007. doi: 10.1029/GL007i010p00821. URL http://dx.doi.org/10.1029/GL007i010p00821.

GEVN. Moment tensor solution. Technical report, GEOFON Virtual Network, Potsdam, Germany, 2013. URL http://geofon.gfz-potsdam.de/eqinfo/event.php?id=gfz2013thyb.

J.-P. Gratier, J. Richard, F. Renard, S. Mittempergher, M.-L. Doan, G. Di Toro, J. Hadizadeh, and A.-M. Boullier. Aseismic sliding of active faults by pressure solution creep: evidence from the San Andreas Fault Observatory at depth. *Geology*, 39(12):1131–1134, 2011. doi: 10.1130/G32073.1. URL http://geology.gsapubs.org/content/39/12/1131.abstract.

G. Grenerczy, A. Kenyeres, and I. Fejes. Present crustal movement and strain distribution in Central Europe inferred from GPS measurements. *Journal of Geophysical Research: Solid Earth*, 105(B9):21835–21846, 2000. ISSN 2156-2202. doi: 10.1029/2000JB900127. URL http://dx.doi.org/10.1029/2000JB900127.

G. Grenerczy, G. Sella, S. Stein, and A. Kenyeres. Tectonic implications of the GPS velocity field in the northern Adriatic region. *Geophysical Research Letters*, 32(16), 2005. ISSN 1944-8007. doi: 10.1029/2005GL022947. URL http://dx.doi.org/10.1029/2005GL022947. L16311.

G. Grünthal. European macroseismic scale EMS-98. Technical report, Cahiers du Centre Europeen de Geodynamique et de Seismologie, 1998.

R. Gutdeutsch and K. Aric. *Geodynamics of the Eastern Alps*, chapter Geophysical Aspects of the Crustal Structures of the Eastern Alps, pages 309 – 324. Deuticke, Wien, 1987.

R. Gutdeutsch, C. Hammerl, I. Mayer, and K. Vocelka. *Erdbeben als historisches Ereignis - Die Rekonstruktion des niederösterreichischen Erdbebens von 1590*. Springer Verlag Wien, Heidelberg, New York, 1987.

B. Gutenberg and C. F. Richter. Frequency of earthquakes in California. *Bulletin of the Seismological Society of America*, 34(4):185–188, 1944. URL http://www.bssaonline.org/content/34/4/185.short.

C. Hammerl and W. Lenhardt. Erdbeben in Niederösterreich von 1000 bis 2009 n. Chr. In *Abhandlungen*, volume 67. Geologische Bundesanstalt, 2013.

J. L. Hardebeck, J. J. Nazareth, and E. Hauksson. The static stress change triggering model: constraints from two southern California aftershock sequences. *Journal of Geophysical Research: Solid Earth*, 103(B10):24427–24437, 1998. ISSN 2156-2202. doi: 10.1029/98JB00573. URL http://dx.doi.org/10.1029/98JB00573.

H. Harjes. Design and siting of a new regional array in Central Europe. *Bulletin of the Seismological Society of America*, 80(6B):1801–1817, 1990.

H. Harjes, M. Jost, J. Schweitzer, and N. Gestermann. Automatic seismogram analysis at GERESS. *Comput. Geosci.*, 19(2):157–166, February 1993. ISSN 0098-3004. doi: 10.1016/0098-3004(93)90113-J.

R. A. Harris. Introduction to special section: Stress triggers, stress shadows, and implications for seismic hazard. *Journal of Geophysical Research: Solid Earth*, 103(B10):24347–24358, 1998. ISSN 2156-2202. doi: 10.1029/98JB01576. URL http://dx.doi.org/10.1029/98JB01576.

R. A. Harris, R. W. Simpson, and P. A. Reasenberg. Influence of static stress changes on earthquake locations in Southern California. *Nature*, 375 (6528):221–224, 05 1995. URL http://dx.doi.org/10.1038/375221a0.

H. Hausmann, S. Hoyer, B. Schurr, E. Brückl, G. Houseman, and G. Stuart. New seismic data improve earthquake location in the Vienna Basin area, Austria. *Austrian Journal of Earth Sciences*, 103/2:2–14, 2010.

H. Hausmann, R. Meurers, and N. Horn. The 2013 earthquakes in the Vienna Basin: Results from strong-motion and macroseismic data. In *Second European Conference of Earthquake Engineering and Seismology*, Istanbul, Turkey, 2014.

D. V. Helmberger and G. R. Engen. Modeling the long-period body waves from shallow earthquakes at regional ranges. *Bulletin of the Seismological Society of America*, 70(5):1699–1714, 1980. URL http://www.bssaonline.org/content/70/5/1699.abstract.

R. B. Herrmann. Computer programs in seismology: An evolving tool for instruction and research. *Seismological Research Letters*, 84:1081–1088, 2013. doi: 10.1785/0220110096.

R. Heyburn, N. D. Selby, and B. Fox. Estimating earthquake source depths by combining surface wave amplitude spectra and teleseismic depth phase observations. *Geophysical Journal International*, 194(2):1000–1010, 2013. doi: 10.1093/gji/ggt140. URL http://gji.oxfordjournals.org/content/194/2/1000.abstract.

R. Hinsch and K. Decker. Do seismic slip deficits indicate an underestimated earthquake potential along the Vienna Basin transfer fault system? *Terra Nova*, 15(5):343–349, 2003. ISSN 1365-3121. doi: 10.1046/j.1365-3121.2003.00504.x. URL http://dx.doi.org/10.1046/j.1365-3121.2003.00504.x.

R. Hinsch and K. Decker. Seismic slip rates, potential subsurface rupture areas and seismic potential of the Vienna Basin transfer fault. *International Journal of Earth Sciences*, 100:1925–1935, 2010. doi: 10.1007/s00531-010-0613-3.

R. Hinsch, K. Decker, and M. Wagreich. 3-D mapping of segmented active faults in the southern Vienna Basin. *Quaternary Science Reviews*, 24 (3-4):321–336, 2 2005. doi: http://dx.doi.org/10.1016/j.quascirev.2004.04.011. URL http://www.sciencedirect.com/science/article/pii/S0277379104001994.

E. Hintersberger, K. Decker, and J. Lomax. Largest earthquake north of the Alps excavated within the Vienna Basin, Austria. In *European Seismological Commission (ESC) 32nd General Assembly*, Montpellier, France, 2010.

N. Hummel and T. M. Müller. Microseismic signatures of non-linear pore-fluid pressure diffusion. *Geophysical Journal International*, 179(3): 1558–1565, 2009. doi: 10.1111/j.1365-246X.2009.04373.x. URL http://gji.oxfordjournals.org/content/179/3/1558.abstract.

E. Husebye, T. Matveeva, and Y. Fedorenko. focal depth estimation using Pn coda phases including pP, sP, and PmP. *Bulletin of the Seismological Society of America*, 103(3):1771–1783, 2013. doi: 10.1785/0120120015. URL http://www.bssaonline.org/content/103/3/1771.abstract.

J.C. Jaeger, N.G.W. Cook, and R. Zimmerman. *Fundamentals of Rock Mechanics*. Wiley, 2007. ISBN 9780632057597. URL https://books.google.at/books?id=FqADDkunVNAC.

S. Jónsson, R. Segall, P.and Pedersen, and G. Björnsson. Post-earthquake ground movements correlated to pore-pressure transients. *Nature*, 424(6945):179–183, 07 2003. URL http://dx.doi.org/10.1038/nature01776.

U. Kastrup, N. Deichmann, and A. Fröhlich. Evidence for an active fault below the northwestern Alpine foreland of Switzerland. *Geophysical Journal International*, 169(3):1273–1288, 2007. doi: 10.1111/j.1365-246X.2007.03413.x. URL http://gji.oxfordjournals.org/content/169/3/1273.abstract.

B. L. N. Kennett. *IASPEI 1991 seismological tables*. Research School of Earth Sciences, Australian National University, 1991.

D. Kilb, M. Ellis, J. Gomberg, and S. Davis. On the origin of diverse aftershock mechanisms following the 1989 Loma Prieta earthquake. *Geophysical Journal International*, 128(3):557–570, 1997. doi: 10.1111/j.1365-246X.1997.tb05318.x. URL http://gji.oxfordjournals.org/content/128/3/557.abstract.

W. Kim, S. Dineva, S. Ma, and D. Eaton. The 4 August 2004, Lake Ontario, earthquake. *Seismological Research Letters*, 77(1):65–73, 2006. doi: 10.1785/gssrl.77.1.65. URL http://srl.geoscienceworld.org/content/77/1/65.abstract.

C.-Y. King, S. Azuma, G. Igarashi, M. Ohno, H. Saito, and H. Wakita. Earthquake-related water-level changes at 16 closely clustered wells in

Tono, central Japan. *Journal of Geophysical Research: Solid Earth*, 104(B6): 13073–13082, 1999. ISSN 2156-2202. doi: 10.1029/1999JB900080. URL http://dx.doi.org/10.1029/1999JB900080.

G. King, R. Stein, and J. Lin. Static stress changes and the triggering of earthquakes. *Bulletin of the Seismological Society of America*, 84(3):935–953, 06 1994.

E. Kissling, G. Hetenyi, and AlpArray-Working-Group. AlpArray – Probing Alpine geodynamics with the next generation of geophysical experiments and techniques. In *EGU General Assembly*, EGU General Assembly Conference Abstracts, Vienna, Austria, 2014.

C. Langston. Depth of faulting during the 1968 Meckering, Australia, earthquake sequence determined from waveform analysis of local seismograms. *Journal of Geophysical Research: Solid Earth*, 92(B11):11561–11574, 1987. ISSN 2156-2202. doi: 10.1029/JB092iB11p11561. URL http://dx.doi.org/10.1029/JB092iB11p11561.

C. Langston. The SsPmp phase in regional wave propagation. *Bulletin of the Seismological Society of America*, 86(1A):133–143, 1996. URL http://www.bssaonline.org/content/86/1A/133.abstract.

W. Lee and J. Lahr. A computer program for determination local earthquake hypocenter, magnitude, and first motion pattern of local earthquakes. *U.S. Geological Survey, Open File Report*, pages 75–311, 1975.

W. Lenhardt, Ch. Freudenthaler, R. Lippitsch, and E. Fiegweil. Focal-depth distributions in the austrian Eastern Alps based on macroseismic data. *Austrian Journal of Earth Sciences*, 100:66–79, 2007.

J. Lin and R. Stein. Stress triggering in thrust and subduction earthquakes and stress interaction between the southern San Andreas and nearby thrust and strike-slip faults. *Journal of Geophysical Research: Solid Earth*, 109(B2):B02303, 2004. ISSN 2156-2202. doi: 10.1029/2003JB002607. URL http://dx.doi.org/10.1029/2003JB002607.

A. Lomax, J. Virieux, P. Volant, and C. Berge. *Advances in seismic event locations*, chapter Probabilistic earthquake location in 3D and layered models: Introduction of a Metropolis-Gibbs method and comparison with linear locations, pages 101–134. Kluwer, Amsterdam, 2000.

S. Ma. Depth determination for moderate and small earthquakes by modeling regional depth phases sPg, sPmP, and sPn. *Bulletin of the Seismological Society of America*, 100(3):1073–1088, 2010. doi: 10.1785/0120090103.

S. Ma. *Earthquake Research and Analysis - Seismology, Seismotectonic and Earthquake Geology*, chapter Focal Depth Determination for Moderate and Small Earthquakes by Modeling Regional Depth Phases sPg, sPmP, and sPn, pages 143–166. InTech, 2012. doi: 10.5772/27240.

S. Ma and G. M. Atkinson. Focal depths for small to moderate earthquakes. *Bulletin of the Seismological Society of America*, 96(2):609–623, 2006. doi: 10.1785/0120040192.

S. Ma and D. W. Eaton. Western Quebec seismic zone (Canada): clustered, midcrustal seismicity along a Mesozoic hot spot track. *Journal of Geophysical Research: Solid Earth*, 112(B6), 2007. ISSN 2156-2202. doi: 10.1029/2006JB004827. URL http://dx.doi.org/10.1029/2006JB004827. B06305.

S. Ma and D. W. Eaton. Combining double-difference relocation with regional depth-phase modelling to improve hypocentre accuracy. *Geophysical Journal International*, 185:871–889, 2011. doi: 10.1111/j.1365-246X.2011.04972.x.

S. Ma and D. Motazedian. Depth determination of small shallow earthquakes in eastern Canada from maximum power Rg/Sg spectral ratio. *Journal of Seismology*, 16:107–129, 2012. ISSN 1383-4649. 10.1007/s10950-011-9252-9.

R. Madariaga. Dynamics of an expanding circular faults. *Bulletin of the Seismological Society of America*, 66/3:639–666, 1976.

M. Manga and C.-Y. Wang. 4.10 - earthquake hydrology. In Gerald Schubert, editor, *Treatise on Geophysics*, pages 293 – 320. Elsevier, Amsterdam, 2007. ISBN 978-0-444-52748-6. doi: http://dx.doi.org/10.1016/B978-044452748-6.00074-2. URL http://www.sciencedirect.com/science/article/pii/B9780444527486000742.

M. Manga, I. Beresnev, E. E. Brodsky, J. E. Elkhoury, D. Elsworth, S. E. Ingebritsen, D. C. Mays, and C.-Y. Wang. Changes in permeability

caused by transient stresses: field observations, experiments, and mechanisms. *Reviews of Geophysics*, 50(2), 2012. ISSN 1944-9208. doi: 10.1029/2011RG000382. URL http://dx.doi.org/10.1029/2011RG000382. RG2004.

S. Mertl and E. Brückl. ALPAACT seismological and geodetic monitoring of ALpine-Pannonian ACtive Tectonics annual report - research year 2009. Technical report, Austrian Academy of Sciences, 2010.

R. Meurers, W. Lenhardt, B. Leichter, and E. Fiegweil. Macroseismic effects of the Ebreichsdorf earthquake of july 11, 2000 in Vienna. *Austrian Journal of Earth Sciences*, 95/96:20–27, 2004.

V. Mifka and E. Trapp. Das Ebreichsdorfer Beben vom 8. November 1938. In *Sitzungsbericht der Akademie der Wissenschaften, Abtl. IIA*, volume 150, pages 57–88, Vienna, Austria, 1941.

S. A. Miller, C. Collettini, L. Chiaraluce, M. Cocco, M. Barchi, and B. J. P. Kaus. Aftershocks driven by a high-pressure CO2 source at depth. *Nature*, 427(6976):724–727, 02 2004. URL http://dx.doi.org/10.1038/nature02251.

J. R. Murphy and B. W. Barker. Improved focal-depth determination through automated identification of the seismic depth phases pP and sP. *Bulletin of the Seismological Society of America*, 96(4A):1213–1229, 2006. doi: 10.1785/0120050259. URL http://www.bssaonline.org/content/96/4A/1213.abstract.

R. M. Nadeau, W. Foxall, and T. V. McEvilly. Clustering and periodic recurrence of microearthquakes on the San Andreas fault at Parkfield, California. *Science*, 267(5197):503–507, 1995. doi: 10.1126/science.267.5197.503. URL http://www.sciencemag.org/content/267/5197/503.abstract.

W. Nagy. New region-dependent travel-time handling facilities at the IDC; functionality, testing and implementation details. Technical Report 96/1179, SAIC, 1996.

A. Nur and J. R. Booker. Aftershocks caused by pore fluid flow? *Science*, 175(4024):885–887, 1972. doi: 10.1126/science.175.4024.885. URL http://www.sciencemag.org/content/175/4024/885.abstract.

Y. Okada. Internal deformation due to shear and tensile faults in a half-space. *Bulletin of the Seismological Society of America*, 82(2):1018–1040, 1992. URL http://www.bssaonline.org/content/82/2/1018.abstract.

H. Peresson and K. Decker. Far-field effects of Late Miocene subduction in the Eastern Carpathians: E-W compression and inversion of structures in the Alpine-Carpathian-Pannonian region. *Tectonics*, 16:38–56, 1997.

J. Plomerova, I. Bianchi, G. Hetényi, H. Munzarová, G. Bokelmann, E. Kissling, "AlpArray-EASI-Working-Group", and "AlpArray-EASI-Field-Team". The Eastern Alpine Seismic Investigation (EASI) project. In *EGU General Assembly 2015*, 2015.

Development Team QGIS. *QGIS Geographic Information System*. Open Source Geospatial Foundation, 2009. URL http://qgis.osgeo.org.

E. Qorbani, I. Bianchi, and G. Bokelmann. Slab detachment under the Eastern Alps seen by seismic anisotropy . *Earth and Planetary Science Letters*, 409:96–108, 2015a. ISSN 0012-821X. doi: http://dx.doi.org/10.1016/j.epsl.2014.10.049. URL http://www.sciencedirect.com/science/article/pii/S0012821X14006761.

E. Qorbani, G. Bokelmann, I. Kováacs, F. Horváath, and G. Falus. Deep deformation pattern for the Carpathian-Pannonian region. *JGR, submitted*, 2015b.

L. Ratschbacher, W. Frisch, H.-G. Linzer, and O. Merle. Lateral extrusion in the Eastern Alps, part 2: Structural analysis. *Tectonics*, 10(2):257–271, 1991. ISSN 1944-9194. doi: 10.1029/90TC02623. URL http://dx.doi.org/10.1029/90TC02623.

J. Reinecker and W. A. Lenhardt. Present-day stress field and deformation in Eastern Austria. *International Journal of Earth Sciences*, 88(3):532–550, 1999. ISSN 1437-3254. doi: 10.1007/s005310050283. URL http://dx.doi.org/10.1007/s005310050283.

J. R. Rice and M. P. Cleary. Some basic stress diffusion solutions for fluid-saturated elastic porous media with compressible constituents. *Reviews of Geophysics*, 14(2):227–241, 1976. ISSN 1944-9208. doi: 10.1029/RG014i002p00227. URL http://dx.doi.org/10.1029/RG014i002p00227.

E. Roeloffs. Persistent water level changes in a well near Parkfield, California, due to local and distant earthquakes. *Journal of Geophysical Research: Solid Earth*, 103(B1):869–889, 1998. ISSN 2156-2202. doi: 10.1029/97JB02335. URL http://dx.doi.org/10.1029/97JB02335.

E. Roeloffs, M. Sneed, D. L. Galloway, M. L. Sorey, C. D. Farrar, J. F. Howle, and J. Hughes. Water-level changes induced by local and distant earthquakes at long valley caldera, california. *Journal of Volcanology and Geothermal Research*, 127(3–4):269–303, 2003. ISSN 0377-0273. doi: http://dx.doi.org/10.1016/S0377-0273(03)00173-2. URL http://www.sciencedirect.com/science/article/pii/S0377027303001732. Crustal Unrest in Long Valley Caldera, California: New interpretations from geophysical and hydrologic monitoring and deep drilling.

S. Rost and C. Thomas. Array seismology: Methods and applications. *Reviews of Geophysics*, 40(3):2–1 – 2–27, 2002. ISSN 1944-9208. doi: 10.1029/2000RG000100. 1008.

L. H. Royden. *Strike-slip deformation, basin formation, and sedimentation*, chapter The Vienna Basin: A thin-skinned pull-apart basin, pages 319–338. SEPM Spec. Publ. 37, 1985.

C. K. Saikia. A method for path calibration using regional and teleseismic broadband seismograms: application to the 21 May 1997 Jabalpur, India earthquake (MW 5. 8). *Current Science*, 79:1301–1315, 2000.

C. G. Sammis, R. M. Nadeau, and L. R. Johnson. How strong is an asperity? *Journal of Geophysical Research: Solid Earth*, 104(B5):10609–10619, 1999. ISSN 2156-2202. doi: 10.1029/1999JB900006. URL http://dx.doi.org/10.1029/1999JB900006.

D. P. Schaff, G. . Bokelmann, W. L. Ellsworth, E. Zanzerkia, F. Waldhauser, and G. C. Beroza. Optimizing correlation techniques for improved earthquake location. *Bulletin of the Seismological Society of America*, 94(2):705–721, 2004. doi: 10.1785/0120020238. URL http://www.bssaonline.org/content/94/2/705.abstract.

M. Schimmel and J. Gallart. Degree of polarization filter for frequency dependent signal enhancement through noise suppression. *Bulletin of*

the Seismological Society of America, 94(3):1016–1035, 2004. doi: 10.1785/0120030178.

S. M. Schmid, D. Bernoulli, B. Fügenschuh, L. Matenco, S. Schefer, R. Schuster, M. Tischler, and K. Ustaszewski. The Alpine-Carpathian-Dinaridic orogenic system: correlation and evolution of tectonic units. *Swiss Journal of Geosciences*, 101(1):139–183, 2008. ISSN 1661-8726. doi: 10.1007/s00015-008-1247-3. URL http://dx.doi.org/10.1007/s00015-008-1247-3.

C. H. Scholz. On the stress dependence of the earthquake b value. *Geophysical Research Letters*, 42(5):1399–1402, 2015. ISSN 1944-8007. doi: 10.1002/2014GL062863. URL http://dx.doi.org/10.1002/2014GL062863. 2014GL062863.

D. Schorlemmer and St. Wiemer. Earth science Microseismicity data forecast rupture area. *Nature*, 434(7037):1086–1086, 04 2005. URL http://dx.doi.org/10.1038/4341086a.

SED. Reviewed regional moment tensor catalog. ONLINE, April 2006. URL http://www.seismo.ethz.ch/prod/tensors/mt_oldcat.

S.A. Sipkin. The use of waveform shapes to automatically determine earthquake focal depth. *Bulletin of the Seismological Society of America*, 90: 248–254, 2000.

R. Stein, G. King, and J. Lin. Change in failure stress on the southern San Andreas fault system caused by the 1992 Magnitude=7.4 Landers earthquake. *Science*, 258:1328–1332, 1992.

R. Stein, A. Barka, and J. Dieterich. Progressive failure on the North Anatolian fault since 1939 by earthquake stress triggering. *Geophysical Journal International*, 128(3):594–604, 1997. doi: 10.1111/j.1365-246X.1997.tb05321.x. URL http://gji.oxfordjournals.org/content/128/3/594.abstract.

S. Stein and M. Wysession. *An Introduction to Seismology, Earthquakes, and Earth Structure*. Wiley, 2009. ISBN 9781444311310. URL http://books.google.at/books?id=-z80yrwFsqoC.

A. Stroujkova. Constraining event depths and crustal velocities using regional depth phases. *Bulletin of the Seismological Society of America*, 99(1): 215–225, 2009. doi: 10.1785/0120080085. URL http://www.bssaonline.org/content/99/1/215.abstract.

A. Stroujkova, D. T. Reiter, and R. H. Shumway. Regional seismic focal depth estimation in complex tectonic environments. *29th Monitoring Research Review: Ground-Based Nuclear Explosion Monitoring Technologies*, 1:501–511, 2007.

S. Toda, R. S. Stein, P. A. Reasenberg, J. H. Dieterich, and A. Yoshida. Stress transferred by the 1995 Mw = 6.9 Kobe, Japan, shock: effect on aftershocks and future earthquake probabilities. *Journal of Geophysical Research: Solid Earth*, 103(B10):24543–24565, 1998. ISSN 2156-2202. doi: 10.1029/98JB00765. URL http://dx.doi.org/10.1029/98JB00765.

S. Toda, R. S. Stein, K. Richards-Dinger, and S. B. Bozkurt. Forecasting the evolution of seismicity in southern California: animations built on earthquake stress transfer. *Journal of Geophysical Research: Solid Earth*, 110(B5), 2005. ISSN 2156-2202. doi: 10.1029/2004JB003415. URL http://dx.doi.org/10.1029/2004JB003415.

E. Umnig, E. Brückl, J. Maras, and R. Weber. Monitoring tectonic processes in Eastern Austria based on GNSS-derived site velocities. *Vermessung und Geoinformation*, 103(2-3/15):198–207, 2015.

M. Uski, T. Hyvönen, A. Korja, and M.-L. Airo. Focal mechanisms of three earthquakes in Finland and their relation to surface faults . *Tectonophysics*, 363(1–2):141–157, 2003. ISSN 0040-1951. doi: http://dx.doi.org/10.1016/S0040-1951(02)00669-8. URL http://www.sciencedirect.com/science/article/pii/S0040195102006698.

J. E. Vidale. Complex polarization analysis of particle motion. *Bulletin of the Seismological Society of America*, 76(5):1393–1405, 1986.

F. Waldhauser and W. L. Ellsworth. A double-difference earthquake location algorithm: method and application to the northern Hayward fault. *Bulletin of the Seismological Society of America*, 90:1353–1368, 2000.

L. M. Warren and P. M. Shearer. Using the effects of depth phases on P-wave spectra to determine earthquake depths. *Bulletin of the Seismological Society of Americawe*, 95(1):173–184, 2005. doi: 10.1785/0120030251.

S. Weginger and E. Brückl. DC moment tensor estimation based on P- and S-waveform stacking. In *EGU General Assembly 2014*, 2014.

P. Wessel, W. H. F. Smith, R. Scharroo, J. Luis, and F. Wobbe. Generic mapping tools: Improved version released. *Eos, Transactions American Geophysical Union*, 94(45):409–410, 2013. ISSN 2324-9250. doi: 10.1002/2013EO450001. URL http://dx.doi.org/10.1002/2013EO450001.

G. Wessely. Zur Geologie und Hydrodynamik im südlichen Wiener Becken und seiner Randzone. *Mitteilungen der österreichischen geologischen Gesellschaft*, 76:27–68, 1983.

C. A.J. Wibberley. Hydraulic diffusivity of fault gouge zones and implications for thermal pressurization during seismic slip. *Earth, Planets and Space*, 54(11):1153–1171, 2002. ISSN 1343-8832. doi: 10.1186/BF03353317. URL http://dx.doi.org/10.1186/BF03353317.

M. Wilde-Piórko, W.H. Geissler, J. Plomerová, M. Grad, V. Babuška, E. Brückl, J. Cyziene, W. Czuba, R. England, E. Gaczyński, R. Gazdova, S. Gregersen, A. Guterch, W. Hanka, E. Hegedüs, B. Heuer, P. Jedlička, J. Lazauskiene, G.Randy Keller, R. Kind, K. Klinge, P. Kolinsky, K. Komminaho, E. Kozlovskaya, F. Krüger, T. Larsen, M. Majdański, J. Málek, G. Motuza, O. Novotný, R. Pietrasiak, Th. Plenefisch, B. Ruzek, S. Sliaupa, P. Środa, M. Świeczak, T. Tiira, P. Voss, and P. Wiejacz. PASSEQ 2006-2008: passive seismic experiment in Trans-European Suture Zone. *Studia Geophysica et Geodaetica*, 52(3):439–448, 2008. ISSN 0039-3169. doi: 10.1007/s11200-008-0030-2. URL http://dx.doi.org/10.1007/s11200-008-0030-2.

ZAMG. Austrian Earthquake Catalogue of earthquakes from 1200 to 2013 A.D. (Austria). Computer File of earthquakes with Ml and defining picks greater equal than 6. E, Central Institute of Meteorology and Geodynamics (ZAMG), 2014.

M. Zhang, D. Tian, and L. Wen. A new method for earthquake depth determination: stacking multiple-station autocorrelograms. *Geophysical Jour-*

nal International, 197(2):1107–1116, 2014. doi: 10.1093/gji/ggu044. URL http://gji.oxfordjournals.org/content/197/2/1107.abstract.

L. Zhu, D. Helmberger, C. Saikia, and B. Woods. Regional waveform calibration in the Pamir-Hindu Kush regions. *Journal of Geophysical Research: Solid Earth*, 102(B10):22799–22813, 1997. ISSN 2156-2202. doi: 10.1029/97JB01855. URL http://dx.doi.org/10.1029/97JB01855.